ANALYSIS OF ORGANIC RANKINE CYCLES CONSIDERING BOTH EXPANDER AND CYCLE PERFORMANCES

ANGELO LA SETA

Master's Thesis

Energy Engineering
DTU Mechanichal engineering, Thermal Energy Section

Ingegneria industriale e dell'informazione
Corso di laurea magistrale in ingegneria energetica
Matr. 787567
Anno accademico 2013/2014

November 2014 –
Lyngby, København

SUPERVISORS

Fredrik Hagind
Leonardo Pierobon
Jesper Graa Andreasen
Giacomo Bruno Persico

ANGELO LA SETA

ANALYSIS OF ORGANIC RANKINE CYCLES CONSIDERING
BOTH EXPANDER AND CYCLE PERFORMANCES

ANALYSIS OF ORGANIC RANKINE CYCLES CONSIDERING
BOTH EXPANDER AND CYCLE PERFORMANCES

Abstract

With the shortage of fossil fuel availability and the deterioration of the environment, new strategies and non-conventional methodologies for energy supply have been proposed. The effective use of low and medium temperature energy sources is one of the main directions to follow to reduce CO_2 emissions and attend to Kyoto protocol. Distributed electricity (and heat) generation, energy-savings as well as renewable sources thus received great attention in these last years. The organic Rankine cycle (ORC) technology has proved a valid alternative for waste heat recovery from different energy sources, e.g. exhausted gas flows from industrial and micro gas turbines, biomass and internal combustion engines. Owing to its feasibility and reliability, ORC power systems have received widespread attention from industries and academia.

This work is focused on the optimization of an axial-flow-turbine design by means of a computational model, capable of evaluating turbine efficiency as a function of expander inlet conditions, and on the coupling of the obtained results into a complete ORC power plant model to achieve a more reliable evaluation of its performances.

The computational model had been aforetime developed in the context of previous studies but it was improved and optimized for the purpose of this work. A new validation process in order to verify its performance and reliability was so performed.

The turbine code was afterwards integrated with the full cycle model. In order to reduce the computational time and ensure convergence, the turbine efficiency map was built.

The full ORC model was applied in the context of the Draughen offshore platform with different boundary conditions and plant configurations. The comparison between the results obtained with a constant-turbine-efficiency model and the ones achieved computing explicitly the expander performance shows, for this latter case, a progressively decrement in turbine efficiency for increasing values of pressure ratio, followed by a progressively flattening power curve.
The reduction in output power is almost 1 MW with respect to a maximum estimated power of 6.3 MW, thereby yielding to a relative reduction of about 15.12% in the most general case.

In the next step, the rotational speed was included among the optimizing parameters and another turbine map was built, allowing to evaluate cycle performances accounting for a turbine with optimized rotational speed. It was found the addition of a

gearbox can significantly improve turbine efficiency, with a benefit in power of about 500 kW that implies a relative increment of 7.5% with respect to the results obtained in the previous case. A first approximated attempt to evaluate the convenience of a gearbox insertion shows this configuration seems profitable; however, more detailed information about gearbox efficiency, weight and volume, as well as data on the effective load regime and utilization factor are required to evaluate properly its profitability, depending the revenue mainly on this latter parameter.

In the end, a different optimization was performed, aiming to minimize the specific cost instead of maximizing turbine efficiency. The results show the economic-best efficiency configuration for the turbine appears to be slightly different from the thermodynamic one, even if the value of obtained specific cost and efficiency are very close.

Sommario

Il progressivo esaurimento dei combustibili fossili e il deterioramento dell'ecosistema terrestre ha comportato nell'ultimo decennio una accesa ricerca di nuove strategie per la produzione di energia. L'uso efficace di risorse energetiche a media e bassa temperatura è una delle principali strade da intraprendere per rispettare il protocollo di Kyoto. Per questo motivo, la generazione distribuita di energia elettrica e calore, il risparmio energetico e le risorse rinnovabili hanno ricevuto sempre più attenzione in questi anni.

L'impiego di fluidi organici si è dimostrato una valida alternativa per il recupero di calore da svariate tipologie di fonti energetiche (correnti gassose provenienti da microturbine e turbine a gas industriali, biomassa, motori a combustione interna e sorgenti geotermiche). Per via della loro affidabilità e semplicità, i cicli ORC hanno ricevuto sempre più interesse sia da parte di industrie che da enti di ricerca.

Lo scopo principale del presente lavoro consiste nell'ottimizzare il design di una turbina assiale monostadio attraverso un codice computazionale, in grado di generare una stima di rendimento dell'espansore per date condizioni in ingresso, e di inserire i risultati ottenuti in un modello completo di ciclo ORC, valutando le prestazioni dell'impianto al variare dell'efficienza della turbina.

Il modello computazionale è stato sviluppato nell'ambito di studi precedenti ma è stato migliorato e ottimizzato per essere impiegato nel presente lavoro. E' stato pertanto necessario validare il codice per comprenderne i suoi reali limiti e potenzialità.

Il codice computazionale è stato successivamente integrato nel modello completo di impianto mediante la realizzazione della mappa di ottimo rendimento della turbina a numero di giri costante.

Il modello di ciclo è stato applicato nel contesto della Draugen offshore platform con differenti condizioni al contorno e configurazioni di impianto. Il confronto tra le prestazioni dell'impianto calcolate assumendo un rendimento di turbina costante e calcolando le prestazioni della macchina mostra, per quest'ultimo caso, una curva di potenza la cui pendenza decresce progressivamente con l'aumentare del rapporto di pressione, causando una riduzione di potenza di circa 1 MW su una potenza massima calcolata di 6.3 MW, con una riduzione relativa del 15.12%.

Nella fase successiva, il numero di giri della macchina è stato ottimizzato ed è stata ottenuta una nuova mappa dell'espansore, consentendo di calcolare le prestazioni del ciclo con una turbina a numero di giri ottimizzato. L'incremento di efficienza dell'espansore consente di aumentare la potenza ottenuta di circa 500 k*W*, con un incremento relativo di circa il 7.5% rispetto ai risultati ottenuti nel test precedente. Una indicazione di massima sulla convenienza economica legata all'impiego di una turbina a numero di giri ottimizzato mostra che questa seconda configurazione sembra essere conveniente. Tuttavia, per una stima più accurata sono necessari ulteriori dati su peso, volume ed efficienza dello stesso, nonché una stima più accurata del fattore di utilizzo e delle effettive condizioni di carico dell'impianto.

Infine, è stato effettuato un ultimo processo di ottimizzazione, scegliendo di minimizzare il costo specifico della turbina anziché ottimizzare il rendimento. I risultati mostrano che la configurazione di minimo costo specifico sono leggermente differenti da quelle ottenute con una ottimizzazione termodinamica, sebbene i valori di efficienza e costo specifico ottenuti nei due processi siano molto vicini.

"So long as you still see the stars as something "above you" you still lack the eye of the man of knowledge."
Friedrich Nietzsche, Beyond Good and Evil

"Everything should be made as simple as possible, but not simpler."
Albert Einstein

PREFAZIONE

Questo lavoro rappresenta il mio progetto di tesi per la laurea magistrale in ingegneria energetica presso il Politecnico di Milano.

L'intero lavoro di tesi è stato svolto presso la Technical University of Denmark (DTU). Il presente lavoro corrisponde a 30 CFU ed è stato svolto dal 12 maggio 2014 al 5 novembre 2014. I supervisors sono il Professor Fredrik Haglind e i Ph.D. candidates Leonardo Pierobon e Jesper Graa Andreasen dalla DTU e il Professor Giacomo Bruno Persico dal Politecnico di Milano.

Vorrei ringraziare il Professor Haglind per avermi concesso l'opportunità di svolgere il mio lavoro di tesi presso questa prestigiosa università e il Professor Persico per essere sempre stato disponibile e presente con i suoi consigli, anche se lontano.

Un ringraziamento speciale è dovuto a Leonardo Pierobon e Jesper Graa Andreasen per la loro pazienza, i loro consigli e il loro supporto.

Questo lavoro avrebbe potuto essere molto dispersivo e il loro consiglio è stato di aiuto fondamentale per me durante la mia permanenza alla DTU.

PREFACE

This present thesis represents my final project for the Master's degree in Energy engineering at Politecnico di Milano.

The whole study has been carried out at Technical University of Denmark (DTU), Thermal Energy section. The Master's thesis consists in a 30 ECTS project and it was performed by the 12th of May 2014 to the 5th of November 2014.

Supervisors were Associate Professor Fredrik Haglind, Ph.D. candidate Leonardo Pierobon, Ph.D. student Jesper Graa Andreasen from DTU and Ph.D. Giacomo Bruno Persico from Politecnico di Milano.

I want to thank Professor Fredrik Haglind for giving me the possibility to perform my final project in this prestigious University and Giacomo Bruno Persico for having been always available, even far away.

My special thanks and gratitude must be given to Leonardo Pierobon and Jesper Graa Andreasen for their patience, their competence, their advice and their support.

This project could have been very dispersive and their advice about which direction to follow have been of fundamental help for me during all my period of permanence at DTU.

SINTESI DEL LAVORO DI TESI

Nel tentativo congiunto di produrre più energia e ridurre le emissioni di biossido di carbonio, i cicli termodinamici alimentati da fluidi organici hanno dimostrato di essere un utile strumento per raggiungere l'obiettivo.

La produzione di potenza da un ciclo termdinamico è strettamente lagata alle prestazioni dell'espansore che, a sua volta, variano in funzione dei parametri termodinamici e del fluido impiegato.

Molti modelli di cicli ORC presenti in letteratura sono realizzati assumendo una efficienza della turbina costante: tuttavia, laddove questa ipotesi non è accetabile, le effettive prestazioni dell'espansore possono significativamente modificare il reale output del ciclo e il suo punto di ottimo da un punto di vista tecnico-economico.

Per ricercare le reali prestazioni di un impianto e trovare il punto di ottimo da un punto di vista termodinamico ed economico, è dunque necessario tenere conto dell'effettivo comportamento dell'espansore all'interno del ciclo termodinamico.

OBIETTIVI DEL LAVORO

Lo scopo principale del presente lavoro consiste nell'ottimizzare il design di una turbina assiale monostadio attraverso un codice computazionale, in grado di generare una stima di rendimento dell'espansore per date condizioni in ingresso, e di inserire i risultati ottenuti in un modello completo di ciclo ORC, valutando le prestazioni dell'impianto al variare della sua pressione di evaporazione. Dal confronto con le prestazioni calcolate per il medesimo impianto assumendo un rendimento di turbina costante, sarà possibile stabilire se tale approccio è in grado di fornire risultati sufficientemente accurati o se un modello più complesso, che tiene conto delle effettive prestazioni dell'espansore, risulta invece necessario.

Per lo scopo di questo lavoro, è stato impiegato un modello computazionale pre-esistente di turbina: sulla base di un set di otto parametri di design, portata massica, temperatura di ingresso e rapporto di pressione totale tra ingresso e uscita, il codice produce una stima dell'efficienza total-to-total della macchina. Qualora inserito in un algoritmo di ottimizzazione, il codice completo può restituire la geometria ottimale che

massimizza l'efficienza della macchina per date condizioni termodinamiche di ingresso e uscita.

Tale codice è stato sviluppato nell'ambito di precedenti studi [12] ma è stato modificato e adattato per le esigenze del presente lavoro. E' stato quindi necessario verificare e validare il codice per valutarne le sue reali potenzialità. nella fase successiva, il codice è stato integrato in un modello completo di ciclo termodinamico ed applicato nel contesto della Draugen offshore platform.

L'integrazione dell'intero modello computazionale avrebbe incrementato ulteriormente il tempo di calcolo richiesto per una singola simulazione e, nel presente caso di studio, causato problemi di convergenza: il design della turbina è stato pertanto ottimizzato per varie condizioni di ingresso e i risultati ottenuti hanno consentito di creare la mappa di ottimo rendimento della turbina, considerando inizialmente un numero di giro costante.

Questi dati sono stati inseriti nel modello completo di ciclo ORC, valutando le prestazioni dell'impianto al variare della pressione di evaporazione del ciclo, tenedo conto simultaneamente del rendimento dell'espansore.

Nella seconda fase, è stata realizzata una nuova mappa della turbina, ottimizzando anche il numero di giri. Le nuove prestazioni dell'impianto sono state valutate nuovamente con questa seconda mappa e alcune considerazioni di natura economica sono state fatte per fornire una prima valutazione di massima sulla convenienza dell'impiego di questa seconda configurazione.

Infine, per valutare se, ed eventualmente in che modo, una diversa ottimizzazione possa portare a differenti risultati, è stato ottenuto un nuovo set di risultati, scegliendo di minimizzare il costo specifico della turbina (in €/kW) piuttosto che massimizzare la sua efficienza.

CODICI E STRUMENTI IMPIEGATI

L'intero modello computazionale è stato realizzato mediante il programma MATLAB fornito da MathWorks® [13]. Le proprietà termodinamiche dei fluidi sono state calcolate utilizzando il database open-source *CoolProp* [14], sviluppato presso la Liege University e il software commerciale *Refprop®* [15].

Alcuni grafici sono stati tracciati mediante Excel 2010, metre alcune figure sono state realizzate mediante il software Autocad 2015, rilasciato da Autodesk® [16]. I vari processi di ottimizzazione sono stati realizzati mediante il *genetic algorithm toolbox* present in MATLAB. Il tempo impiegato da una singola

ottimizzazione può variare da quattro ore a cinque giorni.

METODI E MODELLI

Introduzione al modello computazionale di turbina

Questo paragrafo fornisce solamente uno sguardo di insieme al modello computazionale; una descrizione più dettagliata di alcuni aspetti è riportata nella sezione 3.2 a pagina 18, mentre una trattazione completa ed esaustiva dell'argomento è fornita da Gabrielli [12].

L'intero algoritmo di design della turbina è basato su un set di otto parametri i cui valori, insieme alle condizioni di ingresso e uscita della macchina, consentono di pervenire ad una stima finale del rendimento. Tali parametri, insieme alle condizioni termodinamiche in ingresso e uscita della macchina, sono elencati nella tabella 3.2 a pagina 19. Come riportato, è necessario fornire atri valori oltre a quelli già menzionati, come ad esempio la rugosità superficiale. Tuttavia, questi valori sono scelti per massimizzare l'efficienza compatibilmente con le attuali possibilità tecnologiche e sono tenuti costanti durante l'intero processo di ottimizzazione. Una lista completa di tutti i parametri richiesti dal codice è riportata in tabella B.1 a pagina 95 in appendice B. Per un certo set di valori per i parametri di input riportati in tabella 3.2, il codice restituisce quindi un valore di efficienza total-to-total della macchina, assumendo una componente assiale di velocità costante per tutto lo stadio.

Si noti che questa configurazione non è l'unica possibile, ma per una geometria che non consideri una componente assiale di velocità constante lungo lo stadio, sono necessari altri due parametri di input, ossia la componente assiale di velocità in ingresso C_{a1} e il coefficiente ϕ_r, definito nella equazione 3.2 a pagina 20. questa variante è stata adottata durante la fase di verifica e validazione del codice.

Si noti infine che:

- la valutazione delle perdite è effettuata con il modello di Craig e Cox [4] che risulta essere, secondo precedenti studi, il più completo e adatto allo scopo di questo lavoro [22, 23, 27, 28];

- nella geometria creata dal codice (riportata in figura 3.4 a pagina 21), la forma delle pale rotoriche è sempre convergente, mentre quella delle pale statoriche può cambiare da convergente a convergente-divergente;

- il codice assume flusso monodimensionale e non tiene conto di alcuna variazione in direzione radiale del profilo di velocità nè considera un eventuale svergolamento delle pale.

La struttura principale del modello computazionale è essenzialmente composta da tre parti:

1. Valutazione di tutte le variabili termodinamiche in ingresso e proprietà isoentropiche in uscita. Questo passaggio consente di calcolare il salto entalpico totale isoentropico. Tutti questi valori restano costanti durante le fasi successive del processo;

2. Ottenimento di un set di valori di primo tentativo per angoli di flusso, velocità e proprietà termodinamiche del fluido in tutto lo stadio;

3. Ciclo iterativo: iniziando dai valori di primo tentativo appena ottenuti, viene avviato un processo iterativo finché la convergenza non viene raggiunta.

Se, come precedentemente accennato, questo modello è accoppiato con un opportuno algoritmo di ottimizzazione, per un dato fluido e date condizioni termodinamiche in ingresso[1], è possibile pervenire al set ottimale di parametri che massimizza l'efficienza della macchina. L'algoritmo impiegato è chiamato *algoritmo genetico*, integrato di default nella optimization toolbox del programma MATLAB e la sua logica di funzionamento è brevemente descritta in appendice A a pagina 91.

Per ottenere soluzioni accettabili sia da un punto di vista fisico che tecnologico, è necessario imporre alcuni vincoli geometrici e termodinamici, che si concretizzano in:

- un limite superiore e inferiore per ognuno dei parametri da ottimizzare (richiesto peraltro dall'algoritmo di ottimizzazione);

- un secondo set di vincoli ulteriormente imposto sulla soluzione finale.

Tali vincoli sono stati sostanzialmente stabiliti da Macchi e Perdichizzi [27] e sono riportati nelle tabelle 3.3 e 3.4 a pagina 24.
Come meglio discusso nel paragrafo 3.3.4 a pagina 24, l'imposizione dei vincoli si basa sostanzialmente su tre ragioni:

---

1 Portata massica, rapporto di pressione totale tra ingresso e uscita della macchina, temperatura totale in ingresso, numero di giri (quest'ultimo sarà invece inserito tra i parametri di ottimizzare nella seconda parte del lavoro).

- alcuni sono necessari per assicurare la validità delle correlazioni usate e la compatibilità con la geometria generata dal modello;

- altri sono imposti per ragioni di tipo tecnologico;

- alti ancora sono imposti per contenere l'insorgere di effetti radiali e tridimensionali, di cui il codice, come prima menzionato, non tiene conto.

Caso di studio: la Draugen offshore platform

La Draugen offshore platform si trova nel mar del Nord, a circa 150 km da Kristiansund in Norvegia, distante 200 km dal circolo polare artico.

Svariate compagnie petrolifere possiedono una quota della piattaforma, come Shell, Petoro e BP Norge. La piattaforma estrae petrolio e gas naturale che trasporta in Norvegia mediante la Asgard transport pipeline. Maggiori informazioni sono fornite da Offshore Technology [11] ma alcune di esse sono riportate nella sezione 3.1 a pagina 16.

L'energia necessaria alla piattaforma (carico normale e di picco) è prodotta mediante tre turbine a gas Siemens SGT-500. Si tratta di macchine in grado di produrre potenza tra i 15 e 20 MW. Le specifiche techiche della macchina sono fornite da Siemens [5] e sono riportate in tabella 3.1 a pagina 18.

Nella piattaforma, una di queste turbine rimane spenta e in manutenzione, mentre le altre due forniscono l'energia richiesta.

Nel presenta lavoro verrà esaminata soltanto una turbina a gas, senza considerare il resto dell'impianto presente nella piattaforma. Soltanto in un caso anche la seconda turbina a gas verrà considerata nello schema di impianto.

Si assume di alimentare la macchina mediante gas naturale ma, poichè la turbina Siemens SGT-500 può essere alimentata con una vasta gamma di combustibili, la temperatura minima di scarico dei gas dalla waste heat recovery unit è prudentemente fissata a 145 °C per evitare la formazione di condense acide [29].

Secondo Pierobon et al. [7], la installazione di una unità ORC di recupero di calore dai gas di scarico, comporterebbe due fonti di guadagno: la prima, legata al risparmio sul combustibile, che potrebbe essere pertanto esportato dalla piattaforma e venduto; la seconda, legata alla riduzione delle emissioni di CO_2 legata alla combustione del gas naturale: dal 1991, infatti, il governo norvegese impone una carbon tax sulle emissioni di CO_2 da cobustibili fossili [30]; l'unità installata ridurrebbe quindi

l'ammontare della tassa per via della "mancata" combustione del gas naturale risparmiato.

Modello di impianto

Lo schema di impianto del modello impiegato è riportato in figura 3.15 a pagina 33. Il modello di ciclo è stato realizzato assumendo le seguenti ipotesi:

- Sono considerate solo configurazioni subcritiche (la massima pressione possibile è fissata a $0.9 \cdot P_{cr}$)

- Non sono considerate perdite di carico all'interno dell'impianto;

- La corrente di gas di scarico della turbina a gas è assunta come ideale;

- La localizzazione del ΔT_{pp} nello scambiatore di calore principale può spostarsi dall'ingresso dell'evaporatore all'uscita del rigeneratore, qualora necessario (si veda la figura 3.16 a pagina 35);

Per ridurre il numero di parametri di impianto da ottimizzare, sono state fatte inoltre le seguenti assunzioni:

1. Il ciclopentano è stato scelto come fluido di lavoro risultando, secondo Pierobon et al. [7], la scelta ottimale per il caso in esame;

2. Entrambe le differenze di temperatura di pinch point, ΔT_{pp} e $\Delta T_{pp,rec}$, sono state fissate al minimo (e ottimo) valore riportato da Pierobon et al. [7], rispettivamente 10 e 15 °C;

3. La pressione di condensazione è stata fissata a 1 bar per evitare infiltrazioni di aria che comporterebbero la rapida decomposizione del fluido [21];

4. La temperatura di ingresso in turbina è stata fissata al massimo valore che assicura la integrità chimica del fluido evitandone la decomposizione; tale valore risulta essere 513.15 K [21].

Per quanto appena discusso, entrambe le mappe della turbina sono state ottenute per il ciclopentano[2] considerando una temperatura di ingresso in turbina costante e pari a 513.15 K. Le mappe riportano i valori di efficienza ottenuta in funzione della portata massica e vari valori del rapporto di pressione e sono integrate nel modello di ciclo mediante una funzione la

_____

2 la cui pressione critica è 45.71 bar.

cui sintassi è fornita dalla equazione 3.9 a pagina 32. Si noti che il punto di scarico della turbina influenza la quantità di calore recuperabile dal fluido dopo l'espansione e dunque, il punto di uscita dal rigeneratore. Qualora la localizzazione del ΔT_{pp} sia all'uscita del rigeneratore, questo punto influenza la portata massica di fluido di lavoro attraverso il bilancio energetico dello scambiatore di calore gas-fluido e dunque, infine, il rendimento della turbina. Risulta necessario in questo caso un processo iterativo, la cui convergenza, nel caso in cui l'intero modello computazionale dell'espansore fosse direttamente integrato nel ciclo, risulterebbe estremamente lenta se non impossibile nella maggior parte dei casi, in quanto le fluttuazioni di portata massica presenti durante le iterazioni non potrebbero essere seguite da una simultanea variazione del design della macchina, con un conseguente valore nullo di efficienza mostrato dal codice. L'impiego della mappa della turbina risulta pertanto necessario per ottenere la convergenza nel processo iterativo.

Una lista completa di tutti gli input richiesti dal modello di ciclo è riportata in tabella B.2 a pagina 96.

Stima di massima sulla convenienza dell'impiego di un gearbox

L'ottimizzazione del numero di giri della macchina consente di ottenere una geometria differente con una efficienza più alta, ma comporta anche l'impiego di un riduttore/moltiplicatore di giri. Una stima accurata del profitto economico legato al suo impiego richiederebbe il calcolo del valore attuale netto (VAN) per le due configurazioni di impianto e il loro confronto, comportando pertanto un esame del costo di tutti i componenti dell'impianto. Tale indagine è al di là degli scopi del presente lavoro ma, per ottenere una prima stima di massima sulla eventuale convenienza di impiego una turbina con numero di giri ottimizzato, è sufficiente calcolare il valore attuale netto per un impianto con e senza riduttore, preoccupandosi solo del costo della macchina, generatore elettrico e riduttore e sottrarre i due valori. Infatti, le dimensioni (e il costo) di uno scambiatore di calore sono in prima approssimazione legati alla portata massica che circola e al livello di pressione. Pertanto, per dato rapporto di pressione, è possibile considerare le dimensioni degli scambiatori approssimativamente costanti per i due casi, tenendo a mente anche che, come sarà successivamente discusso, la variazione del rendimento della turbina non cambia significativamente la portata di fluido di lavoro che circola nell'impianto. Il costo della turbina, generatore e riduttore/moltiplicatore di giri è stato stimato mediante le funzioni di costo adoperate da

Astolfi et al. [20], riportate a pagina 38 e 41, mentre i ricavi dell'impianto legati, come già discusso, alla vendita del combustibile risparmiato e alla riduzione della carbon tax sono stati ottenuti mediante la metodologia impiegata da Pierobon et al. [7] e riportata nel paragrafo 3.9 a pagina 39.

Infine, per l'ultimo processo di ottimizzazione, il costo specifico della turbina è stato ricavato impiegando nuovamente la funzione di costo fornita dalla espressione 3.18 a pagina 38 e scegliendo questo parametro come la funzione da minimizzare.

VERIFICA E VALIDAZIONE DEL CODICE

Le prestazioni del modello computazionale di turbina sono state mediante due processi:

1. Una verifica con il codice AXTUR;

2. Una validazione con un set di dati sperimentali ottenuti da Evers and Kötzing [6].

Verifica con AXTUR

AXTUR è un codice sviluppato dal dipartimento di energia del Politecnico di Milano, in grado di ottimizzare il design di una turbina assiale con uno, due o tre stadi. E' stato scelto di riprodurre di simulare una configurazione subsonica con i dati di input riportati in tabella 4.1 a pagina 43. Lo scopo di questo test è verificare se il codice impiegato è in grado di riprodurre, con gli opportuni dati in ingresso, la stessa geometria di AXTUR. Dai dati forniti da AXTUR è stato possibile ricavare i parametrio di input richiesti dal codice e avviare la simulazione.
Si noti che, come il codice in esame, AXTUR fornisce lo stesso design assiale di turbina a raggio medio costante assumendo un flusso monodimensionale.
L'errore è definito mediante l'espressione 4.1 a pagina 42 e i risultati ottenuti, riportati in tabella 4.3 a pagina 44 mostrano un errore relativo massimo del 4.33%. I risultati riportano anche una differenza di circa 20 K nella temperatura allo scarico: è possibile imputare tale differenza al diverso approccio adottato per le proprietà termodinamiche dei fluidi: infatti, mentre AXTUR impiega un modello di gas ideale, nel codice in esame le proprietà termodinamiche dell'aria sono state valutate con il codice *Refprop*.

Evers e Kötzing riportano i dati di una turbina assiale a quattro stadi alimentata ad aria. La geometria è riportata in figura 4.2, mentre i dati adoperati e immagini relative alla geometria delle pale sono riportati in appendice C.

All'ingresso di ogni stadio e all'uscita dell'ultimo, le proprietà termodinamiche del fluido sono state fornite in nove punti lungo l'altezza di pala. Questi dati, insieme alle informazioni sulla geometria delle pale, consentono di ricavare il set di parametri di input necessari al codice. Tutti i valori di input impiegati sono stati estrapolati per mezzo dei dati forniti al raggio medio del particolare stadio. E' stato scelto di validare il codice solo con i dati del primo e ultimo stadio.

I risultati ottenuti per il primo stadio, riportati in tabella 4.6 a pagina 48, mostrano un errore relativo massimo del 22.38% rispetto l'altezza di pala. Tale errore è principalmente imputabile alla non-rappresentatività del valore adoperato di velocità assiale al raggio medio in termini di portata massica: infatti, l'area di passaggio del fluido e, successivamente, l'altezza di pala, sono valutate per mezzo delle equazioni 4.2 e 4.5 a pagina 50; pertanto, per data portata massica e raggio medio, un eventuale "eccesso" legato alla velocità assiale deve essere compensato da una proporzionale riduzione di altezza di pala.

I risultati ottenuti per l'ultimo stadio, riportati in tabella 4.7 a pagina 49, mostrano la stessa tipologia di errore con valori più alti, dovuti alla variazione ancora più marcata del profilo assiale di velocità in direzione radiale, come riportato dai grafici in figura 4.4 e 4.5.

Infine, il grafico in figura 4.3 a pagina 51 mostra la elevata sensibilità dell'angolo di uscita α_3 rispetto all'angolo β_3: risulta dunque possibile comprendere come una piccola incertezza su quest'ultimo angolo risulti in una amplificazione di circa tre volte nell'errore relativo all'angolo α_3, riscontrata nei risultati per entrambi gli stadi.

DISCUSSIONE DEI RISULTATI

I risultati ottenuti si possono dividere in tre gruppi:

1. Risultati riguardanti l'ottimizzazione del design della turbina, raggruppati nelle due mappe di funzionamento della macchina;

2. Risultati riguardanti le prestazioni del ciclo termodinamico;

3. Risultati riguardanti la ottimizzazione tecnico-economica della turbina.

Mappe della turbina

I valori di massimo rendimento ottenuti ottimizzando il design della turbina con numero di giri fisso a 3000 rpm sono riportati nella prima mappa della macchina (figura 5.1 a pagina 54), che mostra l'efficienza in funzione di portata massica e rapporto di pressione. Il rendimento cresce all'aumentare della portata massica e diminuisce all'aumentare del rapporto di pressione. Come meglio discusso nella sezione 5.1, alcuni valori limite imposti dai vincoli sono raggiunti durante il processo di ottimizzazione, ossia il valore massimo del numero di Mach M_{W3} e spesso il valore minimo di $(o/s)_n$ e il numero massimo di pale statoriche.

L'inserimento del numero di giri tra i parametri da ottimizzare consente di avere un grado di libertà in più, che comporta la possibilità di raggiungere efficienze più alte, specialmente nell'intervallo di portata tra 20 e 80 kg/s, ossia l'intervallo di portata massica in cui il numero di giri ottimo risulta marcatamente differente da 3000 rpm (si vedano le figure 5.7 e 5.8 a pagina 58). In questo caso i vincoli più stringenti risultano essere l'angolo di flare del rotore e nuovamente, il numero di Mach M_{W3}.

Prestazioni dell'impianto

Le prestazioni dell'impianto sono state riportate in grafici che mostrano la curva di potenza in funzione del rapporto di pressione tra ingresso e uscita della macchina ossia, per la ipotizzata assenza di perdite di carico, tra pressione di evaporazione e pressione di condensazione. Infatti, per le assunzioni fatte precedentemente, questo parametro risulta l'unico in grado di influenzare le prestazioni dell'impianto. L'intervallo operativo di rapporto di pressione varia da 1 a 41. Per facilitare il confronto, le curve di potenza ottenute calcolando le prestazioni dell'espansore sono state affiancate alle curve di potenza di un impianto in cui è stata assunta un'efficienza di turbina costante. Per la prima parte dei risultati è stata impiegata solo la mappa della turbina a numero di giri costante; la seconda mappa è stata invece impiegata nella fase successiva.

Test con numero di giri fisso

Per il presente caso di studio, il limite sulla temperatura minima di uscita dei gas di scarico risulta essere il vincolo più stringente. Il valore minimo di 145 °C, di fatto limita l'ampiezza del possibile intervallo di rapporto di pressione, come mostrato in figura 5.11 a pagina 60. Come è possibile osservare dal medesimo grafico, minore l'efficienza dell'espansore, maggiore il massimo valore di rapporto di pressione: tale fenomeno è dovuto al fatto che, minore l'efficienza della turbina, maggiore è, a parità di rapporto di pressione, il calore recuperabile nel rigeneratore e pertanto in proporzione è possibile sottrarre meno calore alla corrente di gas di scarico, aumentando la temperatura di uscita dei fumi. Ciò consente in definitiva di raggiungere un rapporto di pressione massimo più elevato compatibilmente con il vincolo di temperatura. Tale comportamento è ulteriormente evidenziato nei grafici in figura 5.12 e 5.13 a pagina 62 in cui si vede come un valore limite della temperatura di uscita dei gas di scarico sempre più basso estende l'intervallo dei possibili valori di rapporto di pressione.

Se questo vincolo viene soppresso, il che coincide con l'ammettere che la temperatura di uscita dei gas di scarico possa raggiungere circa 100 °C, è possibile estendere il rapporto di pressione fino al valore massimo ammesso, come mostra il grafico in figura 5.14 a pagina 62. Questo grafico consente di ottenere una migliore comprensione dell'effetto prodotto dalla variazione di rendimento della turbina. E' possibile osservare che:

- nessuna delle curve di potenza a efficienza di turbina costante riesce a riprodurre l'andamento della curva di potenza ottenuta calcolando le prestazioni dell'espansore. Rispetto alla curva con efficienza di turbina costante pari a 0.8, la potenza massima ottenibile cala da 6.321 *MW* a 5.365 *MW*;

- la curva di potenza ottenuta calcolando le prestazioni dell'espansore mostra una pendenza progressivamente decrescente all'aumentare del rapporto di pressione: questo comportamento è una diretta conseguenza della progressiva diminuzione del rendimento della turbina con il rapporto di pressione, come precedentemente evidenziato nella mappa in figura 5.1 e ancor meglio osservabile in figura 5.15 a pagina 63. Il progressivo appiattimento della curva rende difficile valutare se l'incremento di potenza conseguito oltre un certo valore del rapporto di pressione giustifichi il maggiore investimento economico necessario per raggiungere condizioni operative sempre più severe

e mostra come sia necessario tenere conto delle effettive prestazioni della turbina per indagini successive.

Un secondo test effettuato considera lo sfruttamento di entrambe le turbine a gas presenti nella piattaforma. Lo scopo di questo test è duplice:

- Consente di valutare le prestazioni della turbina in un campo diverso da quello precedente, modificando il range di valori di portata massica nell'impianto;

- Consente di valutare l'eventuale beneficio di installare una unica unità di recupero più grande che sfrutti entrambi i flussi di gas di scarico rispetto a due unità identiche separate; il nuovo schema di impianto è riportato in figura 5.21 a pagina 68.

Il grafico delle curve di potenza ottenute, riportato in figura 5.25 a pagina 71, mostra un comportamento analogo a quello precedente, pur tuttavia con una importante differenza: il valore doppio di portata di gas di scarico implica una portata circa doppia di fluido nel ciclo sottoposto, con un proporzionale incremento della potenza in uscita; tuttavia, mentre per un modello ad efficienza di turbina costante un valore doppio di portata di fluido corrisponde esattamente ad un valore doppio di potenza prodotta, nel caso in cui vengano calcolate le prestazioni della macchina si ha un valore di potenza più che raddoppiato, dovuto al proporzionale miglioramento della efficienza della stessa (si confrontino le figure 5.15 a pagina 63 e 5.26 a pagina 72). Per la massima potenza prodotta di ha un incremento relativo del 6.24%.

Test con numero di giri ottimizzato

L'ottimizzazione del numero di giri, e dunque l'impiego della seconda mappa della turbina, consente di incrementare il rendimento dell'espansore di quasi il 10%, come riportato in figura 5.28 a pagina 73, con un conseguente incremento massimo di potenza di quasi 500 kW[3] (si veda la successiva figura 5.29).

Il grafico di figura 5.30 mostra le curva di potenza ottenuta per tre diversi valori di efficienza di trasmissione meccanica: è possibile osservare come un rendimento inferiore a al 94% sostanzialmente annulli il beneficio dato dalla maggiore complessità impiantistica e il conseguente maggiore investimento economico. Normalmente i rendimenti di trasmissione meccanica sono superiori al 96%, tuttavia questo grafico mostra come

---

3 Per il tracciamento dei grafici è stato utilizzato un rendimento di trasmissione meccanica pari a 0.96.

la maggiore complessità impiantistica sia giustificata solo se tale efficienza è superiore ad un valore minimo. Si noti infine che la quantità di informazioni disponibili in letteratura su sistemi di trasmissione meccanica per potenze di ordini di grandezza pari o superiori a quelle in esame risulta piuttosto contenuta, in quanto tali componenti sono solitamente realizzati sotto specifica commissione per il particolare caso.

Una prima stima di massima sulla convenienza dell'impiego di una turbina a numero di giri ottimizzato è ottenuta come differenza di valore attuale netto tra due configurazioni di impianto, rispettivamente con e senza riduttore. I risultati, riportati nel grafico in figura 5.31 a pagina 78 per due fattori di utilizzo, mostrano come questa configurazione sembri essere conveniente, purché il rapporto di pressione sia superiore a 15. E' interessante notare come il massimo beneficio netto ottenuto risulti pari circa al 5% del valore attuale netto ottenuto nei precedenti studi effettuati da Pierobon et al. [7]. Tuttavia, una analisi più dettagliata e maggiori informazioni sono necessarie per valutare la effettiva convenienza di questa configurazione, soprattutto riguardo l'effettivo fattore di utilizzo dell'impianto nonché peso e volume dei vari componenti, essendo questi due parametri un vincolo importante in una piattaforma offshore.

Ottimizzazione tecnico-economica della turbina

I risultati ottenuti sono riportati nella sezione 5.4, illustrando le curve di costo specifico, efficienza e rapporto di portate volumetriche tra uscita e ingresso della macchina per le ottimizzazioni effettuate minimizzando il costo specifico, insieme agli analoghi risultati ottenuti precedentemente ricercando la massima efficienza della macchina.

Come è possibile notare dal grafico in figura 5.33, i risultati sono abbastanza simili anche se non identici. Per ogni simulazione, il costo specifico risulta sempre minore nel caso della ottimizzazione tecnico-economica, così come il rendimento della turbina risulta sempre maggiore nel caso della ottimizzazione "tradizionale" (figura 5.34).
Da un punto di vista teorico, massimizzare l'efficienza coincide con l'aumento della massima potenza estraibile dalla macchina per date condizioni di ingresso e uscita e dunque, questo comporterebbe la minimizzazione del costo specifico. Tuttavia, il costo di una turbomacchina è più legato al suo volume che alla sua efficienza; una informazione utile sulle dimensioni della macchina è fornita dal size parameter, definito dalla equazione 3.19 a pagina 38 e presente nella funzione di costo impiegata (equazione 3.18). Minimizzare il costo coincide quindi con

la riduzione del size parameter, che per dato rapporto di pressione è funzione solo della portata volumetrica in uscita. Una riduzione di questa ultima coincide con una densità più alta allo scarico e quindi con una minore espansione e comporta, infine, una minore efficienza. Dunque la ricerca della massima efficienza e la riduzione del size parameter non sono due percorsi indipendenti tra loro. I risultati ottenuti mostrano che vi è un certo intervallo di valori di size parameter in cui la riduzione di quest'ultimo ha un effetto benefico sulla riduzione del costo specifico, nonostante la corrispondente diminuzione di efficienza. Tuttavia, tale intervallo di valori, sia in termini di size parameter che di efficienza e costo specifico, risulta molto contenuto, per cui non appare possibile stabilire se l'approccio seguito possa portare a conclusioni apprezzabilmente differenti rispetto a quanto precedentemente ottenuto.

CONCLUSIONI

Un modello computazionale pre-esistente di turbina, in grado di stimare il rendimento di una macchina assiale monostadio, è stato ottimizzato e adattato alle esigenze e gli scopi del presente lavoro. Nella fase di verifica e validazione, il codice ha riportato apprezzabile accordo con un modello computazionale precedentemente sviluppato, ma ha mostrato anche dei limiti di affidabilità qualora siano presenti forti variazioni radiali del profilo di velocità. Per contenere il problema e assicurare la attendibilità dei risultati da un punto di vista fisico e tecnologico, svariati vincoli sono stati imposti restringendo il possibile campo di soluzioni accettabili.

I valori di massimo rendimento ottenuti dal processo di ottimizzazione hanno consentito di tracciare due mappe di efficienza della turbina, che sono state successivamente integrate in un modello completo di ciclo ORC applicato nel contesto della Draugen offshore platform. L'efficienza dell'espansore aumenta all'aumentare della portata massica e diminuisce per valori crescenti del rapporto di pressione.

Il confronto tra le prestazioni dell'impianto ottenute assumendo un'efficienza di turbina costante e calcolando le prestazioni dell'espansore mostra una curva di potenza con pendenza progressivamente decrescente all'aumentare del rapporto di pressione, dovuta alla progressiva diminuzione del rendimento della turbina. Ciò complica la individuazione dell'effettivo punto di ottimo da un punto di vista tecnico-economico e mostra come sia necessario considerare l'effettivo comportamento della

macchina per indagini future.

Un successivo test effettuato raddoppiando la portata di gas di scarico, mostra una potenza prodotta più che raddoppiata, dovuta ad un incremento di efficienza della turbina per valori crescenti di portata massica.

L'ottimizzazione del numero di giri della macchina consente di ottenere un beneficio in termini di efficienza di circa il 10%, a cui può corrisponde un incremento di potenza di quasi 500 k*W*. L'impiego di una turbina a numero di giri ottimizzato comporta comunque un costo aggiuntivo dovuto al sistema di trasmissione meccanica, nonché un maggiore peso e volume complessivo. Una prima stima di massima ottenuta come differenza del valore attuale netto delle due configurazioni impiantistiche riporta che questa seconda configurazione sembra essere conveniente, sebbene indagini e informazioni più dettagliate, soprattutto sull'effettivo fattore di utilizzo e regime di carico dell'impianto, siano necessarie per stimarne la effettiva convenienza nel caso in esame, in cui peraltro peso e volume dei componenti hanno un ruolo non trascurabile.

Infine, un diverso processo di ottimizzazione del design della turbina, scegliendo di minimizzare il costo specifico anziché massimizzare l'efficienza, non mostra una apprezzabile differenza nei risultati finali rispetto alle precedenti ottimizzazioni: sebbene infatti per dato rapporto di pressione vi sia un certo intervallo di valori in cui una riduzione dell'efficienza della macchina ha un effetto benefico sul costo specifico nonostante la riduzione di potenza, tale intervallo di valori, sia in termini di costo specifico che di efficienza, risulta estremamente contenuto e sembra che questo approccio non consenta di ottenere risultati apprezzabilmente diversi dai precedenti.

CONTENTS

NOMENCLATURE

C   absolute fluid velocity $[\text{m} \cdot \text{s}^{-1}]$

C   cost $[\text{€}]$

D   diameter $[\text{m}]$

H   enthalpy $[\text{kJ} \cdot \text{kg}^{-1}]$

I   investment cost $[\text{€}]$

L   work per unit mass $[\text{kJ} \cdot \text{kg}^{-1}]$

M   absolute Mach number

MM   molecular weight $[\text{kg} \cdot \text{kmol}^{-1}]$

M_W relative Mach number

M_{cd} Mach number for converging-diverging nozzle

N   rotational speed $[\text{rpm}]$

P   pressure $[\text{Pa, bar}]$

R   revenue $[\text{€}]$

Re   Reynolds number

S   entropy $[\text{kJ} \cdot \text{kg}^{-1} \cdot \text{K}^{-1}]$

T   temperature $[\text{K}]$

U   peripheral velocity $[\text{m} \cdot \text{s}^{-1}]$

W power $[\text{kW}]$

W relative fluid velocity $[\text{m} \cdot \text{s}^{-1}]$

X   loss coefficient $[\text{kJ} \cdot \text{kg}^{-1}]$

Z   speed of sound $[\text{m} \cdot \text{s}^{-1}]$

$\dot{Q}$ heat rate $[\text{kW}]$

$\dot{V}$ volumetric flow rate $[\text{m}^3 \cdot \text{s}^{-1}]$

$\dot{m}$ mass flow rate $[\text{kg} \cdot \text{s}^{-1}]$

b   profile chord $[\text{m}]$

c   axial chord $[\text{m}]$

c_p isobaric specific heat capacity [kJ · kg⁻¹ · K⁻¹]

h blade height [m]

hhh rotor inlet/nozzle outlet blade height ratio

hu utilization factor [hours/year]

l blade work [kJ · kg⁻¹]

n equipment lifespan [years]

n number of turbine stages (only used in equation 3.18 for the cost-function correlation)

q heat rate per unit mass [kJ · kg⁻¹]

q interest factor

r radius [m]

s blade pitch [m]

t_e trailing edge thickness [m]

z number of blades

Abbreviations and acronyms

CT   carbon tax [NOK/t_{CO_2}]

FL   flare angle [°]

LHV   low heat value [MJ · kg⁻¹]

NOK   norwegian crown

NPV   net present value [€,$]

PEC   purchase equipment cost [€]

PI   profitability index

rpm   rotations per minute

SP   size parameter [m]

TIT   turbine inlet temperature [K]

GA   genetic algorithm

GWP   global warming potential

ORC   organic Rankine cycle

PHE   primary heat exchanger

T-S   temperature-entropy

Greek letters

α   absolute fluid angle [°]

β   relative fluid angle [°]

χ   degree of reaction

Δ   variation symbol

η   efficiency

γ   stagger angle [°]

ω   angular velocity [rad · s⁻¹]

φ   mass flow coefficient C_a/U_m

ψ   Stage load coefficient $(\Delta H_{tot})/(U_m^2/2)$

σ   solidity (b/s)

θ   blade angle [°]

ζ   backbone lenght [m]

o   throat section [m]

Subscripts

0   total condition

1   nozzle inlet

2   rotor inlet

21   nozzle outlet

3   rotor outlet

a   axial

cond condenser

cr   critical

e.r.   emission rate

el   electric

f   fuel

gas   related to exhausted gas flow

gear gearbox

HE	heat exchanger
i	generic element
IR	internal recuperator
is	isoentropic
m	average
max	maximum available value
min	minimum value
min	minimum, relative to nozzle throat
n	nozzle
net	net
ng	natural gas
out	output,outlet
p	pump
pol	polytropic
pp	pinch point
r	ratio (related to pressure)
r	rotor
rec	recovery
rec	recuperator
sf	saved fuel
spec	specific
t	turbine
tot	total condition
ts	total-to-static
tt	total-to-total
u	eulerian (referred to blade work)

INTRODUCTION

In the contemporary attempt to convert more energy and reduce CO_2 emissions for a worldwide growing population, organic Rankine cycles have been proved a useful tool to fulfill this goal. However, the production of such power systems strongly relies on expander efficiency which, in turn, varies depending on inlet thermodynamic conditions and on the adopted fluid.

Most of organic Rankine cycle models in scientific literature relies on the assumption of constant turbine efficiency: however, if this assumption is not consistent, the real expander performance can significantly alter the output of the cycle and its best efficiency point.

In order to calculate the effective cycle performance and find the optimum point for a thermodynamic and economic point of view, it is therefore necessary to couple both turbine and cycle, accounting for real expander behaviour.

1.1 AIMS OF THE WORK

First aim of this work is to couple a computational model of turbine, capable of generating a reliable estimation of expander efficiency, with a complete organic Rankine cycle power plant model and compare the obtained performances with a constant-turbine-efficiency cycle model. From their comparison it would be possible to state whether the assumption of constant turbine efficiency (irrespective to cycle thermodynamic parameters) leads to realistic estimations or if, conversely, a more complex model accounting for both cycle and expander performance should be adopted.

For the purpose of this work, a pre-existing turbine computational code, previously developed and validated in the context of other works [12], has been utilized; for a given set of eight turbine design parameters, mass flow rate, inlet temperature, rotational speed and inlet/outlet total pressure ratio it produces an accurate estimation of turbine total-to-total efficiency.

Due to the high-required computational cost, this code has been optimized and simplified to be subsequently implemented in the whole ORC power plant model, but a new validation process was required to verify its performance.

After the validation, the turbine code was integrated in a whole ORC model and applied in the context of the Draughen offshore platform.
The integration of the full turbine routine into a cycle model would have significantly increased the required computational time and led to numerical convergence issues, so the expander design was first optimized for several combinations of pressure ratio and mass flow rate.
These results were then gathered into a map and this array was coupled with the cycle model. Several tests have been performed, evaluating cycle output in all the available operative range.

Secondly, another thermodynamic optimization process has been performed, looking also for the best rotational speed. In this context some techno-economic considerations have been made to discuss the convenience of a gearbox insertion.

In the end, in order to find out whether and to what extent different expander optimization processes can affect the optimal turbine design and eventually cycle configuration, a turbine techno-economic optimization has been performed: in this process the specific cost (in €/kW) was chosen as the parameter to be optimized, instead of the total-to-total efficiency.

1.2 COMPUTATIONAL TOOLS

The whole Simulation model has been built in the commercial program MATLAB provided by MATHWORKS® [13]. MATLAB, acronym for Matrix Laboratory, is a numerical computing environment and fourth generation programming language.
The thermodynamic properties were calculated using the open-source database provided by *CoolProp* [14], developed at the University of Liege and by the commercial software *Refprop®* [15]. Some plots have been built using the commercial package EXCEL 2010, while some figures have been realized with the commercial software AUTOCAD 2015 provided by AUTODESK® [16]. The optimization processes have been performed with the genetic algorithm toolbox present in MATLAB. The computational time ranged from four hours to five days for a single simulation.

1.3 STRUCTURE OF THE WORK

The following chapters are structured as follows:

- Chapter 2 provides the background for the present study;

- Chapter 3 describes the case of study, models and methodology adopted in this work;

- Chapter 4 is dedicated to the verification and validation of the code;

- In chapter 5 the obtained results are discussed;

- Finally, in chapter 6 the achieved conclusions are summarized and some advice for future work are given.

BACKGROUND

A very interesting overview of organic Rankine cycles and related fluid selection is provided by Quoilin et al. [9].

In this chapter the most important concepts about ORC configuration, fluid selection and organic fluid turbine design are summarized for a better comprehension of the present work.

2.1 GENERAL OVERVIEW OF OF ORGANIC RANKINE CYCLES

The basic Rankine cycle engine consists of a feed pump, vaporizer, power expander and condenser. These four elements form a closed cycle that exploits a fluid to produce power. The original (and most widely used even today) working medium is water: it is available, not expensive and has good thermodynamic properties.

In the lower temperature regime ($< 400\,°C$) there are definitely better working fluids available for the Rankine engine rather than water. These working fluids usually have high molecular weight and can provide high cycle efficiencies in less complex and less costly turbine expanders; they are categorized as *organic fluids*.

The modern interest in organic Rankine cycles is basically concern the following fields of application:

- Solar energy;

- Geothermal energy;

- Power generation for underwater, space and remote terrestrial applications;

- Bottoming or waste heat recovery; together with geothermal application, this is the most common use. In order to improve energy utilization, it can be easily combined with other thermodynamic cycles, such as thermoelectric generators, fuel cells, internal combustion engines, microturbines and so on.

The ORC is a good candidate for all of these because [17]:

1. Use of an appropriate working fluid allows the ORC to achieve high efficiency with simple few-stages turbomachinery even with moderate peak temperatures;

2. Working fluid properties frequently allow regeneration, allowing heat to be added at higher temperatures in the cycle, thereby increasing thermodynamic efficiency;

3. The moderate temperatures imply the use of conventional materials, long life, reliability and low cost.

The electrical efficiency of the ORC process generally lies between 6 and 30%.
Figure 2.1 shows a T-S diagram of the properties of water-steam together with cyclohexane and R245fa with isobars of 1, 10 and 25 bar for all three fluids. The enthalpy differences for organic substances are significantly lower compared with water; this would imply higher mass flows for the same power output [8].
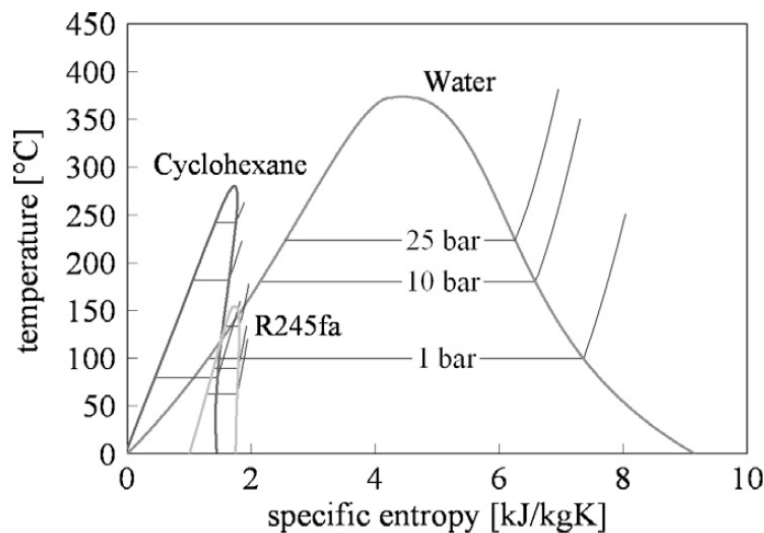
Figure 2.1.: T-S diagram of water-steam, cyclohexane and R245fa, Schuster et al. [8].

2.2 WORKING FLUID SELECTION AND CYCLE SET-UP

A detailed review of all available working fluid for ORC application is provided by Bao and Zhao [18]. The selection of the working fluid is of paramount importance with respect to the optimization of the thermodynamic cycle, the design of the expander, and other technical and nontechnical aspects. Fluid selection indeed affects all the most important design variables, and has a large influence both on system and components performance, as well as cost. Its choice is basically (but not only) determined by the particular application and the waste heat level. Because of the great variety of working condition and heat source nature, The source average temperature varies in

a huge range of possible values: from low-temperature heat source of 80 °C (namely, geothermal or solar collector [19, 20]), to high temperature of 500 °C heat source (e.g. biomass).

ORC cycles enable the use of once-trough boilers, which avoids steam drums and recirculation. This is due to the relatively smaller density difference between vapour and liquid for high molecular weight organic fluids [9].

It can be said that, from a theoretical viewpoint, all kinds of organic and inorganic fluids could be used in a ORC system.

Despite the multiplicity of the working fluid studies, no single fluid has been identified as optimal for a "generic" ORC cycle [18]. This is because:

1. The extent of fluid candidates varies;

2. Different types of heat source and working conditions lead to different optimal working fluids;

3. Different performance indicators result in different best working fluid.

To sum up, there is not a working fluid suitable for any organic Rankine cycle system. At the same time, working fluid selection should also consider other aspects apart from thermodynamic performance and system economy, such as the maximum and minimum bearable temperature and system pressure, expander design, fluid cost, toxicity, flammability, global warming potential (GWP), availability and so on.

For a general approach, from a viewpoint of thermodynamic cycle performance and turboexpander feasibility, it is desirable to employ organic fluids formed by complex molecules (large heat capacity) and with high critical temperature. Indeed, due to the positive slope of their saturation curve in the T-S diagram, the vapour expansion in the turbine is completely dry; thus, high superheating in order to avoid liquid in the exhaust vapour is not necessary any more. In addition, for each organic fluid, there is a maximum available temperature due to chemical instability problems [21]. However, high superheating of the vapour is favourable for better efficiencies[1], but this could lead to very large heat exchangers due to the low value of heat exchange coefficient [9]. If the fluid is "too dry", the expanded vapour will leave the turbine substantially "superheated", so that more heat needs to be theoretically released in the condenser.

---

1 When optimizing an ORC it is important for efficiency to reach the highest average heat addition temperature consistent with the temperature of the heat source; thus, organic working fluids that are stable at temperatures up to 500 °C are desirable [9].

A regenerator is so usually used to recycle these exhaust vapour to increase cycle efficiency. However, it is important to point out that the use of regenerative ORC is not justified for all fluids from the thermal efficiency point of view, because it can result in a limited exploitation of the main heat source, implying moreover the additional cost of one more heat exchanger. Thus, the use of a recuperator appears useful mainly when a lower limit on the exit temperature of heat source exists [19]. In this case the recuperator allows to rescue more heat, increasing the efficiency within the constraint on minimum outlet temperature of the heat source (whatever its nature, geothermal brine, exhausted gas flow etc.). However, the insertion of a recuperator always increases the system initial investment and complexity, so a trade-off process exists. The basic two configuration for ORC plants are reported in figure 2.2.
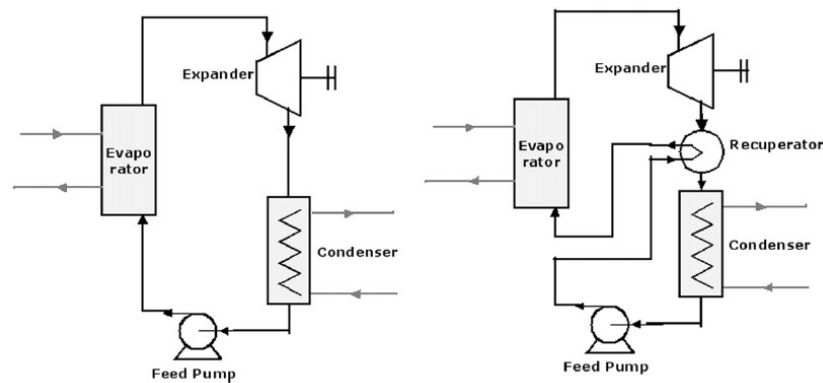
Figure 2.2.: Schematic view of an ORC with (right) and without (left) recuperator, Quoilin et al. [9].

2.3 TURBOEXPANDERS FOR ORGANIC RANKINE CYCLES

The behavior of an ORC system is strongly influenced by the performance of its expander. The most diffused choice relies on turbomachinery, both axial or radial, which still appear the most convenient solution in terms of durability and manteinence operation, even if for small-power scales various types of positive displacement machines such as piston scroll or screw expanders are also available [22]. This present work will focus only on axial-flow turbines, more appropriate for large-scale ORC units [9].

Due to the particular combination of thermodynamic and thermophysical properties, the process that leads to a final optimal geometry for an organic-fluid turbine undergoes several steps that must account for a simultaneous optimization of many geometric variables [23].

From the turbine design point of view, most of organic fluids exhibit small enthalpy drop, low speed of sound, large expansion and volumetric flow rate ratio. The contemporary occurrence of small enthalpy drop (leading to low number of stages) and high volume ratio for organic fluid yields a larger variation of volumetric flow rate per stage than those usually adopted in steam and gas turbine stages.

Fundamentals of turbomachinery theory are comprehensively discussed in Osnaghi [10] or in Saravanamuttoo et al. [24]. Here follows a brief summary of the main used parameters in the context of this present work.

2.3.1 *Turbine efficiency*

When dealing with turbine stages, it is common practice to account for two different definitions of efficiency: total-to-total and total-to-static efficiency. For a turbine, the first one is defined as follows [10]:

$$\eta_{tt} = \frac{H_{01} - H_{03}}{H_{01} - H_{03is}} \tag{2.1}$$

while the total-to-static efficiency is defined as:

$$\eta_{ts} = \frac{H_{01} - H_{03}}{H_{01} - H_{3is}} \tag{2.2}$$

where the suffix "0" indicates a total condition. The difference between these two efficiencies relies in the different way these parameters account for the outlet velocity: the first one accounts for the exit kinetic energy as a component to be still recoverable, while the second one, conversely, considers it an energy loss. Due to its definition itself, the total-to-total efficiency appears to be more suitable for the inner stages of a turbine; on the contrary, for a single-stage turbine, as well as for the last stage of multi-stage turbine, the total-to-static version seems the best alternative since no kinetic energy is recovered in a following stage.
However, when inserting a turbine in a cycle model, the total-to-total efficiency appears to be a more suitable definition since it can account also for the velocity recovery and the friction pressure loss in the diffuser [24].
Two more expressions are defined: isoentropic efficiency and polytropic efficiency.
The first one is defined as:

$$\eta_{is} = \frac{\Delta H_{13}}{\Delta H_{13,is}} \tag{2.3}$$

The second one can be defined as the isoentropic efficiency of an infinitesimal expansion: the difference between isoentropic and polytropic efficiency, is this latter one accounts for reheat occurring during fluid expansion: while passing through turbine channels and expanding, the viscous losses acts as an heating on the fluid, which leads to a dilatation and hence to both an increase of work exchanged by the stage and by the following one in a multistage machine; the difference in the two final power outputs is called reheat effect. The topic is exhaustively discussed in Beccari [25]; here it is just reported that, for an infinitesimal expansion, the two definitions lead to the same result, because the recovery work L_{rec} tends to zero. For a finite expansion, conversely, it is possible to estimate a slightly higher value of power output, due to the contribution of L_{rec}.

According to what previously reported, in this thesis work it was chosen to employ the total-to-total efficiency as the value to maximize in the turbine-design optimization process.

2.3.2 Velocity triangles
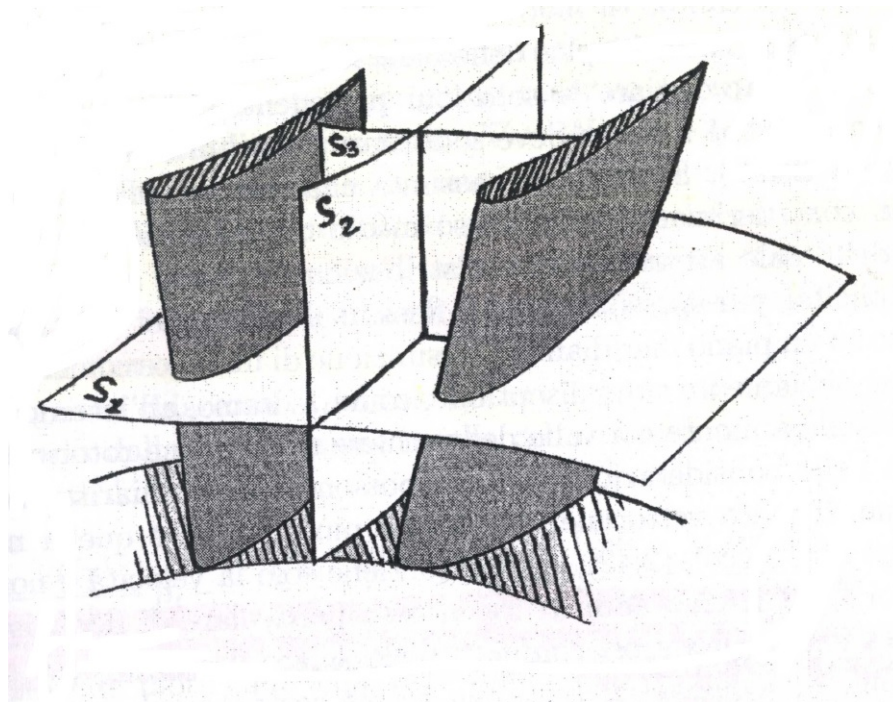
Figure 2.3.: Sketch of the three conventional surfaces in turbomachinery study, Osnaghi [10].

Fluid flow in turbomachinery is usually analysed by means of three conventional surfaces (see fig. 2.3):

- Blade-to-blade surface (S1 area in figure 2.3): this is the surface of the main flux;

- Meridian surface (S2 area in figure 2.3): useful to visualize flow variations along the radial direction;

- Secondary surface (S3 area in figure 2.3): due to the fact that in turbomachinery channels flow is not directionally uniform, its projection on this surface is not in general null, and it is conventionally named *secondary flux*.

The work exchanged between fluid and rotor blades is evaluated by means of velocity triangles, which are a graphical vectorial representation of fluid velocity at the inlet and outlet rotor sections. In this scheme, the absolute rotor inlet and outlet fluid velocities C_2 and C_3 are expressed as the vectorial sum of the blades relative fluid velocities W_2 and W_3 and the peripheral rotor blades velocity U_2 and U_3, where:

$$U_i = \omega \cdot r_i \tag{2.4}$$
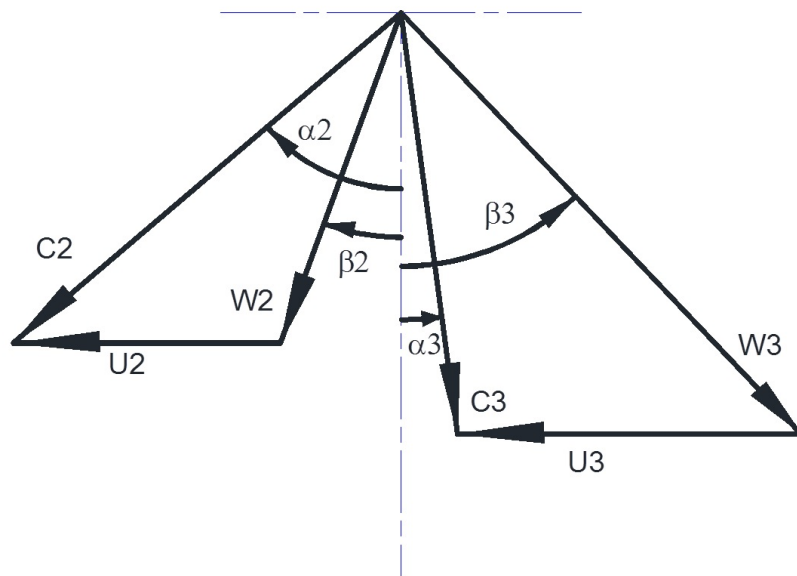
Figure 2.4.: Sample velocity triangles with fluid angles.

Figure 2.4 shows a sample scheme of velocity triangles with relative fluid angles. In this present work fluid angles will be always measured from axial direction with the sign convention adopted in figure 2.4.; absolute fluid angles will be named with letter α, relative fluid angles with β and blade angles with letter θ. The difference between inlet fluid angle and blade angle is called *incidence angle*.
Fluid angles play a key role in axial turbomachinery, being the work at blades due to fluid deflection given by blade shape.
    It should be observed that the shape of velocity triangles varies along blade height because the peripheral velocity U, by

its definition, is a function of radius. For this reason, it is common practice in turbomachinery to design on conditions at the average radius and then twist the blades in order to account for this phenomenon [24].

2.3.3 *Eulerian work*

The eulerian work represents the work per unit mass exchanged between fluid and rotor blades and it is defined as [24]:

$$ł_u = U_2 C_2 \sin \alpha_2 + U_1 C_1 \sin \alpha_1 \tag{2.5}$$

Where in this case suffixes 1 and 2 are for inlet and outlet rotor section respectively and angles are measured from the axial direction.

It is worth noting that l_u may or may not coincide with a total enthalpy drop ΔH_{tot}, being this latter therm a function of the chosen control volume [10]: if section 1 and 2 coincide with the inlet and outlet of the *blades* is possible to state:

$$ł_u = \Delta H_{tot,1-2} \tag{2.6}$$

If, on the contrary, 1 and 2 coincide with the inlet and outlet section of the *machine*, the two expressions are not equal any more, essentially due to disk friction losses (see section 2.3.6).

2.3.4 *Degree of reaction*

The degree of reaction, defined as [25]:

$$\chi = \frac{H_2 - H_3}{H_1 - H_3} \tag{2.7}$$

It is a measure of the fraction of the enthalpy drop that takes place in the rotor with respect to the overall enthalpy drop. The degree of reaction is theoretically always comprised between 0 and 1 but in some real situations it is possible to have $\chi < 0$ or $\chi > 1$ [10]. A turbine characterized by a zero value of reaction degree is called impulse turbine, while a reaction turbine has typically $\chi = 0.5$.

Figures 2.5 and 2.6 show the velocity triangles for these two conventional configurations.

According to Macchi [23], both typical impulse and 50% reaction stages are not attractive for organic fluids: the first ones would exhibit supersonic relative inlet velocity for values of volumetric flow ratio larger than five, the latter ones would require prohibitive blade height variations.
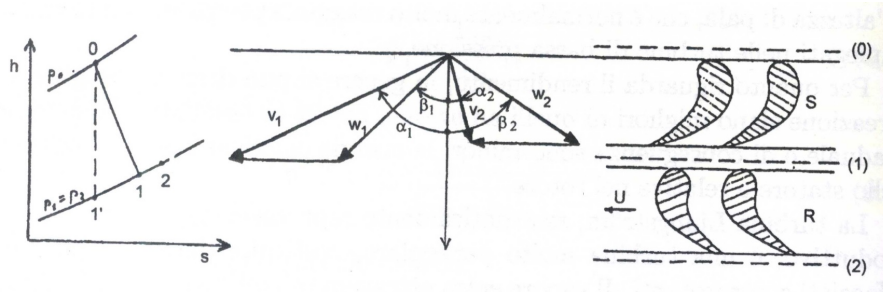
Figure 2.5.: Impulse sample velocity triangles with enthalpy drop and blade shape, Osnaghi [10].
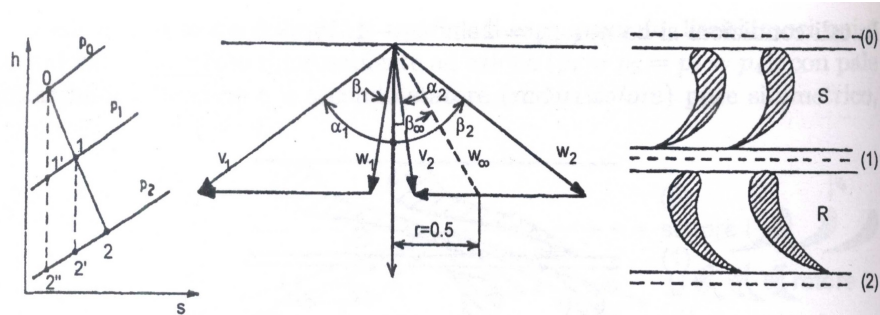
Figure 2.6.: 50%-reaction degree sample velocity triangles with enthalpy drop and blade shape, Osnaghi [10].

As it will be discussed, axial-flow turbines for ORC applications are characterized by values of reaction degree usually comprised within the range $0.1 - 0.45$; these values allow to obtain a compromise between excessive relative Mach numbers (which problem impulse stages are affected by) and prohibitive blade height variations (a problem that would arise, as written above, for a 50% reaction stage turbine).

2.3.5 Mach number

The Mach number is a useful parameter, commonly used to evaluate the "sonic" condition of the fluid; it is defined as the ratio between a fluid velocity (absolute or relative) and the local speed of sound:

$$M = \frac{C}{Z} \tag{2.8}$$

$$M_W = \frac{W}{Z} \tag{2.9}$$

where C and W are the absolute and relative fluid velocity at a point and is the speed of sound at the same point. The speed of sound Z is defined as [26]:

$$Z = \sqrt{\left(\frac{\partial P}{\partial \rho}\right)_{is}} \tag{2.10}$$

if $M < 1$, the velocity of the fluid is lesser than the speed of sound and the flow is said subsonic, by definition.
If $M > 1$ the flow is supersonic. Depending on the Mach number level different design concepts and different correlations must be used.

2.3.6 *Turbine losses*

In turbomachinery theory the losses evaluation procedure is not unified but every method accounts for the following physical phenomena:

- Profile (or primary) losses: the main purpose of blades in turbomachinery is to deflect the flux in the tangential direction in order to obtain a useful torque at shaft. Losses are mainly linked to fluid deflection in the blade-to-blade surface; profile losses result from the boundary layer growth on the surface of the profile and from the accompanying friction and blockage effects. Moreover, the finite thickness of the trailing edge leads to mixing wakes and recirculating vortexes, so an optimal distance between two following blade channels exists [10]. From a dimensionless analysis, a representative parameter of this phenomena is the chord/pitch ratio b/s, also defined as solidity σ: for very low values of this parameter the deflection imposed on the fluid takes place in a too short length, with risk of flow detachment; conversely, when this parameter is too high the blade chord is too long with excessive friction losses.

- Secondary losses: they are basically due to energy transfer from blade-to-blade surface to secondary surface; this is mainly the consequence of the turning of the spanwise velocity gradients near the endwalls. The secondary flows are perpendicular to the main flow direction and have a very complex character. These losses are the most difficult to describe because of their highly 3-D configuration and interconnection of the singles phenomena that occur in secondary surface. These losses have an increasing relative influence when the blade height decreases with respect to blade channel section. This effect is more significant in rotors [25], where also tip clearance losses[2] must be accounted for.

---

2 Leakage of mass flow rate at tip, separated from the main flow due to the rotation of the rotor that induces pressure difference between pressure and suction surface of the blade.

- Three-dimensional effects: as already observed, the shape of velocity triangles varies along blade height because the peripheral velocity U is a function of radius. Due to this variation, flow configuration varies along blade height. 3-D effects introduces weak specific loss mechanisms (such as the effects of flaring), but the variation of velocity triangles can significantly increase the incidence angle, with a subsequent increment in profile losses. The influence of 3-D effect is quite complex and is also dependent on blade design. From a dimensionless point of view, the most representative parameter is the blade height/average diameter ratio h/D_m [23]: for high values of this parameter, typical of last stages in steam turbines [24], these effects can introduce significant losses, so blades are usually twisted to account for variation of blade angles along the radial coordinate.

It is common practice in turbomachinery to account for losses by means of subtractive coefficients that reduce the efficiency. In the present thesis work, the loss coefficients X_i are predicted by making use of Craig and Cox method [4], that appears to be the most suitable and complete loss evaluation process for the purpose of this work [22, 23, 27, 28]. In this section the main concepts of this methodology are summarized (for further details see Craig and Cox [4]).

The total amount of losses that occur in a axial-flow turbine is divided into two groups, listed in table 2.1.

Table 2.1.: List of turbine losses according to Craig and Cox method, Craig and Cox [4].

Group 1	Group 2
Nozzle profile loss	Nozzle gland leakage loss
Rotor profile loss	Rotor tip clearance loss
Nozzle secondary loss	Wetness loss
Rotor secondary loss	Lacing wire loss
Nozzle annulus loss (lap and cavity)	Partial admission loss
Rotor annulus loss (lap, cavity and annulus)	Disc windage loss

The total-to-total efficiency is defined as:

$$\eta_{tt} = \frac{l_u}{l_u + \sum (\text{group 1 losses})}$$
$$- \sum (\text{group 2 efficiency debits}) \quad (2.11)$$

This approach basically relies on the fact that the work at blades is obtained by the change in tangential momentum, but the energy released by the fluid is even more, due to the friction on blade profiles and blade wakes (profile losses), friction on walls at tip and hub and other secondary phenomena, losses due to sudden enlargements in fluid path or wall cavities (annulus losses). Losses of group 2, contrarily, account for the fact that not all the fluid passes through rotor blades, because of leakage through diaphragms glands and tip clearances. In addition, partial admission, windage and bearing losses reduce even more the final work at shaft. This second group can be more easily treated as a an efficiency debt to be subtracted to a "blade efficiency", that accounts only for both nozzle and rotor profile together with secondary losses[3].

---

3 It could be said that group 1 losses only account for flow channel losses, without being concern with mass flow leakage or any other loss external to blade channel.

METHODOLOGY

In this chapter a description of the case of study is given and the adopted methodology and used models are described.

3.1 CASE OF STUDY: THE DRAUGEN OFFSHORE PLATFORM

The Draugen oil field is located in the North Sea, situated approximately 150 km north of Kristiansund in Norway, 200 Km far from the Arctic Circle. The Draugen oil field is operated by Norske Shell, which also owns a 26.2% stake in the field. The remaining stake is held by Petoro (47.88%), BP Norge (18.36%) and Chevron (7.56%). The field was shut down in February 2010 due to cold weather and extreme winds. Shell is yet to resume operations at the facility [11]. The Garn West reservoir is connected to the Draugen platform by a 3.3 km-long pipeline. The pipeline laid via the Garn West reservoir connects the Rogn deposit to the project platform. While the oil extracted from the field is transferred to a floating loading buoy, the associated gas is transported to processing plant at Karsto by means of the Asgard Transport pipeline.

Figure 3.1.: Draugen field location, Offshore Technology [11].

The energy requirement of the platform (normal and peak load) is supplied by three Siemens SGT-500 gas turbines. The Siemens SGT-500 industrial gas turbine is a light-weight, high-efficiency, heavy duty gas turbine in the 15 *MW* to 20 *MW*

Image courtesy of Heine Schjølberg

Figure 3.2.: The Draugen offshore platform, Offshore Technology
[11]

power range. The special design features and the fuel flexibility for lower cost fuels of the gas turbine make it suitable for economical base-load power generation. In order to ensure high reliability, a relatively low TIT (850 °C) and turbine outlet temperature (350-450 °C) are utilized [5]; The design point specifications are reported in table 3.1.

The low and high pressure axial compressors are mechanically coupled by two distinct shafts with the low and high pressure turbines, while the power turbine drives the electric generator. In the Draugen platform, three SGT-500 gas turbines are installed, providing the normal and peak load energy supply. Two of them share 50% of the load while the other is on standby for maintenance periods. This present work will only focus on the single gas turbine without considering the overall system in the platform; only in one case the second gas turbine will be included in the plant scheme.
The fuel is assumed to be natural gas. However, it should be noted the SGT-500 gas turbine can be fed with a wide range of both liquid and gas fuels; in case other fuels (crude oil, heavy fuel oil and naphtha) rather than natural gas are combusted, the exit-gas limit temperature is fixed to 145 °C to prevent the condensation of corrosive compounds [29].

According to Pierobon et al. [7], the installation of the waste heat recovery unit would bring two major sources of revenue: the first, associated with fuel saving, which can be so exported and sold to the market; the second, related to the reduction of carbon tax amount due to the combustion on natural gas: in fact, since 1991, Norway imposes carbon tax on oil, mineral

Table 3.1.: Design point specifications for Siemens SGT-500 [5]

Low pressure compressor stages	10
High pressure compressor stages	8
Low pressure turbine stages	1
High pressure turbine stages	2
Power turbine stages	3
Turbine inlet temperature (TIT)	850 °C
Exhaust gas temperature	376 °C
Exhaust gas mass flow	93.5 kg/s
Net power output	17.014 MW
Heat rate	11312 kJ/kWh
Fuel	Naphta, crude oil, heavy fuel oil, bio oil, natural gas, syngas

fuel and natural gas with rates based on fuels carbon content [30]. Thus, the new method would reduce the carbon tax cost associated with the release of CO_2 due to combustion of natural gas.

3.2 GENERAL OVERVIEW OF TURBINE DESIGN CODE

In this section a description of the used single-stage turbine-design code is given. For a more exhaustive and detailed discussion see Gabrielli [12].

As previously anticipated, the whole turbine design process relies on a set of eight parameters, together with some other requirements. These input variables are listed in table 3.2.

Figure 3.3 reports two blades with the main geometric parameters and relative nomenclature that will be used in this work.

In addition to the ones listed in table 3.2, some other values, such as the surface roughness and trailing edge thickness must be given in input. However, these numbers have been chosen to be consistent with the best available technology and are kept constant during the whole work[1]. A complete list of all the input requirements is reported in table B.1 in appendix B.

---

[1] The value of Mach number that makes nozzle geometry switch from convergent to convergent-divergent is set to 1.4, in accordance to Osnaghi [10]. A turbulent flow configuration ($Re \geqslant 10^6$) is also always assumed.

The rotor inlet/nozzle outlet blade height ratio hhh has been set to one to ensure the minimum annulus loss for controlled expansion, according to Craig and Cox' figure 19 reported in appendix B [4].

Table 3.2.: List of Turbine input parameters and boundary conditions

Description	Unit	parameter
Turbine optimizing variables		
absolute nozzle inlet fluid angle	°	α_1
$\Delta H_{tot}/(u_m^2/2)$	-	ψ
Nozzle throat section	m	$(o_{min})_n$
Rotor throat section	m	o_r
Nozzle axial chord	m	c_n
Rotor axial chord	m	c_r
Nozzle outlet section/nozzle pitch	-	$(o/s)_n$
Rotor outlet section/rotor pitch	-	$(o/s)_r$
Thermodynamic requirements		
Mass flow rate	kg/s	m
Total inlet pressure	bar	P_{01}
Total outlet pressure	bar	P_{03}
Rotational speed	rpm	N
Total inlet temperature	K	T_{01}
Fluid type	-	fluid
Fixd inputs		
Mach number for conv.-div. Nozzle	-	Mcd
Reynolds number	-	Re
Nozzle outlet/rotor inlet height ratio	-	hhh

For a given set of input parameters listed in table 3.2, the code returns an output value of total-to-total efficiency. If this model is coupled with an optimization algorithm, for a given fluid and a given set of mass flow rate, inlet/outlet total pressure ratio and rotational speed[2], it is possible to obtain the best set of eight design parameters that lead to the highest turbine efficiency.

---

2 As already mentioned, the rotational speed N is kept constant in the first part of the work, whilst in the second part it is included into the optimizing set of variables.
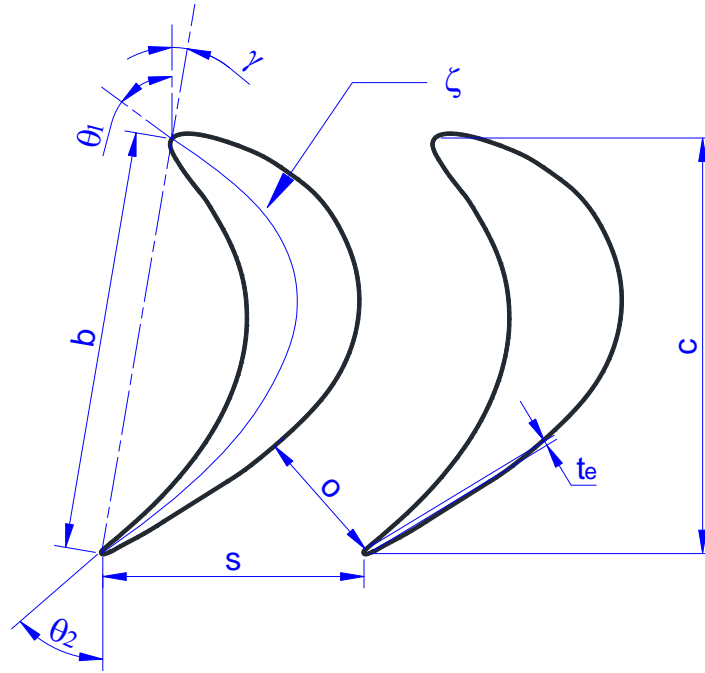
Figure 3.3.: Main geometric blade parameters with relative nomenclature. The subscripts 1 and 2 in this figure are purely illustrative.

3.3 CODE DESCRIPTION

Implementing the procedure that will be now discussed, the used design algorithm provides the final geometry and efficiency for a single-stage axial flow turbine with the assumption of constant axial velocity component and constant average radius; Thus, it will be always assumed (unless otherwise specified):

$$C_{a1} = C_{a2} = C_{a3} \tag{3.1}$$

It is possible to obtain a non-constant axial velocity configuration, but two more parameters are required in input: the inlet axial velocity component C_{a1} and the rotor coefficient ϕ_r[3], defined as:

$$\phi_r = \frac{C_{a3}}{U_m} \tag{3.2}$$

This variant has been adopted in Chapter 4 during the validation process.

Rotor blades are always convergent, while the shape of stator blades can switch from convergent to convergent-divergent. For this reason, the parameter o_{min} and the therm "o" in $(o/s)_n$ coincide only for convergent nozzle blades.

A sketch of the turbine geometry provided by the code is given in figure 3.4.

---

3 The nozzle coefficient ϕ_n is evaluated inside the process.
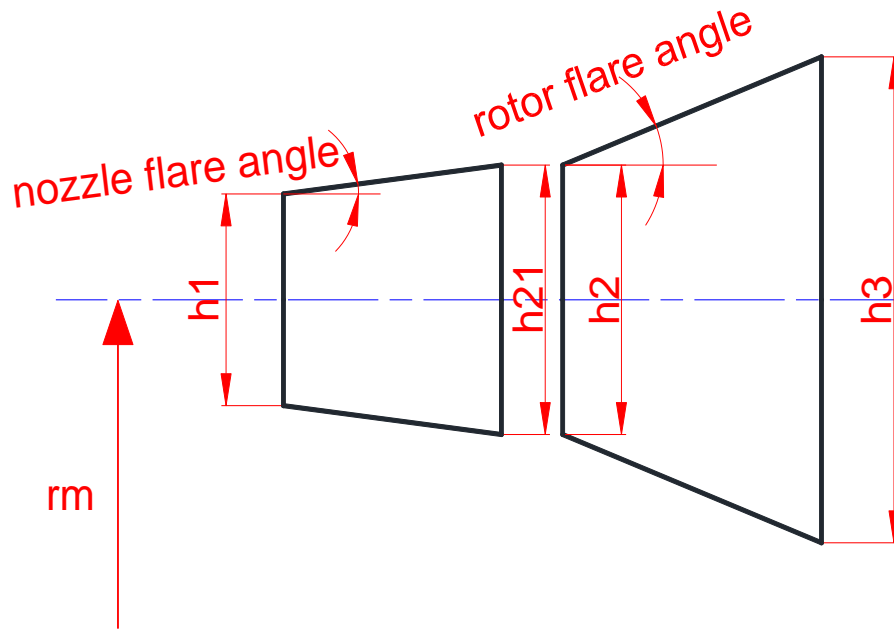
Figure 3.4.: Turbine geometry provided by the code. The values of flare angles are purely illustrative.

With the purpose of inserting the turbine model in a more complex scheme and reducing the required computational time, this code only considers flow at average radius, without accounting for any variation of peripheral velocity in radial direction nor blade twisting. However, ORC turbines are usually characterized by moderate blade height with a small degree of twisting (if present); in addition, several constraints have been put on geometry to contain this problem.

The main structure of the code is essentially composed by three parts:

1. Evaluation of all total inlet thermodynamic variables and total outlet isoentropic properties; this allows to calculate the total isoentropic enthalpy drop. All these values remain constant during the design process;

2. Calculation of a set of first guess values for fluid angles, velocities and thermodynamic properties to be used in the next step;

3. Iterative loop: starting with the provided first guess values, an iterative cycle runs until convergence is reached. The final result can then be displayed.

Here follows a more detailed description of these last two steps.

3.3.1 *First guess values calculation*

This part of the code simply aims at obtaining an approximated set of values for fluid angles, velocities and thermodynamic properties, that will be subsequently updated in the iterative loop. Providing a first guess value for η_{tt}, it is possible to obtain a first guess value for the work per unit mass and then, from ψ, the velocity U. By assuming fluid flow angles coincident with blade angles, α_2 and β_3 are evaluated by the following expressions:

$$\alpha_2 = \arccos \left(\frac{o}{s} \right)_n \tag{3.3}$$

$$\beta_3 = \arccos \left(\frac{o}{s} \right)_r \tag{3.4}$$

The remaining velocities are obtained by trigonometric relations achievable from velocity triangles [12, 24].

With the first guess values for all the kinematic variables it is now possible to start a subroutine that provides a set of first guess values for thermodynamic properties. The detailed description of this process is provided by Gabrielli [12] and is not reported here, being quite complex, cumbersome and not useful for the general understanding of code structure.

3.3.2 *Iterative loop*

The iterative loop is composed by the following steps:

1. Calculation of nozzle blade opening with Deich formula [31]: if the flow is supersonic, this step allows to switch to a converging-diverging shape of nozzle blades;

2. Blades and fluid angles evaluation: θ_{21} and θ_3 are obtained by means of the following expressions:

$$\theta_{21} = \arccos \left(\frac{o}{s} \right)_n \tag{3.5}$$

and

$$\theta_3 = \arccos \left(\frac{o}{s} \right)_r \tag{3.6}$$

for a subsonic case, fluid angles are calculated with Ainley and Mathieson correlation [32], whereas the Vavra correlation is used for supersonic cases [33];

3. Updating velocity calculation with fluid angles;

4. Thermodynamic properties and Mach numbers estimation;

5. Turbine geometry calculation (flare angles, blade height) by means of continuity equation;

6. Updating Mach numbers with Kacker-Okapuu correlation [34] to improve Craig and Cox method for supersonic flow;

7. Losses estimation procedure with Craig and Cox method [4];

8. calculation of total-to-total turbine efficiency;

9. Calculation of the difference with respect to the previous iteration and update of values to start the loop again.

The iterative loop stops when the difference between the new obtained efficiency and the one calculated in the preceding iterations goes below a given tolerance, set at 10^{-4}.

3.3.3 *Optimization process*

For a given fluid, mass flow rate, total inlet temperature and pressure ratio, it is possible to include the turbine code into a more complex function in order to obtain the best geometric configuration that produces the highest efficiency. It is possible to fulfil this goal by coupling the turbine code with an optimization algorithm, called "genetic algorithm". A comprehensive description of this process is provided by Obitko [35]; a general overview is given in appendix A. Here it is only reported that, providing a set of upper and lower bound values for each parameter to be optimized, the algorithm looks for the best combination of optimizing parameters that maximizes (or minimizes) a certain function.
The general syntax has the following expression:

$$[OP] = f(f_{opt}, [LB], [UB], GA_{options}) \tag{3.7}$$

where:

- f_{opt} is the function to be optimized;

- $[OP]$ is the set of optimizing parameters that maximizes or minimizes a certain function f_{opt};

- $[LB]$ and $[UB]$ are the lower and upper bound arrays of values;

- $GA_{options}$ is the set of required options necessary to the genetic algorithm (see appendix A)

3.3.4 *Constraints on the solution*

To provide acceptable solutions both for a physical and technological prospective, some constraints on geometry and thermodynamics have to be given. This basically turns into an upper and lower bound for the optimizing variables, listed in table 3.3 and in some other constraints to be respected by the obtained solutions, provided in table 3.4; these conditions have substantially been established by Macchi and Perdichizzi [27].

Table 3.3.: List of upper and lower bound for the nine turbine design parameters to be optimized.

Parameter	Lower bound	Upper bound	Unit
α_1	-15	15	°
ψ	2	6	—
$(o_{min})_n$	0.002	0.1	m
o_r	0.002	0.1	m
c_n	0.01	0.1	m
c_r	0.01	0.1	m
$(o/s)_n$	0.224	0.7	—
$(o/s)_r$	0.224	0.7	—
N (if optimized)	2000	12000	rpm

Table 3.4.: Other constraints on turbine geometry.

Parameter	Lower bound	Upper bound	Unit
M_{W2}	0	0.8	—
M_{W3}	0	1.4	—
z_n	10	100	—
z_r	10	100	—
FL_n	-25	25	°
FL_r	-25	25	°
h_i/D_m	0.001	0.25	—
c_i/D_m	0	0.2	—

Some comments are necessary:

- Rotor inlet relative Mach number M_{W2} is limited to subsonic values to avoid unique incidence configuration and to ensure the validity of loss correlation [4]; outlet relative Mach number M_{W3} is limited due to the hypothesis

of the assumed converging shape of rotor blades; the restriction on Mach number, however, goes in the direction of the best efficiency, because supersonic inlet velocities with high fluid deflection yield high losses [23].

• Flare angles are limited to ensure a limited influence of radial effects and restrain the efficiency reduction in off-design conditions;

• h/D_m is limited to restrain the three-dimensional effects, related to peripheral velocity variation with blade height (whose influence this model does not account for).

• The limits on axial chords, throat and opening sections, as well as the number of blades, are due to technological reasons [23].

• The limit on $(o/s)_n$ and $(o/s)_r$ is due to contain the maximum deflection $\Delta\alpha$ and $\Delta\beta$. Excessive values of fluid deflection increase the aerodynamic lift per blade and can lead to fluid flow detachment [27];

• The upper and lower bound for ψ are not "limiting" it: from a preliminary set of optimization results it was seen that optimal values for this coefficient are always comprised between 2.5 and 5. The given upper and lower bounds allow the algorithm find the best value being certain it is within the given range.

3.4 INFLUENCE ANALYSIS OF OPTIMIZING VARIABLES

Here follows a more comprehensive description of the influence and effect each design parameter has on the final output. All the optimizing parameters have a certain influence, even though three of them have a more relevant role compared to the others. The following charts have been obtained with a sample set of optimizing parameters, mass flow rate and inlet turbine temperature (see table B.3 in appendix B) and choosing cyclopentane as test fluid.

The design parameters were made vary in pairs of two within the correspondent upper and lower bound values[4], keeping all the other input values constant. The effect of each couple of parameters has been evaluated in charts showing the variation of

---

4 It is necessary to note that, even though each design parameter has his own upper and lower bound, it is not possible to make one (or two) parameter(s) vary within its/their whole possible range keeping all the other values constant. Indeed, for a given fluid, inlet turbine temperature, pressure ratio and mass flow rate, not all the possible combinations of design parameters are acceptable, even with larger constraints.

efficiency and, where relevant, degree of reaction, as a function of the examined couple of values.

It is of paramount importance to note that not all the solution plotted in the following figures are necessarily acceptable, that is, not all of them respect all the constraints given in table 3.3; in order to have a "continuous" solution and understandable trend to be plotted, even in a bounded range of values, just for the purpose of this description, the constraints on flare angles have been enlarged to allow solutions with flare openings up to 40°, the constraint on number of blades has been removed and the limits on Mach numbers have been enlarged.

Here follows a more detailed discussion on each couple of parameters:

3.4.1 *stage load coefficient ψ and absolute turbine inlet angle α_1*

The dimensionless coefficient ψ is defined, as already stated, as:

$$\psi = \frac{\Delta H_{tot}}{U_m^2/2} \tag{3.8}$$

It is one of the three most influencing parameter in the overall turbine design process and its variation significantly affects the efficiency and the shape of velocity triangles.
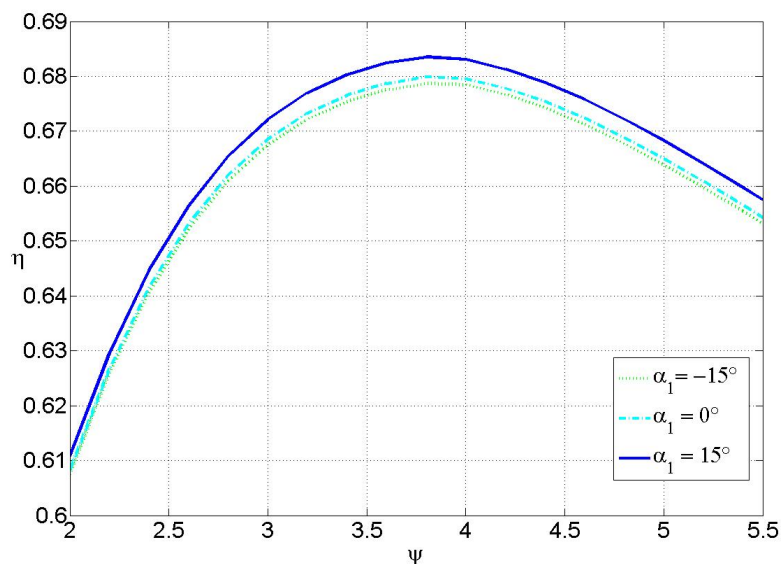
Figure 3.5.: Efficiency variation as a function of ψ for several values of α_1.

The charts in figures 3.5, 3.6 and 3.7 show the variation of efficiency, degree of reaction and average radius as a function of ψ for several values of α_1, whereas figure 3.8 shows the different shape of velocity triangles for two sample values of ψ.
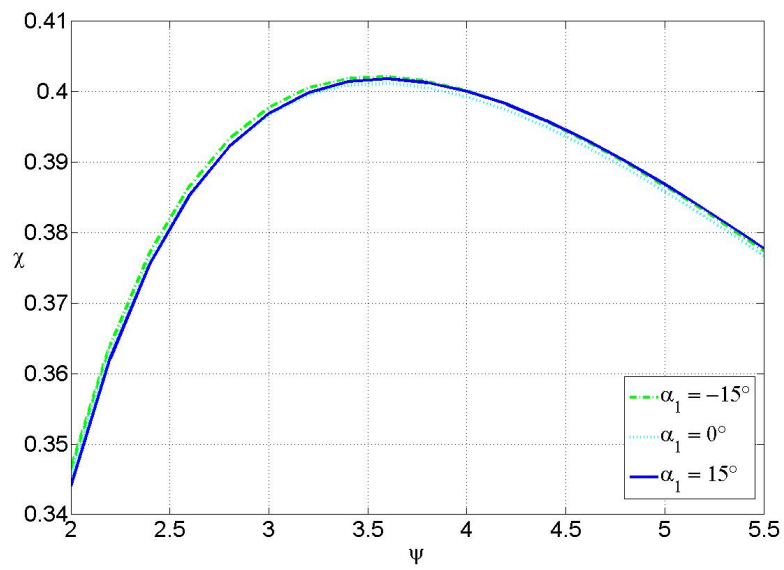
Figure 3.6.: Variation of reaction degree as a function of ψ for several values of α_1.
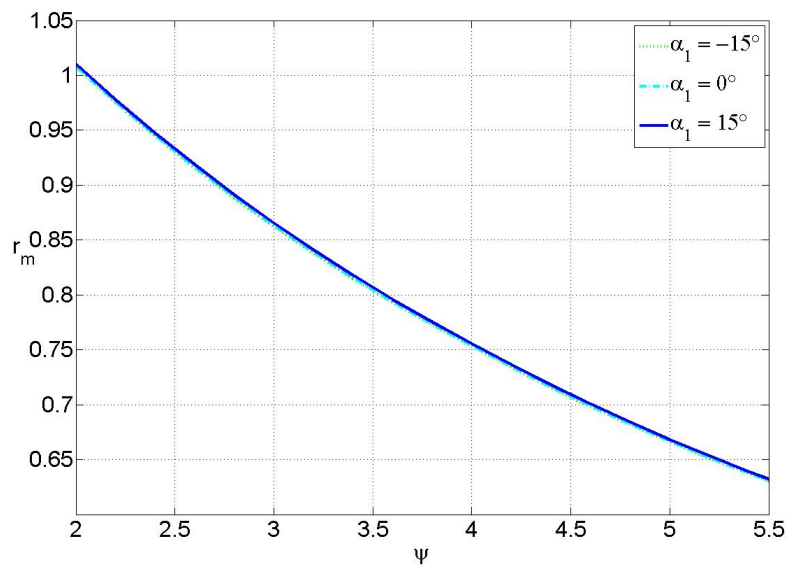
Figure 3.7.: Variation of average radius as a function of ψ for several values of α_1.
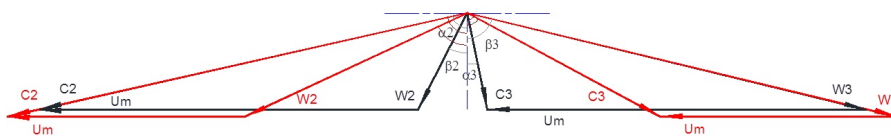
Figure 3.8.: velocity triangles for $\psi = 2$ (black) and $\psi = 5.5$ (red).

Keeping in mind that $U_m = \omega \cdot r_m$, to increase ψ keeping all the other values constant means to increase ΔH_{tot} or to decrease U_m (and so r_m, for a given rotational speed). For given constant values of $(o/s)_n$ and $(o/s)_r$ (so for constant values of θ_{21} and θ_3), the stage is more "loaded" with progressively decreasing values of r_m[5] and velocity triangles tend to "open". About α_1, figure 3.5 shows its influence is within the increment of 1% in efficiency. However, for a general-purpose study this parameter has been considered among the optimizing ones[6].

3.4.2   Throat section/pitch ratio for stator and rotor $(o/s)_n$ and $(o/s)_r$

Together with the stage loading coefficient ψ, these geometric ratios are the most influential design parameters in terms of blade shape and velocity triangles among the eight ones.
Their importance is due to the direct influence those ratios have on blade shape by means of formulas 3.5 and 3.6; Remembering that blade and flow angles are measured from the axial direction, according to these expressions, to increase $(o/s)_n$ or $(o/s)_r$ means to decrease the geometric blade outlet angle θ_2 or θ_3 and so consequentially the fluid exit angles α_2 and β_3.
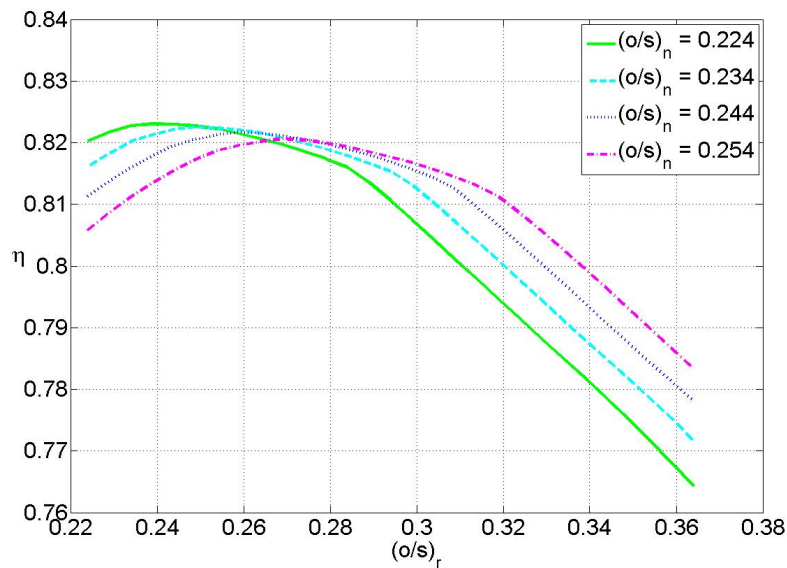
Figure 3.9.: Variation of efficiency as a function of $(o/s)_r$ for several values of $(o/s)_n$.

Figures 3.9 and 3.10 show the influence of $(o/s)_n$ and $(o/s)_r$ on efficiency and reaction degree, while figures 3.11 and 3.12 show different shapes of velocity triangles as a function of sev-

---

5 which cause blade height and so the ratio h/D_m to increase proportionally.
6 It should be noted the practical deflection of the gas at turbine inlet requires an IGV (inlet guide vane), thus adding a small technological complication.
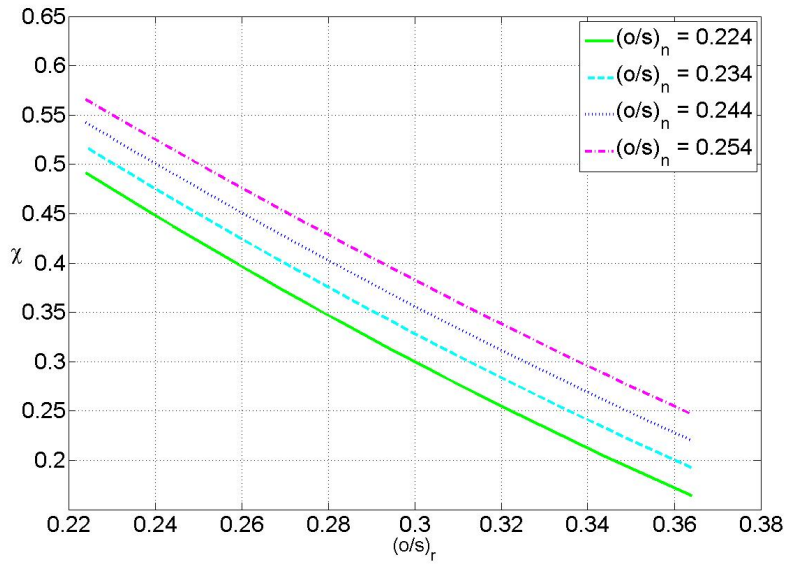
Figure 3.10.: Variation of reaction degree as a function of $(o/s)_r$ for several values of $(o/s)_n$
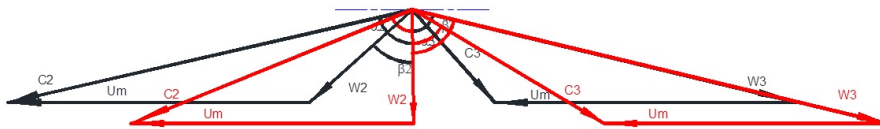
Figure 3.11.: Different velocity triangles for a constant value of $(o/s)_r$=0.238 with $(o/s)_n$=0.224 (black) and $(o/s)_n$=0.374 (red).
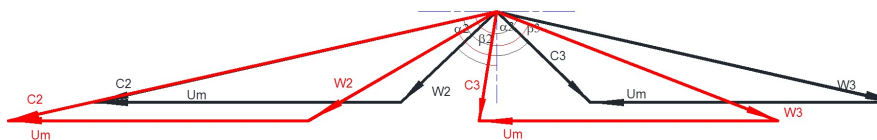
Figure 3.12.: Different velocity triangles for a constant value of $(o/s)_n$=0.224 with $(o/s)_r$=0.224 (black) and $(o/s)_r$=0.364 (red).

eral combinations of $(o/s)_n$ and $(o/s)_r$. As written above, an increase of $(o/s)_n$ causes θ_2 and so α_2 to decrease, as shown in figure 3.11. This basically means that the fluid is less deflected and/or expanded in the nozzle, which causes the degree of reaction to increase.

For the same reason, in figure 3.12, an increase of $(o/s)_r$ causes θ_3 and so β_3 to decrease, and that means the fluid is, in proportion, less deflected and/or expanded in the rotor: this causes a reduction in reaction degree. This is confirmed by the trends in figure 3.10, where the degree of reaction χ decreases for increasing values of $(o/s)_r$. This chart also shows the influence of $(o/s)_n$ that induces the opposite effect: indeed, for a fixed value of $(o/s)_r$, the higher $(o/s)_n$, the higher the reaction degree.

3.4.3 Throat sections $(o_{min})_n$, o_r and axial chords c_n, c_r

The remaining parameters whose influence has not been analysed yet play a somehow different role in the whole turbine design and optimization process. Figures 3.13 and 3.14 show the effect of these parameters on efficiency.
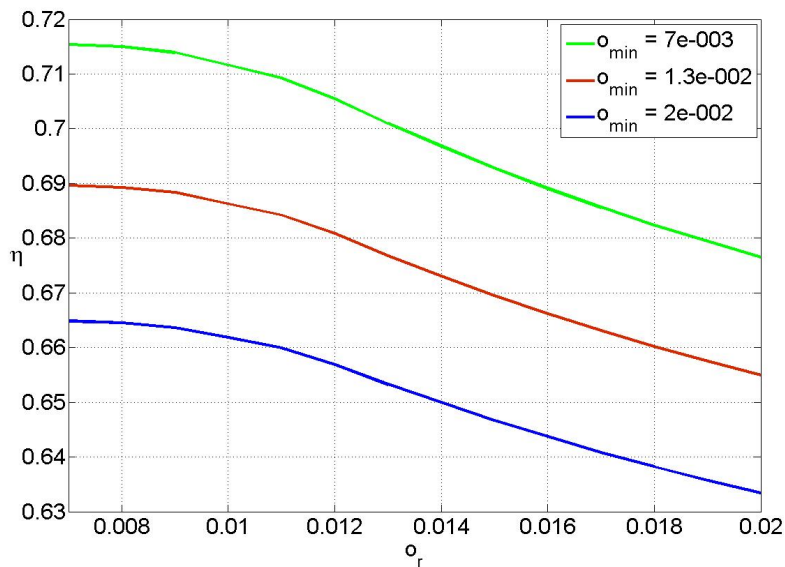
Figure 3.13.: Efficiency variation as a function of o_r for several values of nozzle throat section.

The values of throat sections and axial chords do not modify directly the shape of velocity triangles, but the effect of their variation is considered inside the code while estimating all the remaining geometric variables, most of whom are successively received as an input in the losses evaluation procedure: for example, the values of o_n and o_r are used to evaluate nozzle and rotor pitch (and so the number of blades in stator and rotor)
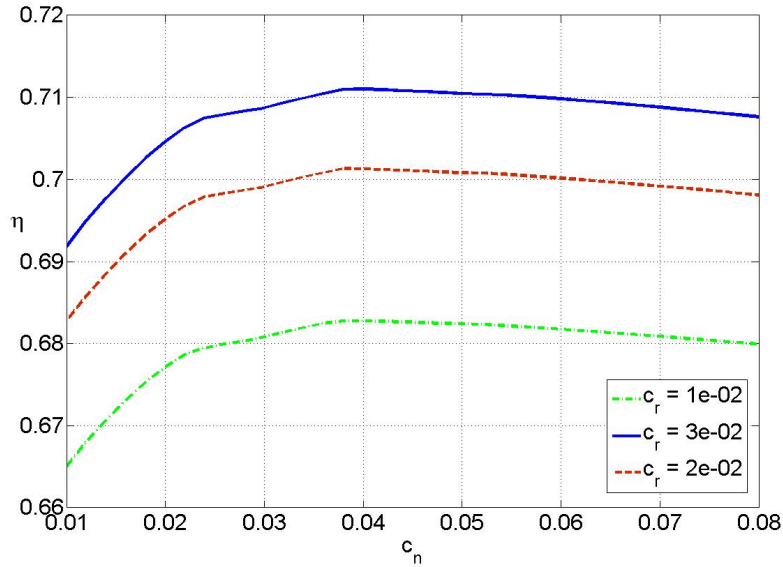
Figure 3.14.: efficiency variation as a function of c_n for several values of c_r.

whereas c_n and c_r are used to evaluate the flare angles and the backbone length ζ, a necessary parameter in the losses evaluation procedure [4].
Their contribution in the overall turbine design process resides in the need itself to make these very parameters change simultaneously with ψ, $(o/s)_n$ and $(o/s)_r$ to obtain an acceptable final solution, that is, a turbine design configuration respecting all the constraints listed in table 3.3 and 3.4.

So, as already discussed, it is not generally possible to vary arbitrarily one or two parameters keeping all the other constant. Indeed the optimization of turbine geometry is a highly non-linear process that must account for the simultaneous variation of all the eight optimizing parameters.
The stage load coefficient ψ, together with parameters $(o/s)_n$ and $(o/s)_r$ dictate the shape of velocity triangles but they need a correspondent variation of throat sections and axial chords to respect all the constraints and produce a feasible solution.

3.5 TURBINE MAP

The required computational time for a single optimization process ranges between four hours and five days[7], depending on the number of optimizing parameters, their upper and lower bound, population size, number of generations and, finally, the occurrence of potential numerical instability in the algorithm

---

7 This happens only in the case where the rotational speed is optimized and numerical instability occurs.

(see section 5.5 and appendix A). The insertion in a complete cycle model would imply the addition of at least two more cycle variables to be optimized (evaporation pressure and turbine inlet temperature), with a further increase in computational time. It also should be considered that, when optimizing a thermodynamic cycle, one is initially more interested in knowing the best efficiency achievable for an expander with certain inlet conditions than knowing its complete geometry. Moreover, as it will be discussed in section 3.6.2, the creation of a map allows to obtain the convergence in the iterative loop of internal recuperator. Thus, it was chosen to optimize expander geometry separately and subsequently integrate the obtained map into the cycle.
For a single fluid, turbine inlet temperature and rotational speed, many optimizations have been performed to plot turbine efficiency as a function of mass flow rate and inlet/outlet pressure ratio; The mass flow rate was varied between 10 and 200 kg/s, with a variation of pressure ratio between 5 and 44. The results are reported and discussed in chapter 5.
In the complete cycle model, the map is embed into a function to return turbine efficiency as follows:

$$\eta_{tt} = f(\dot{m}, P_r) \qquad (3.9)$$

Whenever the values of mass flow rate and pressure ratio are not directly provided in the map, this function interpolates linearly between the two closest values of these variables.

3.6 CYCLE MODEL

For the given case of study, an organic Rankine bottoming cycle model has been set up. The structure of the cycle with the nomenclature that will be used is reported in figure 3.15, while a complete list of cycle input requirements is reported in table B.2 in appendix B. Fluid properties will be referred to with subscript from 1 to 8, while gas temperature will be indicated with subscript from A to D.
For a simpler approach that does not affect the structure of the problem, no pressure losses have been taken into account throughout the cycle; the exhausted gas have been considered as ideal with constant specific heat, which allows to write:

$$\Delta H_{gas} = c_p \cdot \Delta T \qquad (3.10)$$

In the most general case, the complete optimization of a thermodynamic cycle would imply the simultaneous research for the best combination of the following parameters:

- Turbine inlet temperature;
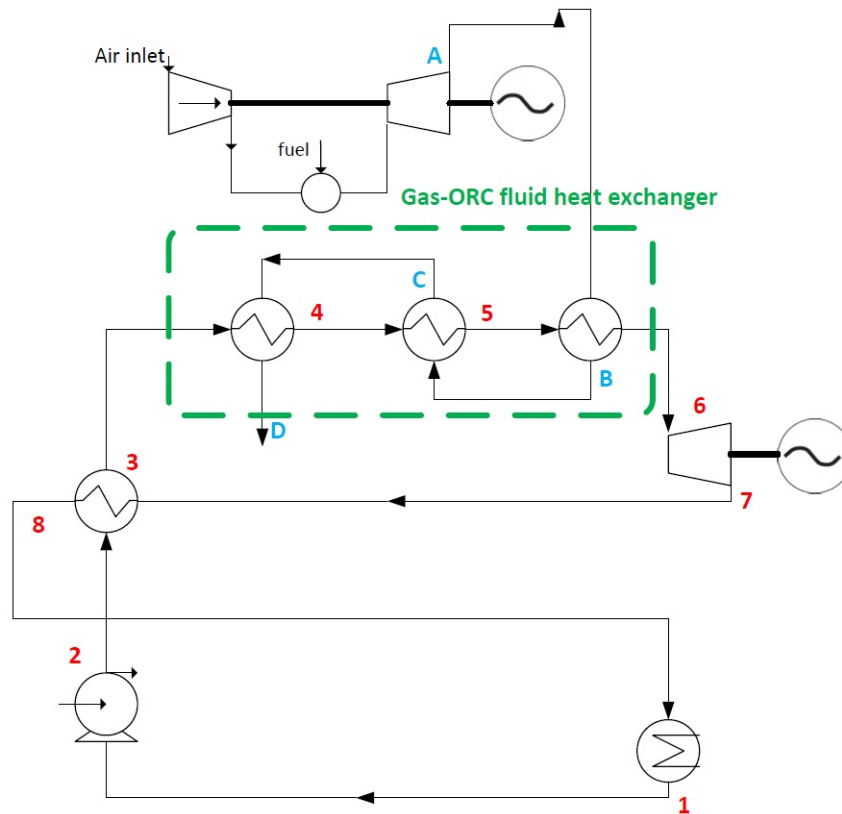
Figure 3.15.: ORC plant scheme.

- Turbine inlet pressure: this parameter influences significantly cycle efficiency, mass flow rate and primary heat exchanger (PHE) area and volume [7, 19];

- Minimum cycle pressure;

- Pinch point temperature difference in PHE (ΔT_{pp}): from a thermodynamic point of view, the lower the pinch point, the higher the heat recovery and the overall plant efficiency, but the higher the PHE area and cost as well [36];

- Pinch point temperature difference in regenerator ($\Delta T_{pp,rec}$): it is the temperature difference between points 2 and 8 (see figure 3.15 and 3.16). This parameter influences the amount of recovered heat and its optimization is important in presence of a limit on minimum outlet temperature of heat source, since a proper recuperator design allows to reach the best compromise between thermodynamic efficiency and exploitation of the particular heat source;

- Selection of working fluid.

For this present work, the number of cycle optimizing parameters has been reduced due to the following considerations:

- Cyclopentane has been chosen as the working fluid, being, according to Pierobon et al. [7], the optimal choice for this case of study;

- Without pressure losses there are only two pressure values, namely the evaporation pressure and the condensation one; this latter tends always to the minimum possible value within the constraints given by thermodynamic fluid properties and operative considerations.
  In this present work the condensing pressure has always been fixed to 1 bar, in order to avoid air leakage into the pipes [9], a problem that would also lead to rapid decomposition of organic working fluid [21, 37];

- From a thermodynamic point of view, the higher the maximum cycle temperature (that is, the turbine inlet temperature), the higher the cycle efficiency. However, as discussed by Ginosar et al. [21], due to chemical instability issues, there is a maximum available operative temperature for the chosen fluid, found to be 513.15 K. It was chosen to build the map for this value of turbine inlet temperature. This assumption implies to work with a constant value of T_6.

- Both ΔT_{pp} and $\Delta T_{pp,rec}$ have been fixed to the minimum value provided by Pierobon et al. [7] and reported in table B.2 in appendix B. Inside the cycle calculation process, if necessary, the location of the ΔT_{pp} is made switch automatically from evaporator inlet to recuperator outlet. Figure 3.16 shows a sample T-S diagram for these two configurations.

It is worth noting this cycle model only provides subcritical configurations. It was chosen to limit the analysis just to this configuration because, for the chosen fluid, a supercritical cycle model would require values of turbine pressure ratio that are too large for being effectively managed in a single-stage turbine. Moreover, supercritical configurations for ORC are still under experimental study and not easily commercially available.
For this reason, the maximum available turbine pressure has been fixed to $0.9 \cdot P_{cr}$[8].

---

8 The critical pressure of cyclopentane is $P_{cr} = 45.71$ bar. Thus, this limit corresponds to a maximum available pressure ratio of 41.
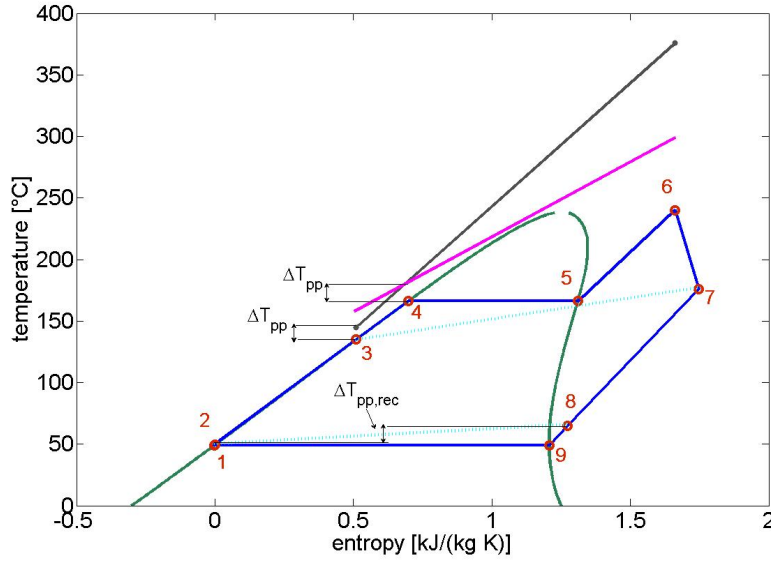
Figure 3.16.: Sample T-S diagram with two heat sources and two different locations of ΔT_{pp}.

3.6.1 *Fluid properties*

Both the aformentioned *Coolprop* and *Refprop®* codes require a similar syntax to calculate the desired thermodynamic properties [14, 15]; the general expression is:

$$A(i) = f(A, B, B_i, C, C_i, \text{fluid name}) \qquad (3.11)$$

where "i" is the desired value of the property A and both B and C are two more thermodynamic properties and B_i and C_i are their correspondent value in "i".

For example, the enthalpy in point 7 in figure 3.15 can be evaluated by the following expression:

$$H_7 = f(H, T, T_7, P, P_7, \text{fluid name}) \qquad (3.12)$$

While estimating thermodynamic properties in saturated condition, the thermodynamic title substitutes the second parameter.

3.6.2 *ORC model description*

Attending to nomenclature shown in figure 3.15 and 3.16, the cycle model is developed as follows:

1. For a given P_6 and T_6, the thermodynamic properties at point 6, 5, 4 and 1 are obtained. With the first assumption of ΔT_{pp} located on evaporator inlet (point 4), the exhausted gas temperature T_C is evaluated as:

$$T_C = T_4 + \Delta T_{pp}$$

and the mass flow rate $\dot{m}_{ORC}$ is obtained through the energy balance of superheater and evaporator sections:

$$\dot{m}_{gas} \cdot c_{p,gas} \cdot (T_A - T_C) = \dot{m}_{ORC} \cdot (H_6 - H_4)$$

Now it is possible to calculate also T_B from the superheater energy balance:

$$\dot{m}_{gas} \cdot c_{p,gas} \cdot (T_A - T_B) = \dot{m}_{ORC} \cdot (H_6 - H_5)$$

2. A *pump* function is created to calculate pump consumption and point 2 properties as follows:

$$(H_2, S_2, T_2, L_p) = f(P_1, P_2, \eta_p, \rho_1, \text{fluid}) \quad [\text{kJ/kg}] \quad (3.13)$$

where L_p and H_2 are respectively calculated as:

$$L_p = \frac{P_2 - P_1}{\rho_1 \cdot \eta_p} \tag{3.14}$$

$$H_2 = H_1 + \eta_p \cdot L_p \tag{3.15}$$

3. The turbine map function is made run as in eq. 3.9. The properties for isoentropic point 7_{is} are evaluated and turbine work is obtained as:

$$L_t = \eta_t \cdot (H_6 - H_{7is}) = (H_6 - H_7) \quad [\text{kJ/kg}]$$

This allows also to calculate H_7.
Now that H_7 is known, all the remaining properties at point 7 are calculated;

4. It is now possible to calculate T_8 as:

$$T_8 = T_2 + \Delta T_{pp,rec}$$

and so the remaining thermodynamic properties in point 8. Through the recuperator energy balance H_3 is obtained as:

$$H_3 = H_2 + q_{rec}$$

where $q_{rec} = H_7 - H_8$. Now it is possible to obtain the remaining thermodynamic properties in point 3 and obtain the exhausted gas exit temperature T_D as:

$$T_D = T_C - \dot{m}_{ORC} \cdot \left(\frac{H_4 - H_3}{\dot{m}_{gas} \cdot c_{p,gas}} \right)$$

5. The location of the pinch point is checked:
if $T_D - T_3 < \Delta T_{pp}$, a new cycle calculation begins with the ΔT_{pp} located in point 3 (recuperator exit);

6. The new mass flow rate has to be evaluated from the primary heat exchanger energy balance:

$$\dot{m}_{gas} \cdot c_{p,gas} \cdot (T_A - T_D) = \dot{m}_{ORC} \cdot (H_6 - H_3)$$

In this case it is not possible to calculate $\dot{m}_{ORC}$ until H_3 is known. But H_3 is a function of the recuperator energy balance which in turn, depends on H_7, calculated with the turbine map function that needs $\dot{m}_{ORC}$ to be run. An iterative process is so performed, described as follows:

- For a first guess turbine efficiency the properties of point 7 are evaluated;

- With H_7, through the recuperator energy balance, H_3 is obtained, and so T_D, being now $T_D = T_3 + \Delta T_{pp}$;

- $\dot{m}_{ORC}$ is now obtained from equation in step 6;

- the map function is called and the new turbine efficiency is obtained and updated; this loop is repeated until a convergence on turbine efficiency set at 10^{-3} is reached.

7. Finally the output power is calculated as:

$$W_{out} = \dot{m}_{ORC} \cdot (\eta_{gen} \cdot L_t - L_p) \quad [kW] \qquad (3.16)$$

while the plant efficiency is defined as:

$$\eta_{ORC} = \frac{W_{out}}{\dot{Q}_{max,gas}} \qquad (3.17)$$

where $\dot{Q}_{max,gas} = \dot{m}_{gas} \cdot c_{p,gas} \cdot (T_A - T_{D,min})$ and $T_{D,min}$ is the minimum allowed exhausted gas exit temperature.

For each test performed, the results are compared to the ones obtained with a similar ORC plant model that considers a constant turbine efficiency $\eta_t = 0.8$. The structure of this second model is the same as the one just described, with the assumption, of course, that expander efficiency is known (and given as an input parameter), so no iterative loop is required to evaluate the mass flow rate in the equation in step 6.

It is worth noting the turbine map has proved to be a useful tool to ensure the convergence of the internal loop: during this routine, the mass flow rate fluctuates and it has been observed that, if the entire turbine optimization process is inserted in the cycle model, it is not possible to reach convergence, because any change in mass flow rate should be followed by a simultaneous variation of all the turbine optimizing parameters, and this is not possible. Thus, if the map had not been used, the algorithm would have always stopped without reaching convergence.

3.7 OPTIMIZATION ACCOUNTING FOR ROTATIONAL SPEED

In the second part of this work, a new turbine map has been generated, considering also the rotational speed as an optimizing parameter. The complete set of input requirements is the same provided in table B.1 in appendix B, but considering N among the optimizing parameters with the upper and lower bound set to 2000 and 12000 rpm (see also table 3.3). Also in this case, the outlet pressure was fixed to 1 bar, turbine inlet temperature was fixed to 513.15 °C and mass flow rate was varied between 10 and 200 kg/s for values of pressure ratio between 5 and 44.

The new map was then inserted into the organic Rankine cycle model and the output power was evaluated as described in section 3.6, with the only addition of a gearbox efficiency fixed to 0.96 [20].

3.8 TURBINE TECHNO-ECONOMIC OPTIMIZATION

To find out whether and to what extent different expander optimization processes can affect the optimal design and eventually cycle configuration, a techno-economic optimization has been performed: in this process, the specific cost (in €/kW) was chosen as the parameter to be minimized instead of maximizing the total-to-total turbine efficiency.

The specific cost was computed by means of the cost function developed by Astolfi et al. [20]:

$$C_t = C_0 \cdot \left(\frac{n}{n_0}\right)^{(0.5)} \cdot \left(\frac{SP}{SP_0}\right)^{1.1} \tag{3.18}$$

where n is number of stages (always one, in this present work), $n_0 = 2$, $C_0 = 1230 \cdot 10^3$ € and $SP_0 = 0.18$ m. SP is the *size parameter*, defined as:

$$SP = \frac{\sqrt{\dot{V}_{out}}}{\Delta H_{is,stage}^{3/4}} \quad [m] \tag{3.19}$$

The electric power produced by the turbine is computed as:

$$W_t = \eta_{gen} \cdot \dot{m}_{ORC} \cdot \Delta H_{tot} \tag{3.20}$$

and so the specific cost is defined as:

$$C_{spec,t} = \frac{C_{turb}}{W_{turb}} \tag{3.21}$$

in €/kW.
The specific cost was optimized for three different values of

pressure ratio, as a function of mass flow rate and compared with the specific cost obtained for the conventional thermodynamic optimization.

3.9 ESTIMATION OF GEARBOX PROFITABILITY

A techno-economic estimation has been performed to evaluate the profitability of a gearbox insertion.
The difference between the present value of cash inflows and the present value of cash outflows is called "net present value" (NPV) [38] and it is mathematically defined as [39]:

$$NPV = \sum_{i=0}^{n} \frac{R_i}{(1+q)^i} - I_{tot} \qquad (3.22)$$

where R_i is the annual revenue, q is the interest factor, n is the equipment lifespan and I_{tot} is the total investment cost. As stated by Pierobon et al. [7], the total investment cost can be calculated as a function of the sum of purchase equipment cost (PEC) of plant components:

$$I_{tot} = 3.7 \cdot (PEC_{HE} + PEC_p + PEC_{turb} + PEC_{cond} \\ + PEC_{IR} + PEC_{gen} + PEC_{gear}) \qquad (3.23)$$

For the present case of study, as previously introduced, two major sources of income with the installation of the ORC unit are expected: the first is associated with the fuel saving, the second with the CO_2 tax.

The power produced by the ORC unit allows to reduce the load of the other gas turbine operating on the platform: the saved fuel can then be exported and sold to the marked, becoming an additional revenue.

According to turbine data provided in tables 3.1 and 3.5, the saved mass flow rate of fuel can be calculated as:

$$\dot{m}_{sf} = \frac{W_{ORC,net} \cdot 3600}{LHV_f \cdot HR} \qquad (3.24)$$

where $W_{ORC,net}$ is the net output power of waste heat recovery unit, LHV is the low heating value of natural gas and HR is the gas turbine heat rate.

The annual revenue R_{sf} due to saved fuel (in €/year) is estimated as follows:

$$R_{sf} = \dot{m}_{sf} \cdot hu \cdot 3600 \cdot C_{ng} \qquad (3.25)$$

where hu is the utilization factor [7] and C_{ng} is the price of natural gas [40].

Table 3.5.: Parameter assumed for the economic analysis

parameter	Symbol	Unit	Value
Natural gas price [40]	C_{gn}	NOK/MMBTU	24.04
Energy conversion factor [41]	-	GJ/MMBTU	1.054615
utilization factor [7]	hu	hours/year	7000
Low heating value [7]	LHV	MJ/kg	48.530
Carbon tax [30]	CT	NOK/t_{CO_2}	410
Carbon dioxide emission rate [42]	$CO_{2\,e.r.}$	$kgCO_2/kgCH_4$	2.75
Maintenance [7]	Ma	-	0.9
Equipment lifespan [7]	n	years	20
Interest factor [7]	q	-	10%
Conversion factor [43]	-	€/NOK	0.1224
Generator efficiency [7]	η_{gen}	-	0.98
Gearbox efficiency	η_{gear}	-	0.96

The income R_{CO_2} (in €/year) related to the CO_2 saving is computed as:

$$R_{CO_2} = \dot{m}_{sf} \cdot hu \cdot 3600 \cdot CO_{2\,e.r.} \cdot \frac{CT}{1000} \qquad (3.26)$$

where $CO_{2\,e.r.}$ is the carbon dioxide emission rate and CT is the carbon tax.
The annual revenue R_i is therefore defined as:

$$R_i = R_{s.fuel,i} + R_{CO_2,i} \qquad (3.27)$$

According to equation 3.23, a complete techno-economic analysis must account for all plant components and it is out of the purpose of this present work. However, in order to evaluate the profitability of a gearbox purchase, a full analysis is not necessary, being an estimation of the sought information given by the following difference:

$$NPV_{diff} = NPV_{gear} - NPV_{no-gear} \qquad (3.28)$$

where the subscripts *gear* and *no-gear* respectively indicate a plant configuration where the gearbox is considered and not. In fact, for a given evaporation pressure, it is possible to consider heat exchangers dimensions approximately constant for the two cases in pair, being the heat exchanger dimensions influenced by pressure and mass flow rate, and being this latter approximately the same for the two configurations once established the pressure ratio (see also section 5). Following this

approach, considering the pump as a fixed-cost component as well, all these values basically disappear in equation 3.28; the result is positive when the gearbox insertion is convenient.

Thus, in this present work only turbine, electrical generator and gearbox cost are considered. The first one is calculated with equation 3.18, while the second one is calculated as suggested by Astolfi et al. [20]:

$$C_{gen} = C_0 \cdot \left(\frac{W_{el}}{W_{el,0}} \right)^{0.67} \tag{3.29}$$

where $W_{el,0} = 5000$ kW and $C_0 = 200$ k€. In case a gearbox is present, its cost is considered equal to 40% of the electrical generator cost.

It was chosen to assume a value of 96% for gearbox efficiency, thereby reducing of one point the value of 97% adopted by Astolfi et al. [20]: indeed, as a consequence of the lack of more detailed information about this component, it was chosen to consider a slightly less effective performance.

VERIFICATION AND VALIDATION OF THE CODE

In this chapter the performances of the code are tested and compared with two cases:

1. A similar computational code, capable of producing an optimized turbine design;

2. A set of experimental data regarding a four-stage turbine provided by Evers and Kötzing [6].

In all the analyses performed in this chapter the code has not been coupled with the optimization routine and the ϕ_r coefficient, as well as the inlet axial velocity C_{a1}, is provided as an input value; this allows to have a non-constant axial velocity component throughout the stage, which is the real physical configuration for both the examined cases.

4.1 VERIFICATION WITH AXTUR CODE

AXTUR is a code developed by the department of energy in Polytechnic of Milan [44]. Provided the requested input data, it can produce the optimal design of an axial-flow turbine with one, two or three stages. It employs the same correlation as the examined single-stage code to estimate fluid angles and losses.

It was chosen to reproduce a subsonic case with the values listed in table 4.1.

These values, together with the useful results given by AXTUR output, provide the input values for the single-stage model computational code. The purpose of this test is to check if, provided the correct input data, the turbine code can reproduce the same results as AXTUR. It should be noted that, just like the employed design code, AXTUR does not account for any radial equilibrium problem.

The complete set of input values for the single-stage model code is listed in table 4.2, while both the output values obtained by the two codes are provided and compared in table 4.3. The relative error is defined as:

$$\epsilon = \left| \frac{\xi_{obtained} - \xi_{axtur}}{\xi_{axtur}} \right| \cdot 100 \tag{4.1}$$

where ξ is a generic parameter.

Figure 4.1 shows the velocity triangles for this case.

Table 4.1.: Provided input data for AXTUR

Parameter	Unit	Value
Fluid	—	Ideal gas
molecular configuration	—	biatomic
MM	kg/kmol	28.4
$\dot{m}$	kg/s	10
T_{01}	K	1123.15
P_{01}	bar	2
P_{03}	bar	1
N	rpm	10000
Number of stages	—	1
α_1	°	0
Re	—	10^5
M_{cd}	—	1.4

Table 4.2.: Input data provided for turbine code.

Parameter	Unit	Value
Fluid	—	air
$\dot{m}$	kg/s	10
T_{01}	K	1123.15
P_{01}	bar	2
P_{03}	bar	1
N	rpm	10000
Re	—	10^5
M_{cd}	—	1.4
α_1	°	0
ψ	—	2.1457
$(o_{min})_n$	m	0.01091
o_r	m	0.01139
c_n	m	0.0354
c_r	m	0.0354
$\left(\frac{o}{s}\right)_n$	—	0.25086
$\left(\frac{o}{s}\right)_r$	—	0.31762
ϕ_r	—	0.3475
C_{a1}	m/s	89.2
hhh	—	1.04

Table 4.3.: Comparison between the results showed by AXTUR and the ones obtained by the code.

Parameter	Unit	Model	Axtur	Error(%)
η_{tt}	—	0.92461	0.92657	0.211533
χ	—	0.48045	0.46851	2.548505
r_m	m	0.40172	0.39331	2.138262
h_1	m	0.071386	0.07462	4.333959
h_{21}	m	0.072219	0.07462	3.217636
h_2	m	0.075122	0.07762	3.217636
h_3	m	0.074982	0.07759	3.361258
z_n	—	58	57	1.754386
z_r	—	70	69	1.449275
C_1	m/s	89.2	89.2	0
C_{a1}	m/s	89.2	89.2	0
C_{a2}	m/s	114.41	112.3601	1.824378
C_2	m/s	460.74	452.3	1.866018
C_{a3}	m/s	146.18	143.1558	2.11253
C_3	m/s	146.64	143.5931	2.121924
W_2	m/s	117.33	115.4	1.672444
W_3	m/s	456.23	446.6	2.156292
α_1	$^\circ$	0	0	0
α_2	$^\circ$	75.61	75.617	0.009257
β_2	$^\circ$	12.605	13.165	4.253703
β_3	$^\circ$	71.312	71.305	0.009817
α_3	$^\circ$	4.4968	4.464	0.734767
M_1	—	0.13616	0.1314	3.622527
M_2	—	0.73287	0.6985	4.920544
M_{W2}	—	0.18663	0.1782	4.73064
M_{W3}	—	0.75507	0.7224	4.522425
ψ	—	2.1457	2.1457	0
$(o_{min})_n$	m	0.01091	0.01091	0
o_r	m	0.01139	0.01139	0
c_n	m	0.0354	0.0354	0
c_r	m	0.0354	0.0354	0
$(\frac{o}{s})_n$	—	0.25086	0.250862	0.000904
$(\frac{o}{s})_r$	—	0.31762	0.317624	0.001289
ϕ_n	—	0.27197	0.272785	0.298757
ϕ_r	—	0.3475	0.34755	0.014349
T_{out}	K	957.6	935	2.417112

Figure 4.1.: Velocity triangles for AXTUR test case.

As reported in table 4.3, the obtained results are in agreement with the ones provided by AXTUR. The highest error is the one concerning the inlet blade height (about 4.33 %).

Some words should also be dedicated to the different values obtained for the outlet temperature T_{out}; this discrepancy could be attributed to the different assumptions made about fluid nature in the two codes: indeed, AXTUR utilizes an ideal-gas model, while for the computational code the *Refprop* database has been used. This can lead to slightly different values for the thermodynamic properties that can also affect Mach number and blade height, being it evaluated through the mass flow rate continuity equation.

4.2 VALIDATION WITH EVERS AND KÖTZING

Evers and Kötzing [6] describe a test case of a four-stage air axial-flow turbine. A meridional view of the machine section is reported in figure 4.2.

Figure 4.2.: Flow path with measuring stations $0-4$, Evers and Kötzing [6].

Table 4.4.: Turbine design data, Evers and Kötzing [6]

Parameter	Unit	Value
N	rpm	7500
$\dot{m}$	kg/s	7.8
P_{in}	bar	2.6
T_{in}	K	413
P_{out}	bar	1.022
T_{out}	K	319
η	–	0.913
Coupling power	kW	703

For the inlet of each stage and for turbine outlet several measurements are available in nine different points on blade height; thus, for each station, nine values of total pressure, static pressure, total temperature, absolute velocity, absolute flow angle and radial flow angle are provided. The turbine was basically designed to have the same blade section in all stages at a given radius. The blades are twisted according to the free-vortex theory with a 50% reaction degree in the middle section of the *last* stage. The geometry of stator and rotor blades is reported in appendix C. For several heights along the blade (five for the nozzle and six for the rotor) the values of the following parameters are provided:

- Stagger angle;

- Solidity: $\sigma = b/s$, where b is the profile chord and s is the blade pitch;

- profile chord b;

- blade angles $\theta_1, \theta_{21}, \theta_2, \theta_3$;

These values, the thermodynamic measurements and the turbine input values listed in table 4.4, allow to evaluate all the input parameters necessary for the code. It has been chosen to validate the code just for the first and fourth stage of the turbine, being them the ones with the highest amount of experimental data.

All the input values requested by the code have been extrapolated using the thermodynamic values at the average radius for the particular stage; it is worth noting that the blade height values which the geometric parameters are given for, do not coincide with the height values used to provide thermodynamic data (see also appendix C); it was so necessary to interpolate

Table 4.5.: Final set of input values to test the code for first and fourth stage.

Parameter	Unit	Stage I	Stage IV
α_1	$^\circ$	-5.4	-5.5
ψ	$-$	2.383453	1.952544
$(o_{min})_n$	m	0.012109	0.014929
o_r	m	0.013922	0.01409
c_n	m	0.045927	0.0485
c_r	m	0.038832	0.036657
$(o/s)_n$	$-$	0.332067	0.373582
$(o/s)_r$	$-$	0.38636	0.353413
ϕ_r	$-$	0.584305	0.563299
C_{a1}	m/s	67.4	73.85
$\dot{m}$	kg/s	7.8	7.8
P_{01}	bar	2,588	1.348
T_{01}	K	406.44	339.6
P_{03}	bar	2.129	1.1052
N	rpm	7500	7500

between two blade data to obtain the correspondent value at average radius.

The set of input values obtained to validate the code for the first and last stage are reported in table 4.5.

The results of validation test for first and fourth stage are reported in tables 4.6 and 4.7, where the error is defined again as in eq. 4.1. Before proceeding with the analysis of the results it should be noted that:

- The value of efficiency provided in table 4.4 is defined as:

$$\eta = \frac{\Delta H_{I-IV} + (C_{I,in}^2 - C_{IV,out})/2}{\Delta H_{is,I-IV} + C_{I,in}^2/2}$$

  where $C_{I,in}$ is the absolute velocity at first stage inlet and $C_{IV,out}$ is the absolute velocity at fourth stage outlet, and it is related to the overall turbine efficiency. Thus this value is a useful indicator to consider, but can not be a parameter which the single stage total-to-total efficiency can be properly compared to. Moreover, the overall turbine efficiency is usually slightly higher than the single stage one, because some unconverted flow energy is then recuperated throughout the machine [25];

- The geometry modelled by the code is different from the real one of this test case. So at least, a minimum level of

discrepancy between the obtained results and the experimental ones is expected;

- Data of both velocities and thermodynamic properties between nozzle and rotor of the same stage are non provided.

Table 4.6.: Results of validation test for stage I.

Parameter	unit	obtained value	experimental data	error %
η_{tt}	—	0.884782	0.913	3.090724
χ	—	0.542232	—	—
r_m	m	0.163103	0.1701	4.113264
z_n	—	28	29	3.448276
z_r	—	28	30	6.666667
C_3	m/s	76.50949	79.3	3.518924
α_3	°	12.09528	0	—
θ_1	°	10	10	0
θ_{21}	°	70.60571	70.59588	0.013927
θ_2	°	23.3426	23.3426	0
θ_3	°	67.27181	67.2634	0.012508
T_{03}	K	385.3479	384.8	0.142392
P_3	Pa	207321.6	206900	0.203786
h_1	m	0.04977	0.0595	16.35289
h_3	m	0.052396	0.0675	22.37641
α_2	°	64.94738	—	—
β_3	°	62.56876	—	—
β_2	°	8.334964	—	—
ϕ_n	—	0.501755	—	—
ϕ_r	—	0.584	—	—
M_2	—	0.381995	—	—
M_{W3}	—	0.41434	—	—

Table 4.7.: Results of validation test for stage IV

Parameter	unit	obtained value	experimental data	error %
η_{tt}	—	0.848922	0.913	7.018449
χ	—	0.721565	0.5	44.31291
r_m	m	0.179183	0.1871	4.231459
z_n	—	28	29	3.448276
z_r	—	28	30	6.666667
C_3	m/s	83.73556	84.7	1.138653
α_3	°	18.87892	5.4	249.6096
θ_1	°	10	10	0
θ_{21}	°	68.06333	68.0626	0.001071
θ_2	°	−2.8233	−2.8233	0
θ_3	°	69.30377	69.3022	0.002261
T_{03}	K	319.8864	319.3	0.183642
P_3	Pa	101237.4	101200	0.036966
h_1	m	0.065751	0.0892	26.28781
h_3	m	0.074611	0.103	27.56209
α_2	°	61.73962	—	—
β_3	°	64.72768	—	—
β_2	°	−22.904	—	—
ϕ_n	—	0.437797	—	—
ϕ_r	—	0.563	—	—
M_2	—	0.356869	—	—
M_{W3}	—	0.520362	—	—

4.2.1 *Discussion of Results*

Stage I

As shown in tables 4.6 and 4.7 the obtained values for stage I show a better agreement than the correspondent ones for the last stage. As discussed above, due to geometry difference, the obtained average radius r_m is slightly smaller than the experimental one[1].

The main reason of discrepancies in both the stages is due to the non-representative behaviour of the assumed axial velocity at average radius in terms of mass flow rate: as exhaustively discussed by Saravanamuttoo et al. [24], the axial velocity profile is never constant along blade height and the whirl component of flow at nozzles outlet makes static pressure and temperature vary across the annulus. The employed model considers a uniform density and velocity profile along blade height: this means the mass flow rate can simply be evaluated by the expression:

$$\dot{m} = \rho A C_{ax} \qquad (4.2)$$

However, figure 4.4 shows the inlet axial velocity profiles for stage 1 and 4. As illustrated, the assumed value for axial velocity is not representative of the whole profile. An infinitesimal element of mass flow rate $d\dot{m}$ can be expressed as [24]:

$$d\dot{m} = \rho\, C_{ax}\, 2\pi r\, dr\, d\vartheta \qquad (4.3)$$

and in reality, the total mass flow rate is obtained performing the integration:

$$\dot{m} = \int_0^{2\pi} \int_{r_{hub}}^{r_{tip}} \rho\, C_{ax}\, 2\pi r\, dr\, d\vartheta \qquad (4.4)$$

According to equation 4.2, to ensure the mass flow rate conservation, for a given density, an eventual *over-contribution* from axial velocity must be compensated by a proportional reduction in area which, in turn, is a function of r_m and h:

$$A_i = 2\pi r_m h_i \qquad (4.5)$$

where i is a generic stage section. So for a given value of r_m, a reduction in area leads to a reduction in blade height[2].

---

[1] In the real geometry of the turbine described by Evers and Kötzing [6] the hub radius is constant, while the tip radius increases along the axial direction. This causes the average radius to increase as well. for a generic stage, the average radius is so computed as the half-sum of the inlet and outlet radii, as follows:

$$r_{m,i} = \frac{r_{m,iIN} + r_{m,iOUT}}{2}$$

[2] The calculated values of density along blade height show an almost null variation in radial direction.
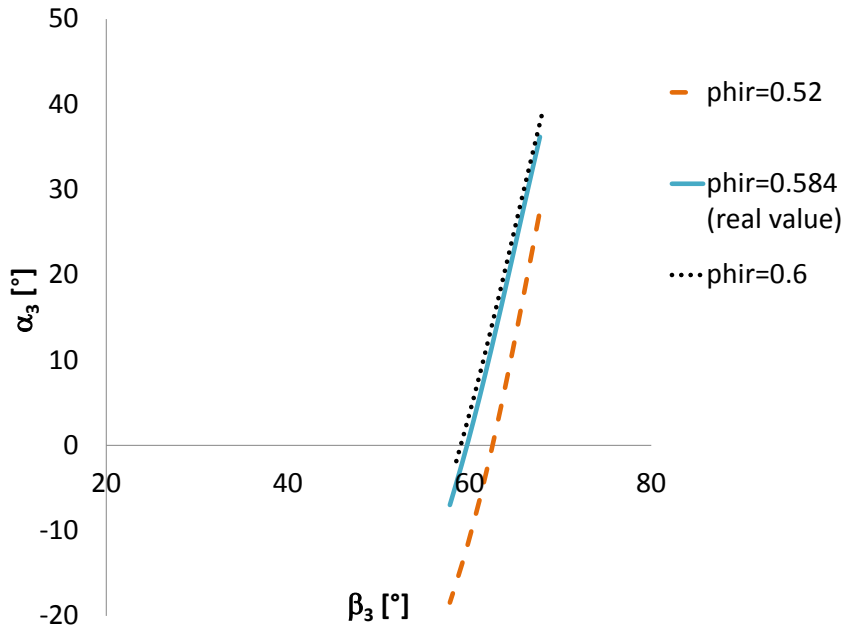
Figure 4.3.: Influence of rotor relative fluid exit angle β_3 on absolute rotor exit angle α_3 (stage I).

Some comments must be expressed also about absolute flow exit angle α_3[3]. According to Saravanamuttoo et al. [24], the flow angle α_3 is obtained by the expression:

$$\alpha_3 = \arctan\left(\tan\beta_3 - \frac{1}{\phi_r}\right) \tag{4.6}$$

so, α_3, depends on the flow angle β_3 which is evaluated, for a subsonic case, through the Ainley and Mathieson correlation [32]. However, eq.4.6 seems to be extremely sensitive to even small variation of β_3, as shown in figure 4.3: an eventual decreasing in β_3 of about three degrees would bring α_3 to zero, as provided in the experimental data. So a small uncertainty on β_3 would lead to a bigger error in the value of α_3.
Anyway, the obtained efficiency or the first stage is just slightly lower than the value accounting for the overall expander performance.

---

3 in table 4.6 the relative error is undefined because, for this particular case, the experimental angle has a zero value: this makes the error defined in equation 4.1 tend to infinity.

Stage IV

The errors obtained for the fourth stage show a bigger discrepancy with experimental data (table 4.7): as reported in figure 4.4 and 4.5, in this last stage the variation of axial velocity along radial direction, both for inlet and outlet, is much more significant than in the first stage. The axial velocity profile is decreasing from hub to tip, a phenomenon that the code can not account for with a single axial velocity distribution. Due to this, the error in blade height is more consistent than in the first stage, with a consequent under-estimation of efficiency. Both for first and last stage, lower values for C_{a1} and ϕ_r would be more representative in terms of overall stage performances and mass flow rate, leading both to higher values for blade length and efficiency. Moreover, according to equation 4.6, a lower value of ϕ_r would also reduce the error in α_3.
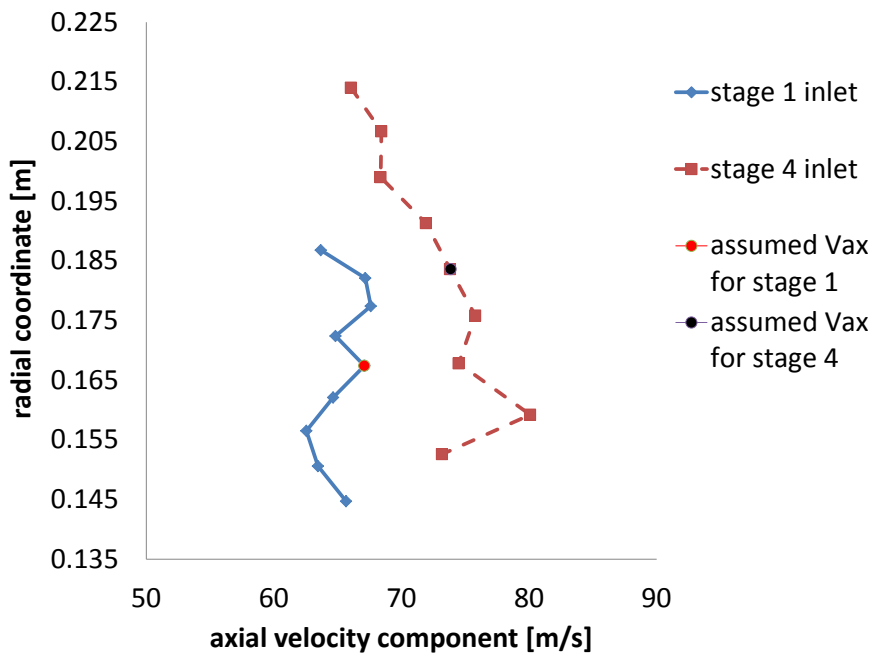
Figure 4.4.: Axial velocity profile for inlet section of stage I ad IV.

Finally, it is worth mentioning again that in all the stages, especially in the last ones, the "real" blades are highly twisted to account for fluid variation in radial direction and increase the efficiency, an aspect that is not taken into account, as previously anticipated, in the employed code.
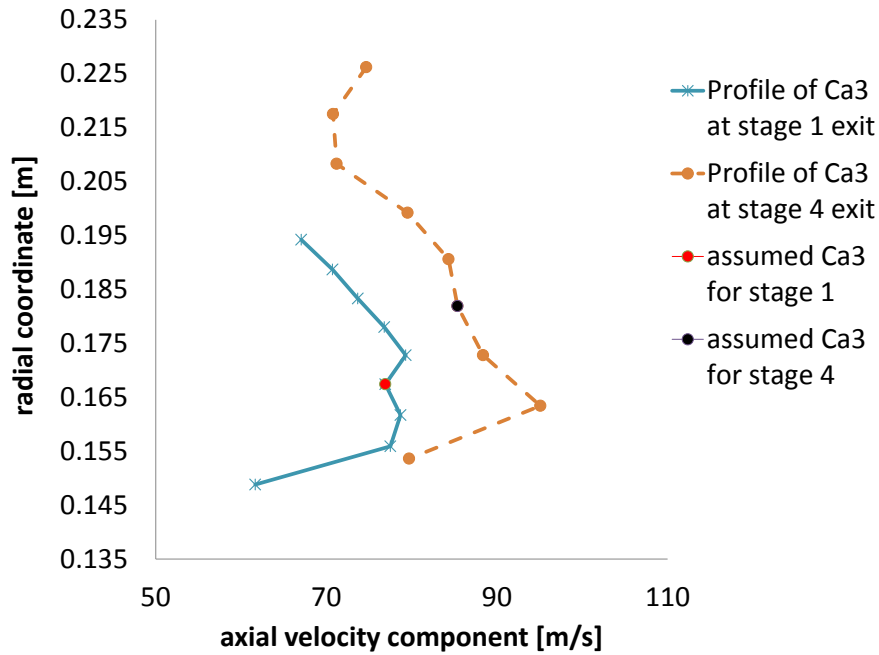
Figure 4.5.: Axial velocity profile for outlet section of stage I ad IV.

4.3 CONCLUSIONS

From the results obtained in this chapter it is possible to state that:

- The computational code has shown satisfactory accuracy with reliable previous similar models (maximum relative error of 4.33%);

- Whenever three-dimensional variations of flux are present but still not significantly pronounced, the model is still capable of giving acceptable results in terms of efficiency, even if with bigger error in blade geometry, especially in blade height (up to 22%);

- In circumstances when three-dimensional effects are significant and velocity profile can not be represented by only one component at mean radius any more, the results are not trustable and a more complex approach is necessary.
  However, organic fluid turbines typically exhibit moderate blade height, therefore the model is expected to give satisfactory results in the context of the present work.

DISCUSSION OF RESULTS

In this chapter all the obtained results are reported and discussed.

5.1 TURBINE MAPS

5.1.1 *Map for constant rotational speed*
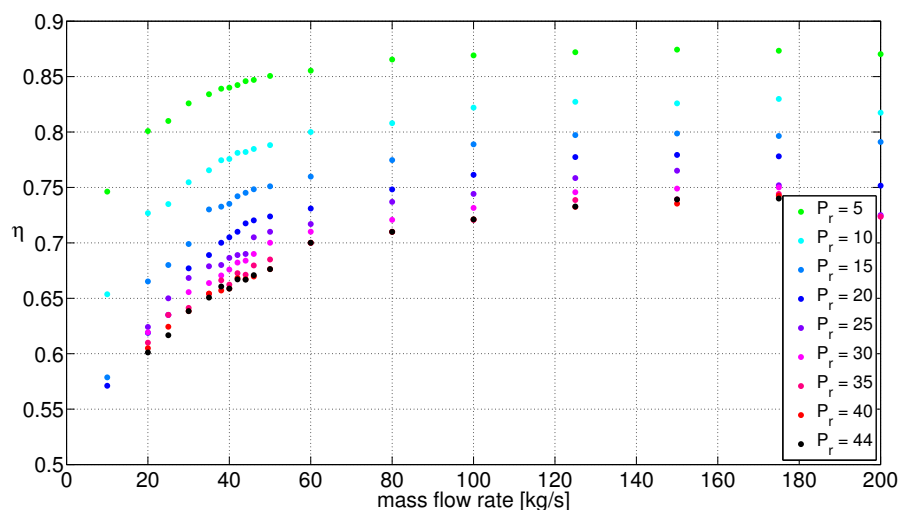
Figure 5.1.: Turbine efficiency map for constant rotational speed.

The results obtained for the first set of turbine design optimizations with $N = 3000$ rpm are reported in figure 5.1, which shows the trends of total-to-total efficiency as a function of mass flow rate and pressure ratio $P_r = P_{01}/P_{03}$. The efficiency grows up when the first one increases and the second one decreases, and its variations are more significant when mass flow rate is lower than 100 kg/s and pressure ratio ranges from 5 to 30. Higher values of mass flow rate lead to larger turbine for the same pressure ratio, with bigger blade channels and reduce the relative influence of boundary layers and secondary losses.

For high values of pressure ratio the iterative loop requires more iterations, thereby increasing the overall computational time. Moreover, for values of pressure ratio higher than 30, the curves start showing some fluctuating behaviour. The following pictures show the trends of the most interesting parameters. In accordance with the results obtained by Macchi [23] the degree of reaction (figure 5.2) is, as expected, comprised between 0.2 and 0.5. The higher the pressure ratio, the lower the degree

of reaction to restrain blade height variation within the respect of all the other constraints.

Figure 5.2.: Values of reaction degree for optimal design geometries, as a function of mass flow rate and pressure ratio.
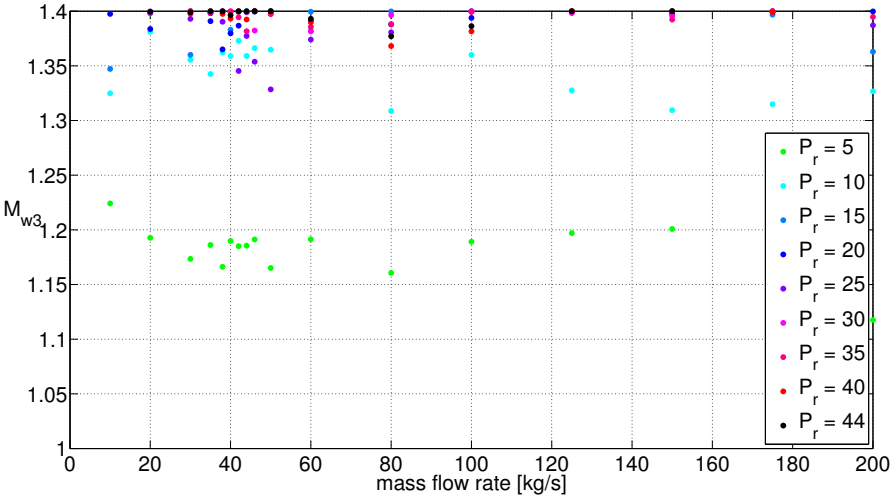
Figure 5.3.: Values of M_{W3} for optimal design geometries, as a function of mass flow rate and pressure ratio.

The limit on Mach number M_{W3} is one of the most active constraints: as shown in figure 5.3, with the exception of low values of pressure ratio the upper bound is almost always reached. The values of $(o/s)_n$ are close to the lower bound (figure 5.4), which is often reached. Remembering equation 3.5 and being the nozzle exit flow angle related to θ_{21}, the lower $(o/s)_n$, the higher the blade outlet angle and the achieved fluid deflection in nozzle.

The obtained values of nozzle throat section are reported in figure 5.5. For low mass flow rates and high values of pressure ratio, the optimal value is close to the lower bound; however, if

desirable, values of o_{min} smaller than the ones obtained would be impractical in many cases, due to the high number of blades, which often already reaches the maximum admitted value (figure 5.6).
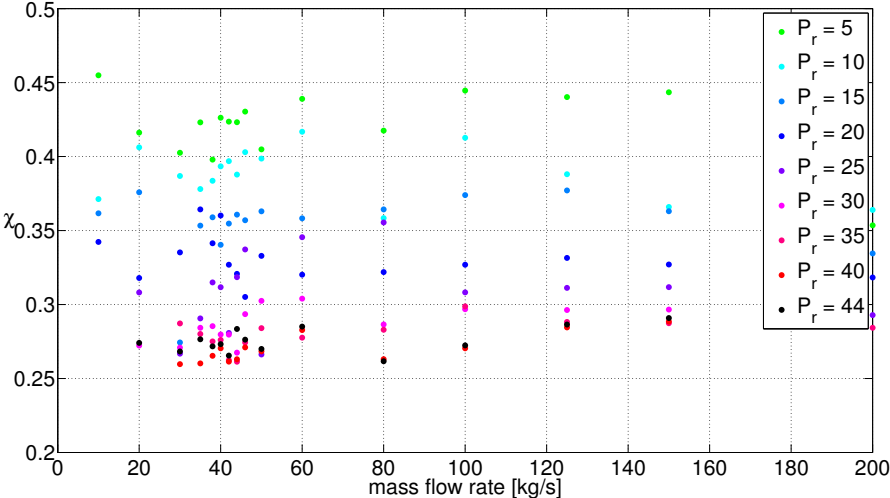

Figure 5.4.: Values of $(o/s)_n$ for optimal design geometries, as a function of mass flow rate and pressure ratio.
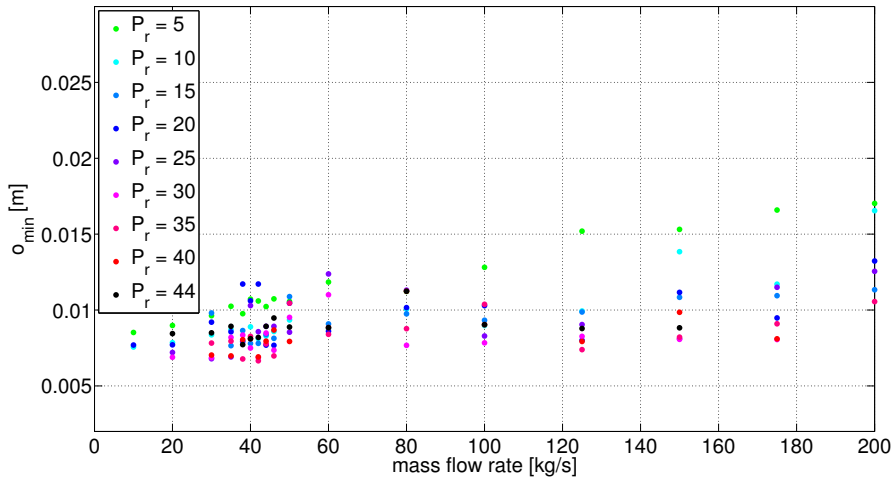
Figure 5.5.: Values of o_{min} for optimal design geometries, as a function of mass flow rate and pressure ratio.
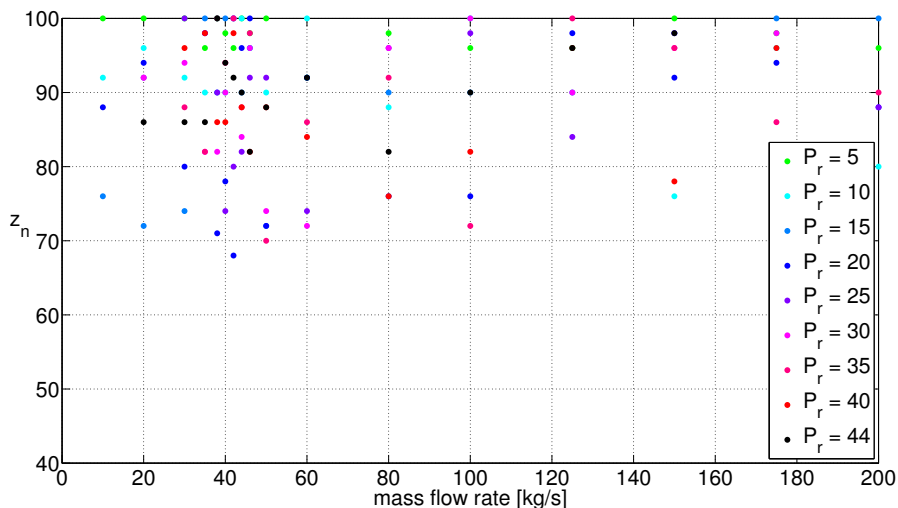
Figure 5.6.: Number of nozzle blades for optimal design geometries, as a function of mass flow rate and pressure ratio.

5.1.2 *Turbine map for optimized rotational speed*

If rotational speed is considered among the optimizing variables, the obtained map of efficiency changes significantly, as shown in figure 5.7. The obtained values of efficiency are remarkably higher than in the previous test: just for a few cases expander performance drops down below 0.75 and never reaches 0.7. The main difference between these new data and the ones reported in figure 5.1 is obtained for values of mass flow rate lower than 100 kg/s that is, substantially, the operative range where the optimal rotational speed significantly differs from 3000 rpm (figure 5.8).
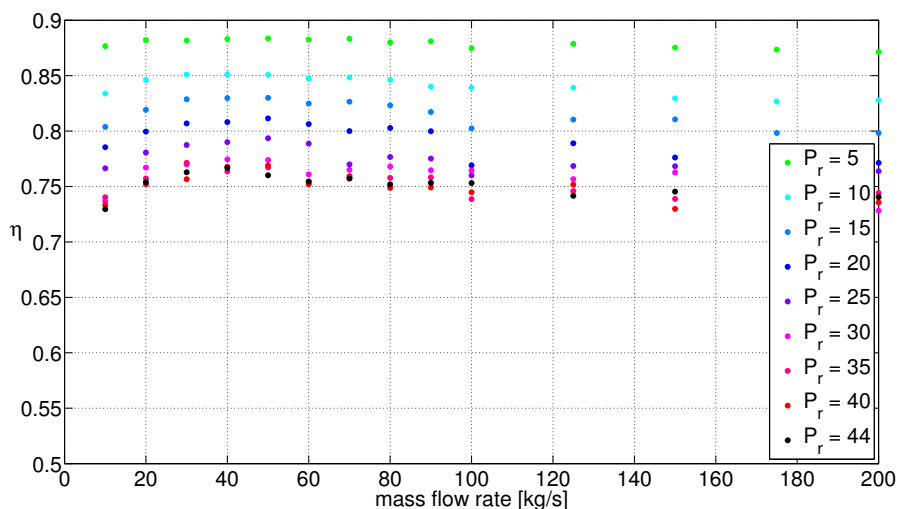
Figure 5.7.: Turbine efficiency map for optimized rotational speed.
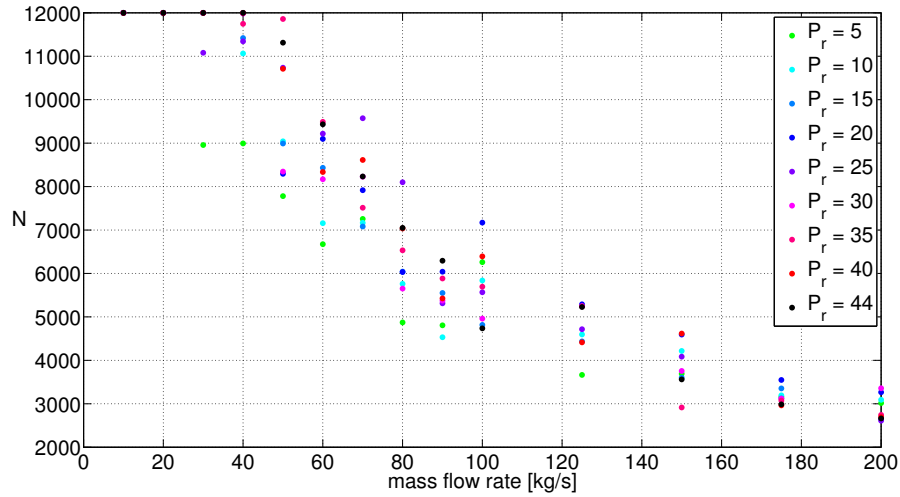
Figure 5.8.: Optimal rotational speed as function of mass flow rate and pressure ratio.

The optimal rotational speed reaches the upper bound for relatively low values of mass flow rate: indeed, for a given shape of velocity triangles (so for a given U) and mass flow rate, the possibility to vary N allows to modify turbine diameter and proportionally vary blade height. This has a beneficial effect especially for low mass flow rates, because an increment in N allows to reach higher values of efficiency, implying the proportional increase of blade height whose non-optimal value, for gas and vapour turbines, appears to be one of the most significant causes of losses [23, 24].

Rotor flare angles almost always reach the upper bound, as shown in figure 5.9; for this second set of turbine efficiency optimizations, this limit is one of the most active constraints[1].
The other key role is played, again, by Mach number M_{W3} which, from values of pressure ratio higher than 10, always reaches the upper bound (figure 5.10).

---

1 The limit value of 25° refers to the half-opening of the flare, as previously illustrated in figure 3.4.
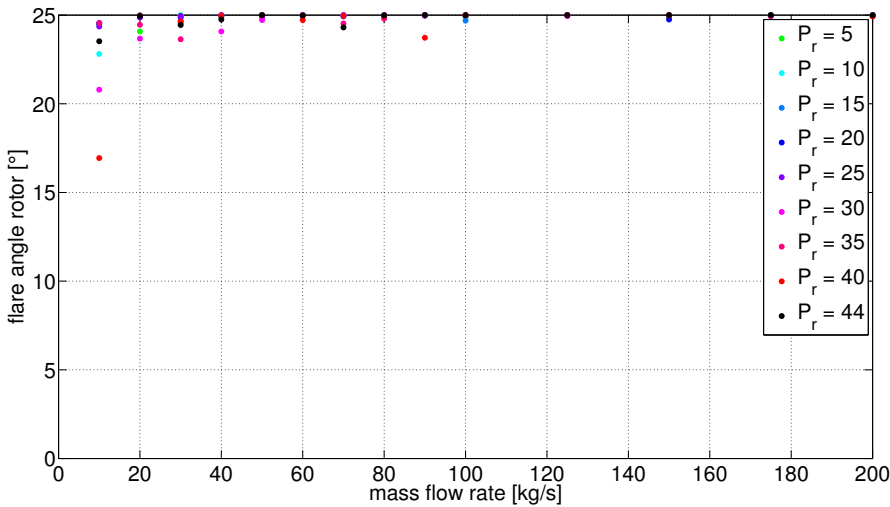
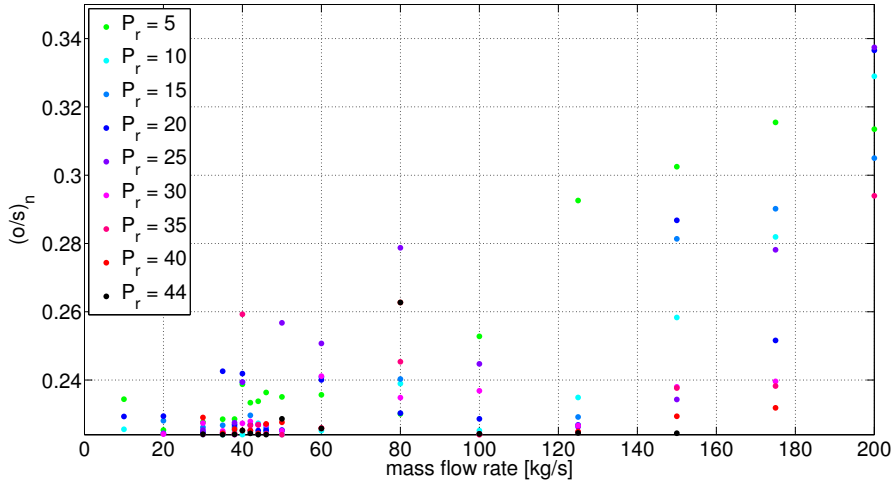**Figure 5.9.:** Flare angles for optimal design geometries, as a function of mass flow rate and pressure ratio.
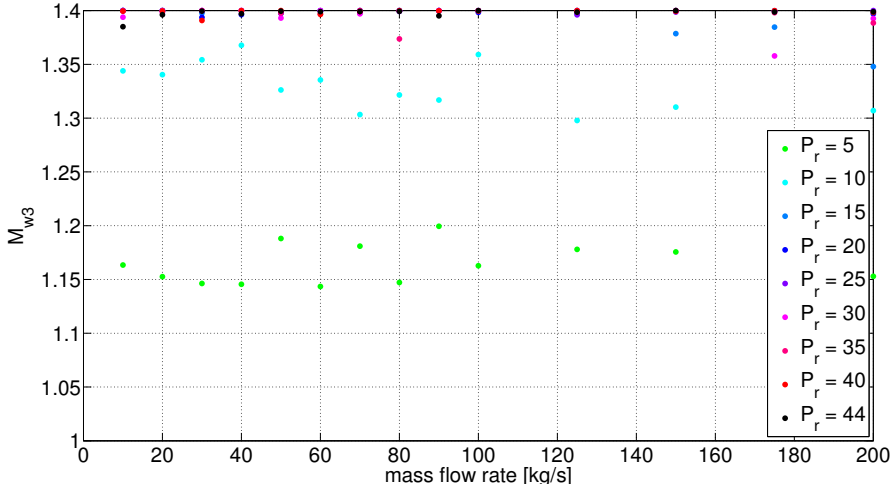
Figure 5.10.: Values of M_{W3} for optimal design geometries, as a function of mass flow rate and pressure ratio.

5.2 CYCLE TESTS

The obtained results are presented and compared in charts showing the most important trends as a function of pressure ratio $P_r = P_6/P_7$: in fact, considering that our attention is restricted to the cases where both T_6 and the two ΔT_{pp} are fixed, this parameter results to be the only active one in terms of thermodynamic cycle configuration. The following charts mark the difference in final power output between the two different ways of accounting for turbine efficiency. It is worth noting that, for this particular fluid and level of heat source, the pinch point of primary heat exchanger is *always* located at recuperator outlet.
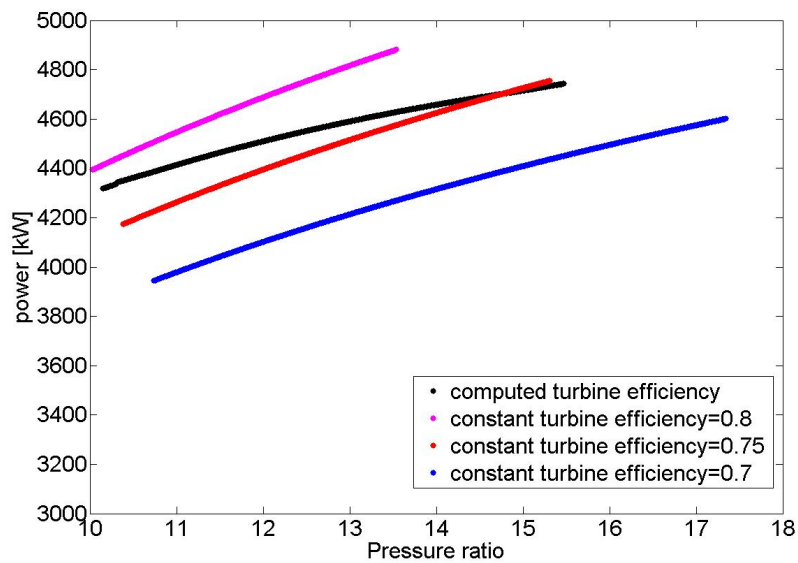
Figure 5.11.: Power output for three different values of constant turbine efficiency, in comparison with the computed-efficiency curve.

The chart in figure 5.11 shows the power output for three assumed levels of turbine efficiency in comparison with the values obtained computing expander performance. The trend of efficiency is reported later, in figure 5.15.
In this present case of study, the most restrictive constraint, in terms of cycle design, is the minimum outlet temperature of exhausted gas T_D: when imposing a maximum value of T_6 consistently smaller than the inlet temperature of heat source (more than 100 °C, as reported in figures 5.17 and 5.18), for the fixed value of ΔT_{pp}, the outlet gas temperature decreases with a steep slope and, for a fixed value of T_6, the higher the pressure ratio, the lower the amount of heat available in the recuperator.
Moreover, if the value of T_6 is decreased, the amount of q_{rec} also decreases progressively. So, for the used value of T_6, the temperature T_D decreases rapidly, and there is a limit value

of pressure ratio, depending on the correspondent value of η_t, above whom the temperature drops down below the constraint value of 145 °C.

As illustrated in figure 5.11, the maximum available pressure is higher for a progressively decreasing turbine efficiency: this is because expander performance decreases with increasing pressure ratio, so, in proportion, more heat is available in the internal recuperator. It is therefore possible to subtract less heat from the gas flow and have a lower decrement in outlet temperature, allowing to reach a higher maximum evaporation pressure compatible with the constraint.
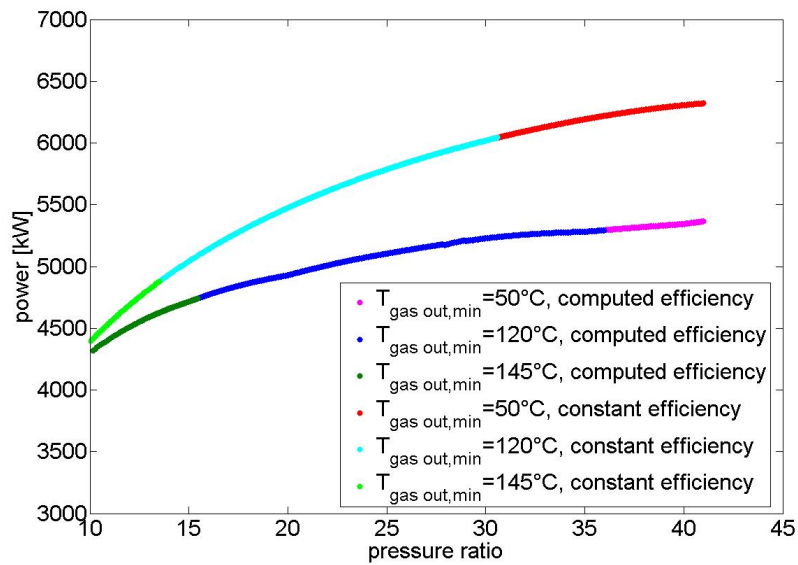
Figure 5.12.: Power output for $T_6 = 513.15$ K and three different minimum outlet gas temperature, for constant and nonconstant turbine efficiency.

The role played by the constraint on T_D is also underlined in figures 5.12 and 5.13, where the output power is reported in two curves, one obtained with a constant-efficiency set equal to 0.8, whilst the other one obtained computing expander performance through the map. The two curves are also reported as a function of three different minimum outlet gas temperatures. As illustrated, a lower value of minimum outlet gas temperature simply extends the available range of pressure: The lower the minimum outlet temperature, the longer the available range for the curves and the higher the difference between the two.

The effect of computing expander performances is reflected in the different trend of the correspondent curve in figure 5.11: moving from the 0.8-constant-efficiency curve to the computed performance one the maximum available power drops down from 4.9 MW to 4.65 MW.
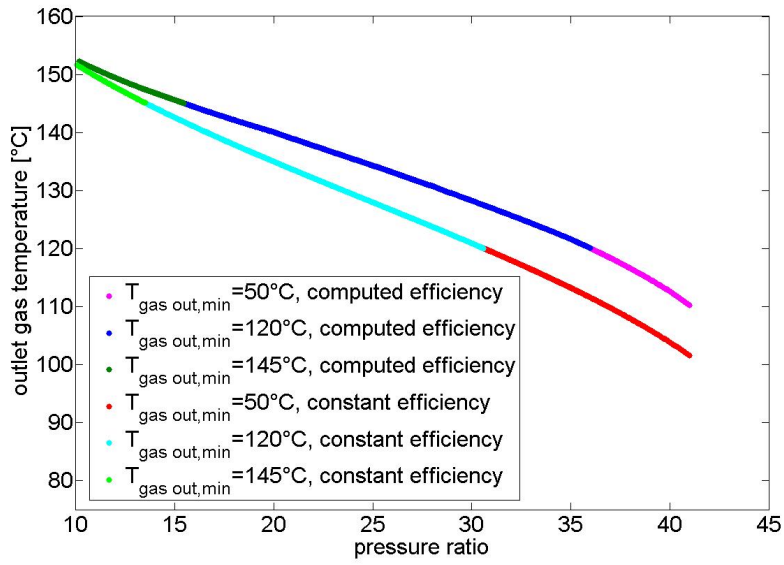
Figure 5.13.: Curves for three minimum values of T_D and $T_6 =$ 513.15 K, for constant and non-constant turbine efficiency.
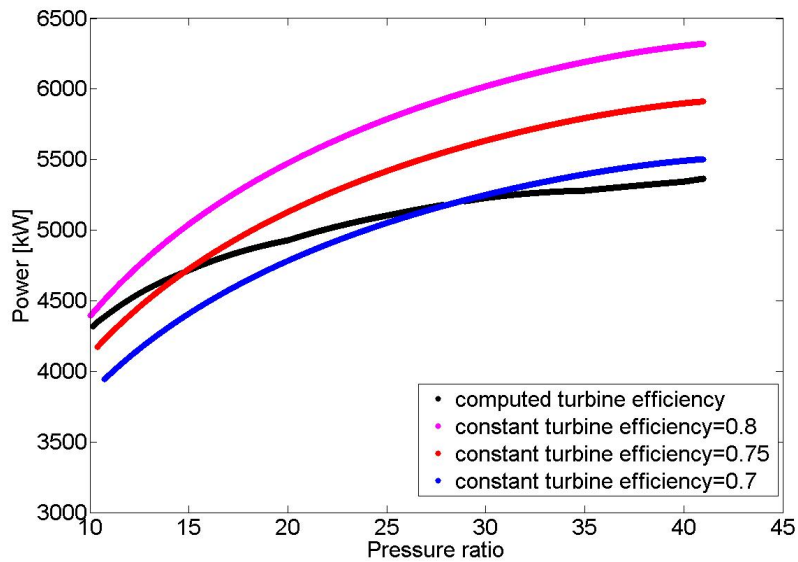
Figure 5.14.: Power output for three different values of constant turbine efficiency in comparison with the computed-efficiency curve (no constraint on minimum outlet gas temperature).

Figure 5.14 shows the same chart without the constraint on exit gas temperature; for a hypothetical minimum value of 50 °C (never reached, however, as shown in figures 5.13 and 5.16) the maximum power output drops down approximately from 6.321 *MW* to 5.365 *MW*.

The plot in figure 5.14 gives a more comprehensive global vision: irrespective of the assumed value of η_t, none on the constant-efficiency curves represents well the whole trend of the computed-efficiency one (black curve); this is due to the progressive decrement of expander performance with increasing pressure ratio, reported in figure 5.15.
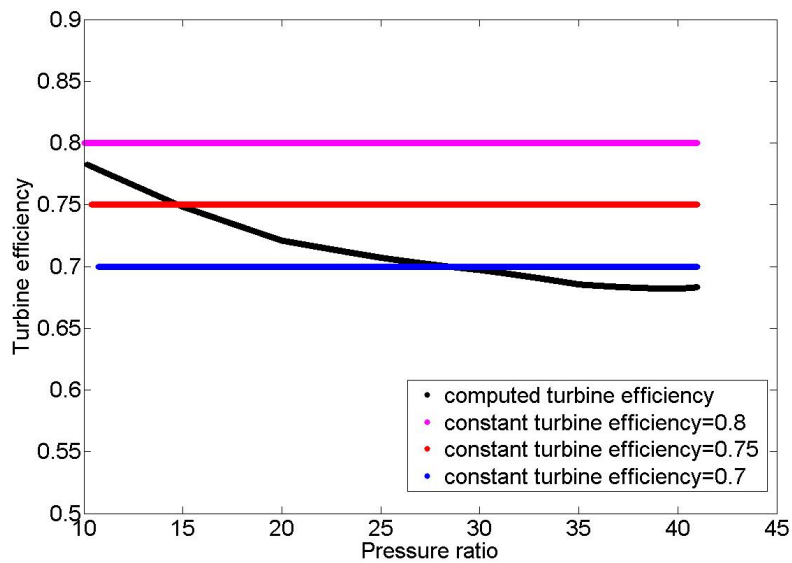
Figure 5.15.: Computed turbine efficiency in comparison with three constant values (no constraint on minimum outlet gas temperature).

The computed value of η_t progressively decreases from 0.7826 to 0.67, crossing the horizontal lines of constant efficiency. The crossed points correspond to the values of pressure ratio for which η_t coincides with the assumed constant value.

The outlet gas temperature chart (figure 5.16) shows an inverse trend: considering that, for a given TIT and pressure ratio, the higher the expander performance, the lower the exploitable heat in the recuperator (so the lower the outlet gas temperature), the slope of the computed-turbine efficiency curve progressively decreases, accounting for the increasing recoverable heat at turbine outlet.

As reported, in the most general case the limit on power is the maximum available pressure ratio. This means that a further increment in electric output could be achievable increasing the evaporation pressure even more. However, the power curve in
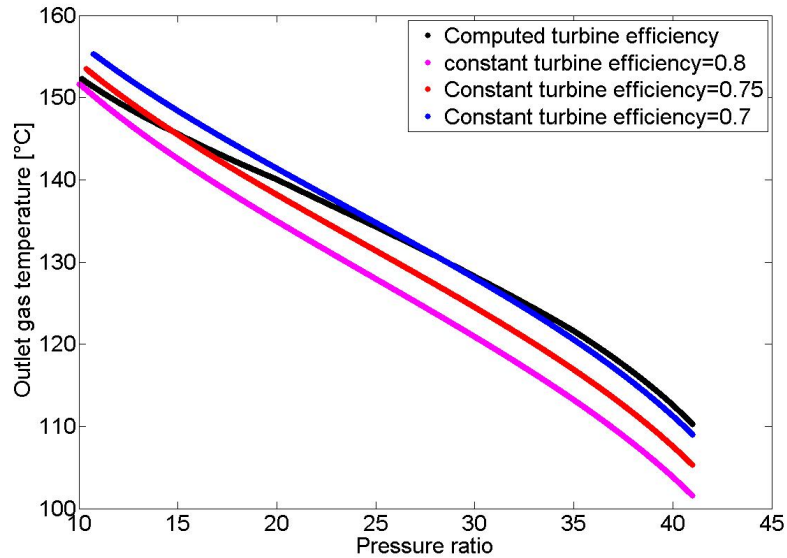
Figure 5.16.: Trends of outlet gas temperature for three different values of constant-turbine efficiency, in comparison with the computed-efficiency curve (no constraint on outlet gas temperature).

figure 5.14 obtained computing turbine efficiency, shows a progressively flattening trend for increasing values of pressure ratio. So, after a certain threshold, the increment in power could not be enough significant to justify the technological (and economic) effort to reach higher pressure levels. Thus, it should be noted that, for the sake of a complete techno-economic optimization, it is necessary to compute the effective expander performance, being the slope of power curve flattening with pressure ratio: this can deeply modify the effective revenue and so the real profitability of a high-pressure cycle, considering that high pressures lead to higher investment costs and increased complexity [9].

The T-S diagram of the two maximum-power configurations accounting for the limit on outlet temperature is now presented in figure 5.17, while the most important parameters are reported in table 5.1. Figure 5.18, in the end, reports The T-S diagram for the maximum-power configuration without the constraint on outlet gas temperature.

As already discussed, the maximum available evaporation pressure is the one consistent with the constraint on minimum T_D. That explains why in figure 5.17 point 7 (turbine outlet) is the same for both the cases.
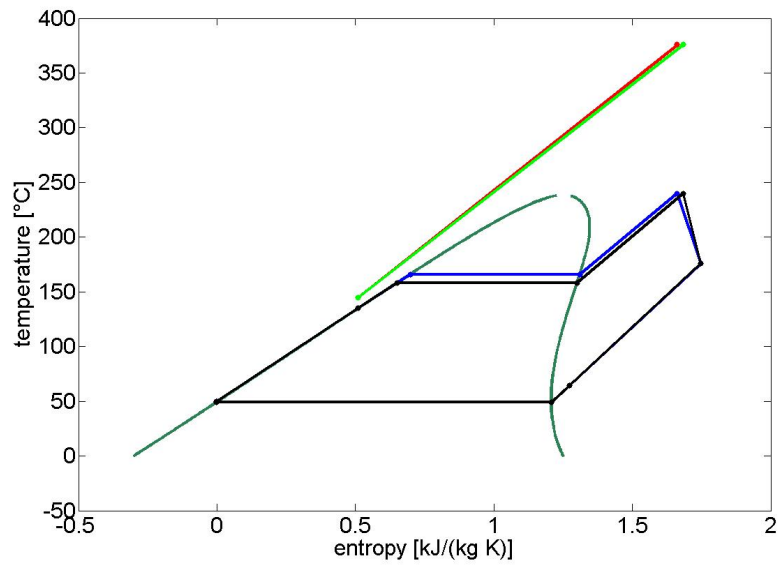
Figure 5.17.: T-S diagram for the two maximum-power configurations for both the computed and constant turbine-efficiency case (blue and black, respectively).

Table 5.1.: Cycle parameters for the two maximum-power configurations, with constant and computed turbine efficiency.

Parameter	Unit	$\eta_t = 0.8$	computed η_t
W_{el}	MW	4.881	4.711
P_6	bar	13.54	15.9
T_6	K	513.15	513.15
T_D	°C	145	145
η_{ORC}	—	0.2056	0.198
η_t	—	0.8	0.7346
$\dot{m}_{ORC}$	kg/s	45.64	46.054
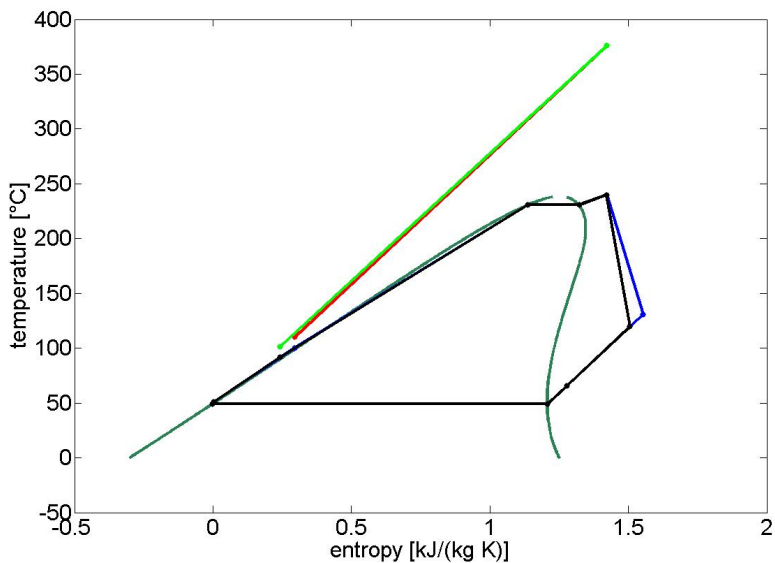
Figure 5.18.: T-S diagram for the two maximum-power configurations for both constant and computed turbine efficiency cases (black and blue, respectively), with no constraint on outlet gas temperature.
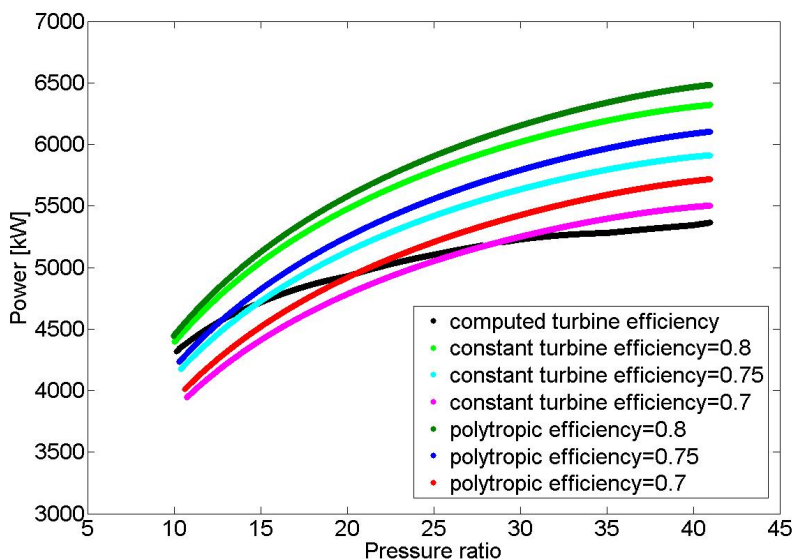
Figure 5.19.: Output power for three different constant-turbine efficiencies, computed expander performances and polytropic efficiency.
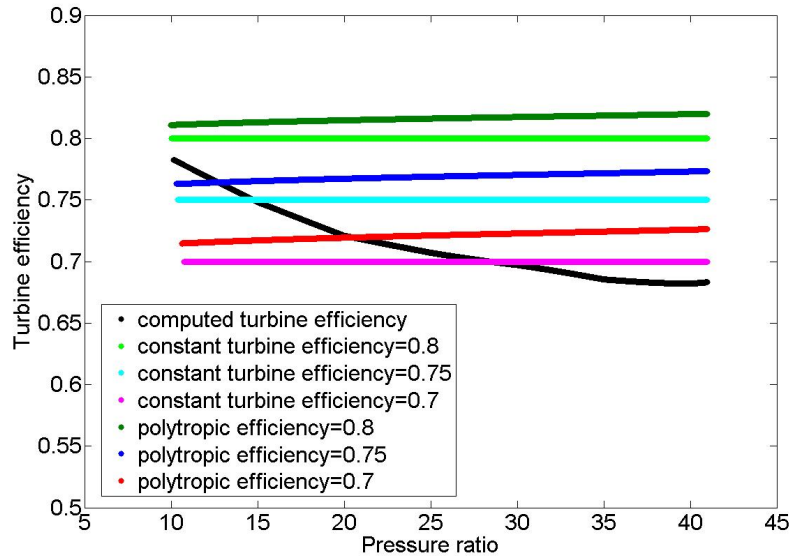
Figure 5.20.: Computed turbine efficiency, both with η_{pol} and map, in comparison with three different constant values.

Finally, figures 5.19 and 5.20 show the comparison with the results obtained assuming a polytropic efficiency. As discussed in section 2.3.1, the polytropic efficiency allows to account for a partial recovery of work throughout the expander. This means there is a slight benefit for high values of pressure ratio in comparison to the constant-efficiency assumption. However, with respect to the behaviour predicted by the map, the difference is even higher, because the latter shows a progressive decrement in efficiency with increasing pressure ratio, which far overbalances the little benefit due to energy recovery.

5.2.1 *Test with double exhausted gas mass flow rate*

The purpose of this test is twofold:

1. It allows to observe the different behaviour of turbine efficiency shifting the range of mass flow rates towards higher values in the map in figure 5.1;

2. It has also a relevant interest for this specific case of study: as previously described in section 3.1, there are three gas turbines on the offshore platform, two of whom are constantly operative; until now, it has only been considered to link the waste heat recovery unit only to one of the two exhausted gas flows. One could also be interested in exploiting both the fluxes of exhausted gas: this test shows that there is a benefit in output power if just one waste heat recovery unit is built exploiting both the two flows

rather than two smaller separate bottoming cycles, each of them linked just with one gas turbine. The plant scheme is now the one reported in figure 5.21.
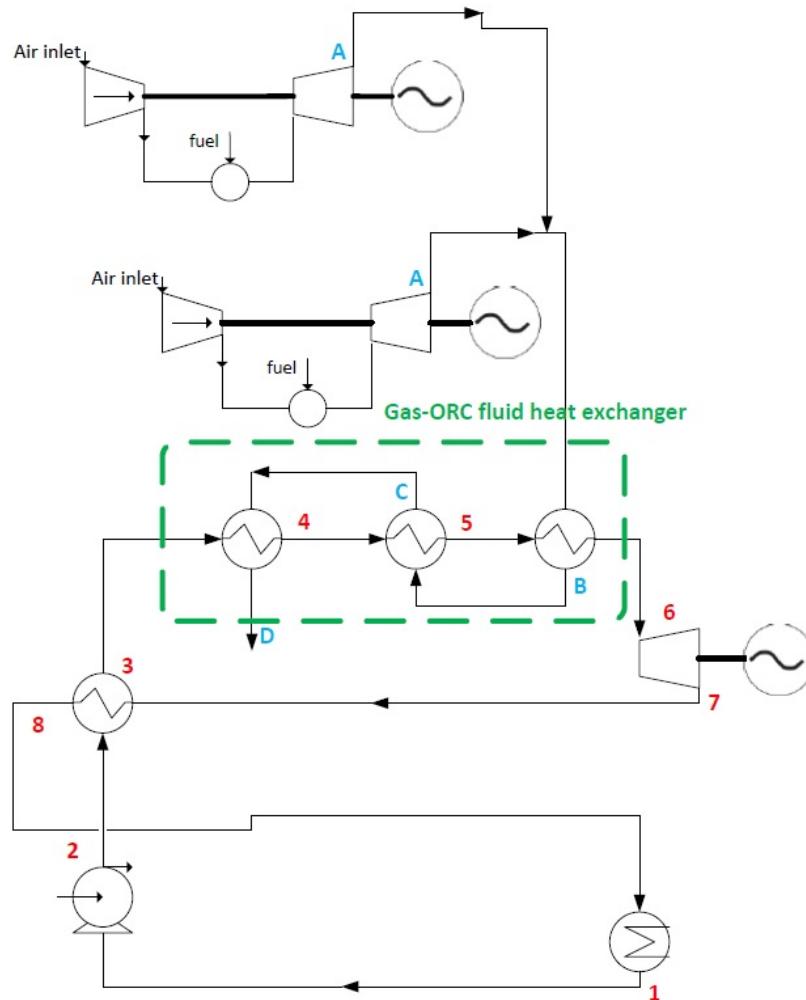
Figure 5.21.: ORC plant scheme for the case with double exhausted gas mass flow rate.

The main difference in the ORC plant is the possibility to have almost a doubled mass flow rate with respect to the previous case (figures 5.22 and 5.23). As reported in figures 5.24 and 5.25, the trend of power and mass flow rate curves is the same as the previous test: however, the power obtained in the computed-efficiency curve is proportionally higher than in the previous case, being the obtained values of turbine efficiency higher as well, as shown in figure 5.26, which accounts for the most general case with no outlet gas temperature constraint.
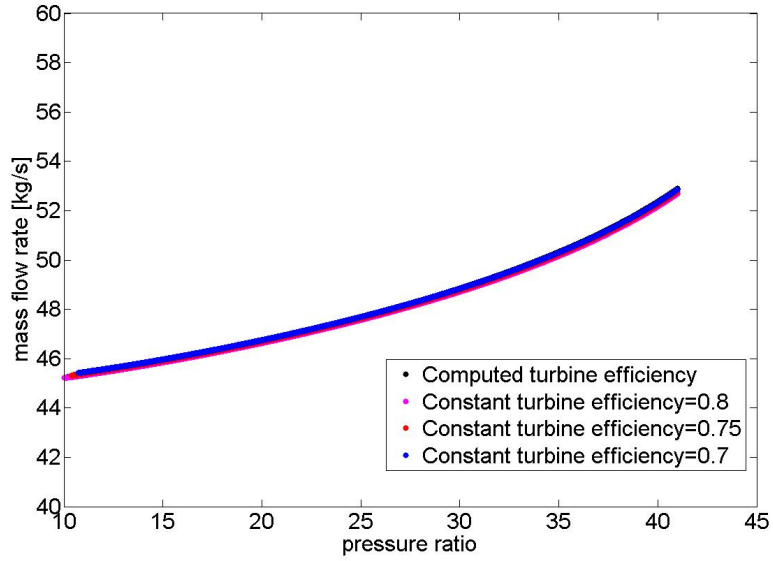
Figure 5.22.: Mass flow rate for three levels of constant turbine efficiency and computed-performance test (no constraint on outlet gas temperature.)
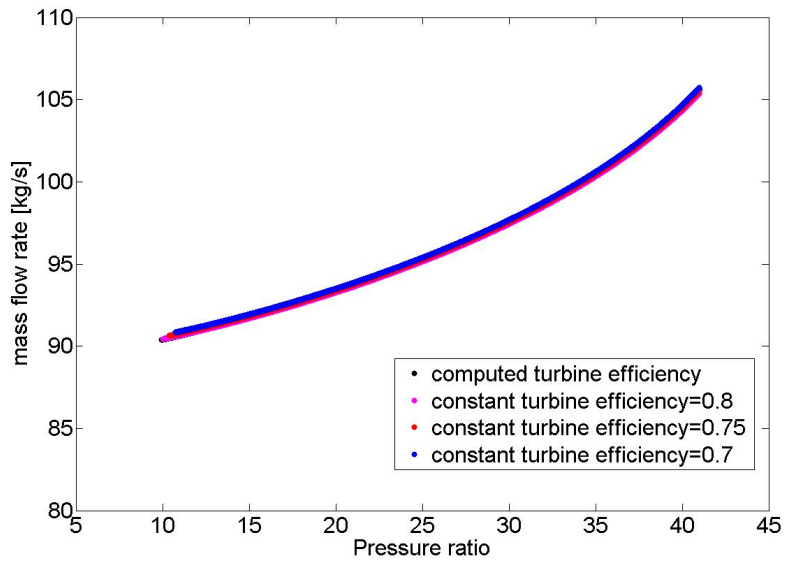
Figure 5.23.: Mass flow rate for 3 levels of constant turbine efficiency and computed-performance test, for a doubled value of exhausted gas mass flow rate (no constraint on outlet gas temperature.)

As illustrated in figures 5.24 and 5.27, with the aforementioned constraint on outlet gas temperature, the pressure leading to the maximum power, both for the 0.8-efficiency curve and the computed-efficiency one is almost the same, being this time the computed efficiency close to 0.8. The most important results for the two maximum-power configurations, accounting for the constraint on T_D, are listed in table 5.2. It is worth noting that, for the constant-turbine-efficiency test, the obtained results are exactly the same as the ones reported in table 5.1 on page 65, with the obvious exception of the doubled values of mass flow rate and power. Indeed, for the same T-S diagram, a double value of exhausted gas mass flow rate simply leads to a double $\dot{m}_{ORC}$. The obtained results for the computed-efficiency test are conversely different than the ones in table 5.1, due to the different value of expander efficiency. Table 5.2 reports the benefit in power output due to the increment in exhausted gas mass flow rate and turbine efficiency is more than doubled. The power increases from 4700 kW (value obtained in the previous test) to 9719 kW, with a relative increment of about 3.4%. In the most general case, without accounting for the outlet gas temperature constraint, the power rises from 5.635 MW to 11.4 MW, with a relative increment of 6.24%.

Table 5.2.: Cycle parameters for the two maximum-power configurations with a double value of exhausted gas mass flow rate, for constant and computed turbine efficiency.

Parameter	Unit	$\eta_t = 0.8$	computed η_t
W_{el}	MW	9.763	9.719
P_6	bar	13.54	13.86
T_6	K	513.15	513.15
T_D	°C	145	145
η_{ORC}	—	0.2056	0.2046
η_t	—	0.8	0.7903
$\dot{m}_{ORC}$	kg/s	91.29	91.4
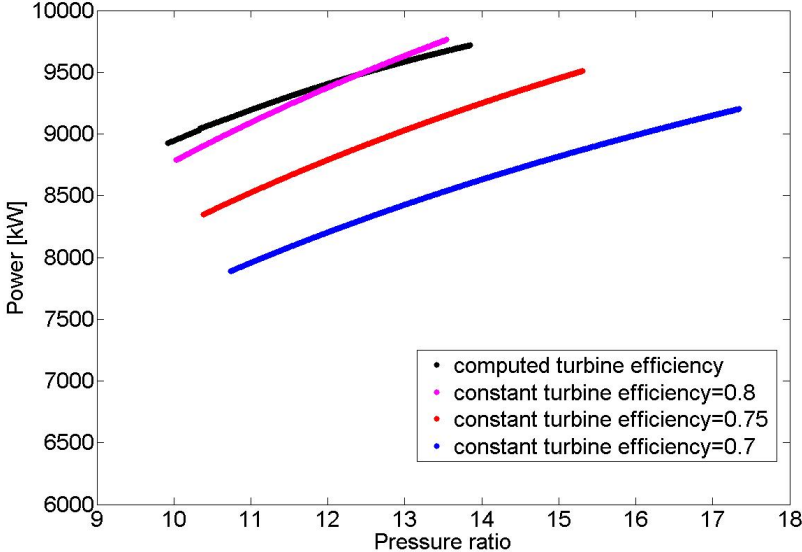
Figure 5.24.: Power output for three levels of constant turbine efficiency and computed-efficiency test, for a doubled value of exhausted gas mass flow rate.
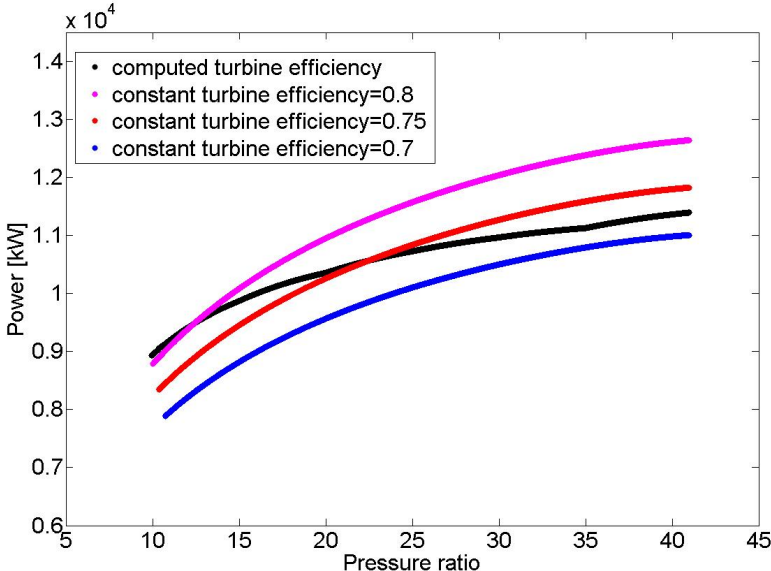
Figure 5.25.: Power output for three levels of constant turbine efficiency and computed-efficiency test, with no constraint on outlet gas temperature.
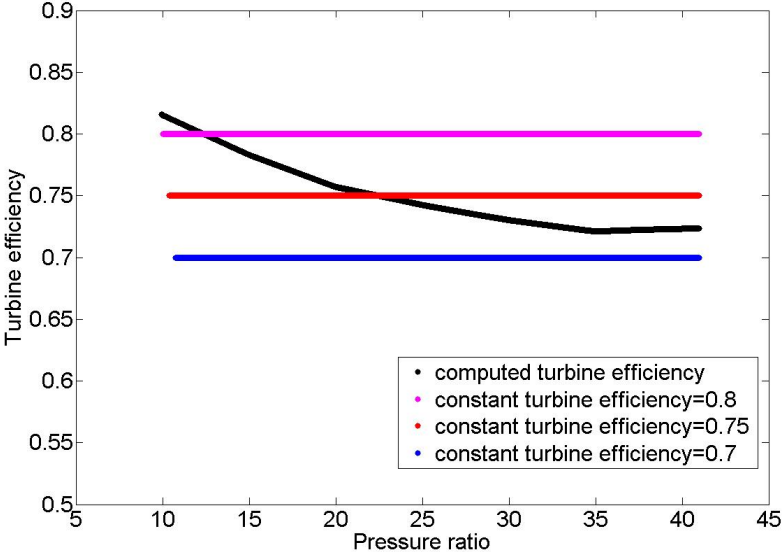
Figure 5.26.: Three levels of constant turbine efficiency in comparison with the computed-efficiency curve (no constraint on outlet gas temperature).
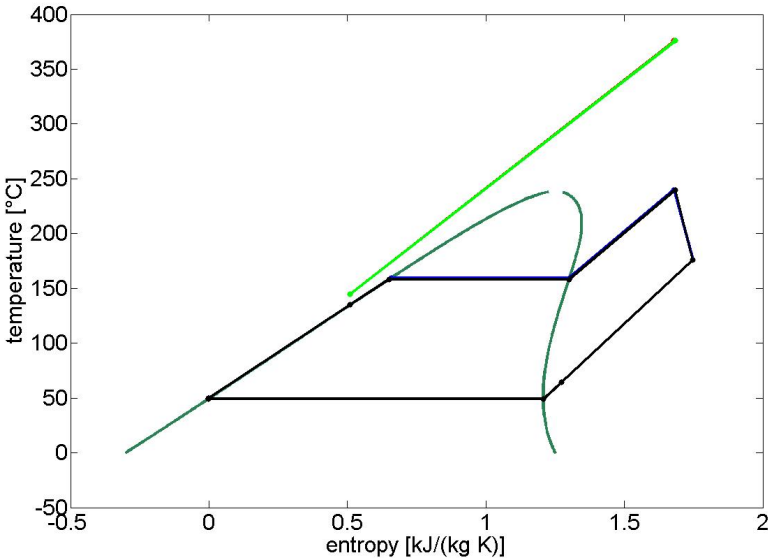
Figure 5.27.: T-S diagram for the two maximum-power configurations with constant and computed turbine efficiency (double exhausted gas mass flow rate).

In this section the effect of a gearbox insertion is examined with respect to the whole cycle performance. For a more general overview, only the charts without constraint on outlet gas temperature are reported.
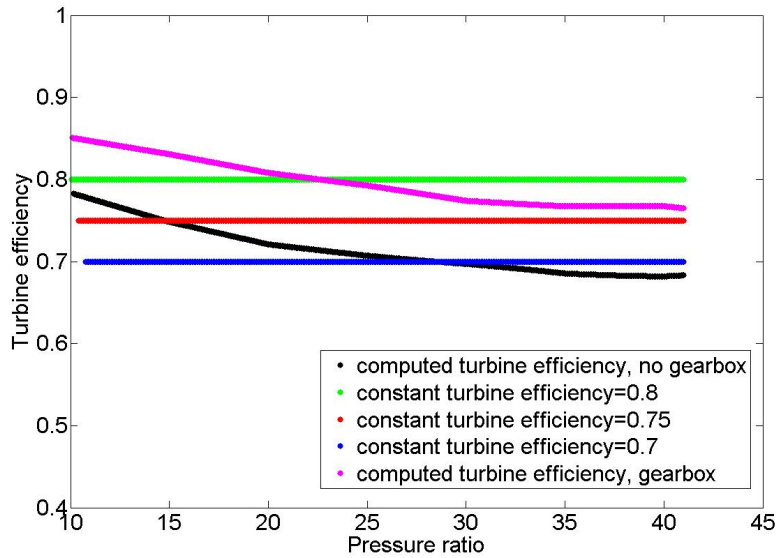
Figure 5.28.: Turbine computed efficiency both for fixed and optimized rotational speed, in comparison with constant efficiency lines.
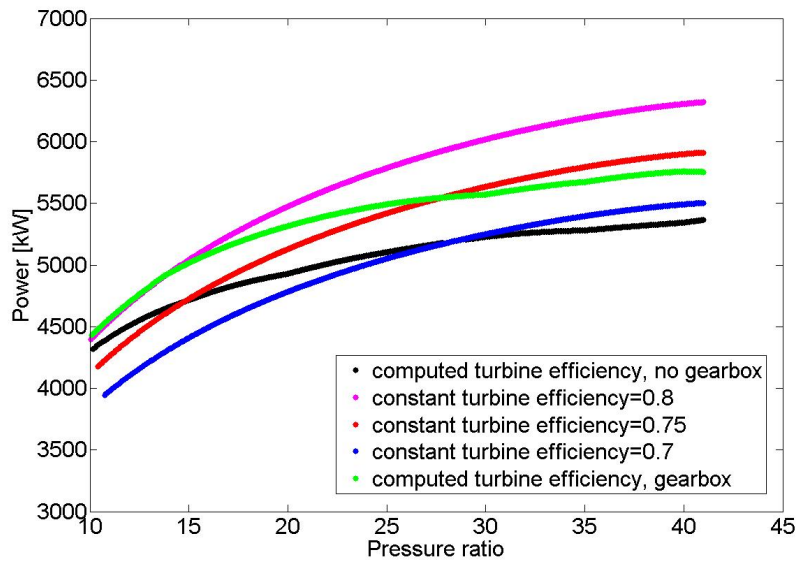
Figure 5.29.: Electric power for both the tests with fixed and optimized rotational speed, in comparison to the trends obtained with constant-efficiency assumption.

As reported in figure 5.28, the new degree of freedom allows to achieve a higher turbine efficiency, leading to a benefit of about 500 kW in comparison with the case where rotational speed is fixed to 3000 rpm (figure 5.29). This is because, as already shown in figure 5.8, the optimal value of rotational speed, in the range of mass flow rate of interest, appears to be significantly different from 3000 rpm. The trend of the two computed-efficiency curves is similar:

- Both of them cross the power curves obtained with a "constant efficiency" assumption, showing that a map is necessary for both the cases to account for real expander performance in the whole possible range of solutions;

- both of them tend to flatten after a pressure ratio of about 30, making the effort to reach more severe cycle operating conditions of questionable effectiveness.
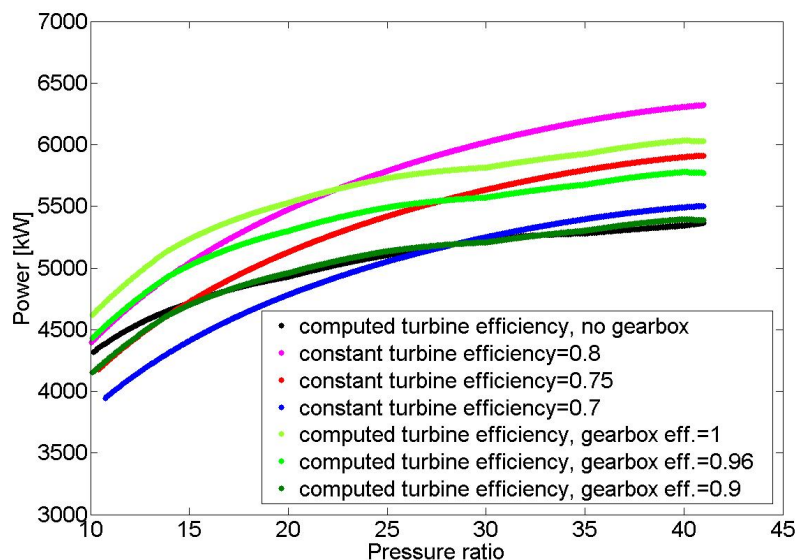
Figure 5.30.: Cycle electric power for three different values of gearbox efficiency.

Some comments are also necessary about gearbox efficiency. In figures 5.28 and 5.29 a value of $\eta_{gear} = 0.96$ has been used to account for losses in mechanical transmission: the gearbox is not, indeed, an ideal component and its efficiency could play an important role in final power output; the chart in figure 5.30 shows the generated power for three different values of gearbox efficiency. As illustrated, even with a better expander performance, a value of η_{gear} below 0.9 invalidates the benefit of its insertion with respect to the curve for fixed rotational speed. This analysis is also important considering that detailed information about weight, cost and efficiency of gearboxes are not

easily available in literature, being these components expressly realized under specific order for the particular turbine. Usually the efficiency in mechanical transmission is higher than 95%, but figure 5.30 underlines the more complex and expensive turbine set up is justified only if the mechanical transmission efficiency is above this value. Moreover, for this present case of study, the weight and volume of the gearbox should also be at least estimated, being an important issue in offshore platforms [7].

Finally, an estimation of the possible economic benefit due to gearbox insertion is given in terms of net present value difference. For three values of pressure ratio, identifying three correspondent cycle configurations, the net present value difference between the tests with and without gearbox is provided[2]; the examined level of pressure ratio are:

- $P_r = 41$: for this value the maximum power output is reached for both the cases;

- $P_r = 28.3$: from this value on, both the curves of power in figure tends to flatten, reducing the increment in power output for higher pressure ratio;

- $P_r = 12.8$ for the case with gearbox and $P_r = 15.45$ for the case without gearbox: these two values of pressure ratio are the maximum available for the two configurations when the constraint of minimum outlet gas temperature is considered.

The net present value difference is obtained through the methodology described in section 3.7 and the results are reported in table 5.3. Even if with a certain level of approximation, the results show the gearbox insertion seems profitable. The utilization factor h_u plays obviously a key role: as reported in table 5.4, a value of $h_u = 50\%$ (4380 hours/year) almost halves the net present value difference and revenue, estimating also the non-profitability of gearbox insertion for low values of pressure ratio.

The chart in figure 5.31 reports the trend of the net present value difference as a function of pressure ratio for the examined two values of utilization factor (4380 and 7000 hours per year, corresponding to 50% and 80% of total hours per year). It is interesting to note that, when the utilization factor is set to 7000, the maximum amount of net present value difference, that is, the net profit due to gearbox insertion, corresponds almost to 5% of the NPV found by Pierobon et al. [7], whose

---

2 For this test, again, a value of $\eta_{gear} = 0.96$ has been used.

Table 5.3.: Results of net present value difference for the three examined configurations and $hu = 7000$.

Parameter	Unit	no gearbox	Gearbox
W_{el}	kW	5364.9	5753.5
P_r	–	41	41
$\dot{m}_{ORC}$	kg/s	53	53
η_{ORC}	–	0.16	0.1717
η_t	–	0.683	0.7629
$T_{gas,out}$	°C	110.24	104.85
NPV_{diff}	€	–	$9.0915 \cdot 10^5$
W_{el}	kW	5188.9	5553.6
P_r	–	28.3	28.3
$\dot{m}_{ORC}$	kg/s	48	48
η_{ORC}	–	0.1548	0.1657
η_t	–	0.7	0.78
$T_{gas,out}$	°C	130.37	124.72
NPV_{diff}	€	–	$8.9217 \cdot 10^5$
W_{el}	kW	4741.9	4800
P_r	–	15.45	12.8
$\dot{m}_{ORC}$	kg/s	46	45
η_{ORC}	–	0.19972	0.2022
η_t	–	0.74581	0.84
$T_{gas,out}$	°C	145	145
NPV_{diff}	€	–	$1.1687 \cdot 10^5$

results are reported in table 5.5. A different estimation, assuming a constant specific cost of $C_{spec} = 1000$ €/kW according to Quoilin et al. [9], seems to confirm the obtained results, even with different values.

In this test, for the case with gearbox, the cost of this latter component has been calculated as the 40% of the generator cost, expressed in equation 3.29 in section 3.7 and added to the total cost. Figure 5.32 reports the obtained values of net present value for two different utilization factors. It is worth noting the assumption of $C_{spec} = 1000$ €/kW seems however optimistic if compared to the specific cost obtained by Pierobon et al. [7] (see table 5.5).

To conclude, from all discussed above, the gearbox insertion seems to increase the revenue for values of pressure ratio greater than 15. Nevertheless, its profitability requires further inquiries, especially a realistic estimation of working time and effective load regime.

Table 5.4.: Results of net present value difference for the three examined configurations and $hu = 4380$.

Parameter	Unit	no gearbox	Gearbox
W_{el}	KW	5364.9	5753.5
P_r	—	41	41
$\dot{m}_{ORC}$	kg/s	52,894	52,751
η_{ORC}	—	0.16	0.1717
η_t	—	0.683	0.7629
$T_{gas,out}$	°C	110.24	104.85
NPV_{diff}	€	—	$4.018 \cdot 10^5$
W_{el}	KW	5188.9	5553.6
P_r	—	28.3	28.3
$\dot{m}_{ORC}$	kg/s	48,422	48,322
η_{ORC}	—	0.1548	0.1657
η_t	—	0.7	0.78
$T_{gas,out}$	°C	130.37	124.72
NPV_{diff}	€	—	$4.2146 \cdot 10^5$
W_{el}	KW	4741.9	4800
P_r	—	15.45	12.8
$\dot{m}_{ORC}$	kg/s	45,974	45,323
η_{ORC}	—	0.19972	0.2022
η_t	—	0.74581	0.84
$T_{gas,out}$	°C	145	145
NPV_{diff}	€	—	$-1.2 \cdot 10^5$

Table 5.5.: Estimated total investment cost and net present value for the case of study, Pierobon et al. [7].

Parameter	Unit	Value
Output power	MW	6.43
NPV	M$	20.1
hu	hours/year	7000
conv. Factor [43]	$/€	0.7936
Total investment cost	M€	10.95247
Specific cost	€/kW	1703
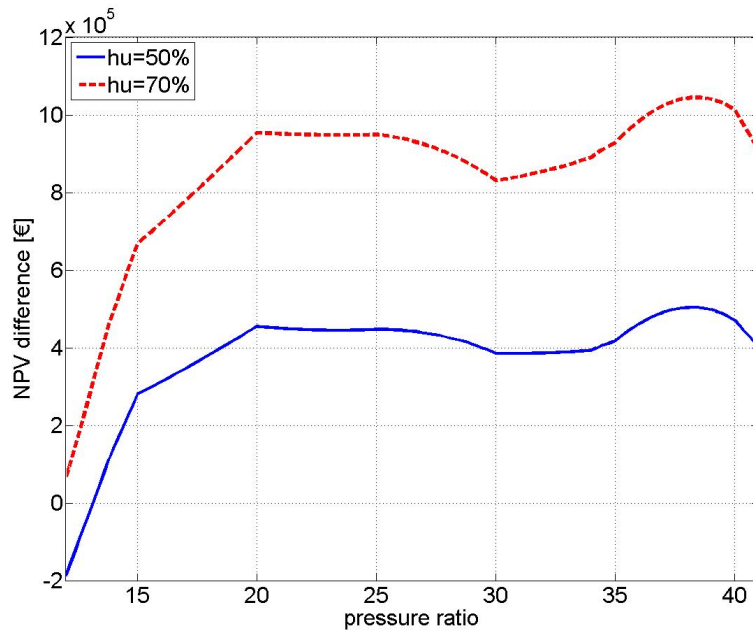
Figure 5.31.: Net present value difference between the cases with and without gearbox, for two different values of utilization factor.
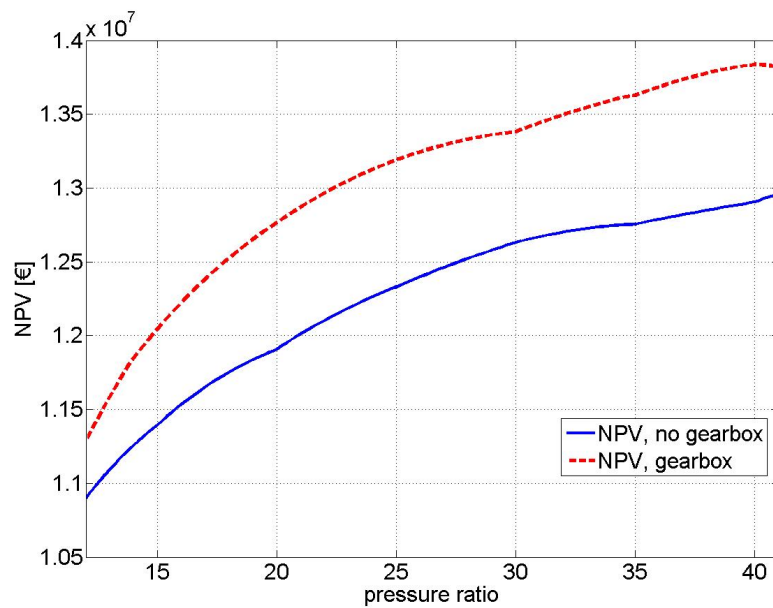
Figure 5.32.: Net present values obtained for $C_{spec} = 1000$ €/kW and $hu = 7000$ hours/year.

5.4 TURBINE TECHNO-ECONOMIC OPTIMIZATION

The results obtained for the specific-cost optimization are presented in the following charts, in comparison with the correspondent values obtained for the "traditional" turbine optimization process. As reported in figure 5.33, the results are quite similar but not identical: for each test performed, the specific cost is always lower for the techno-economic optimization. However, the difference between the two correspondent obtained results is always relatively small.
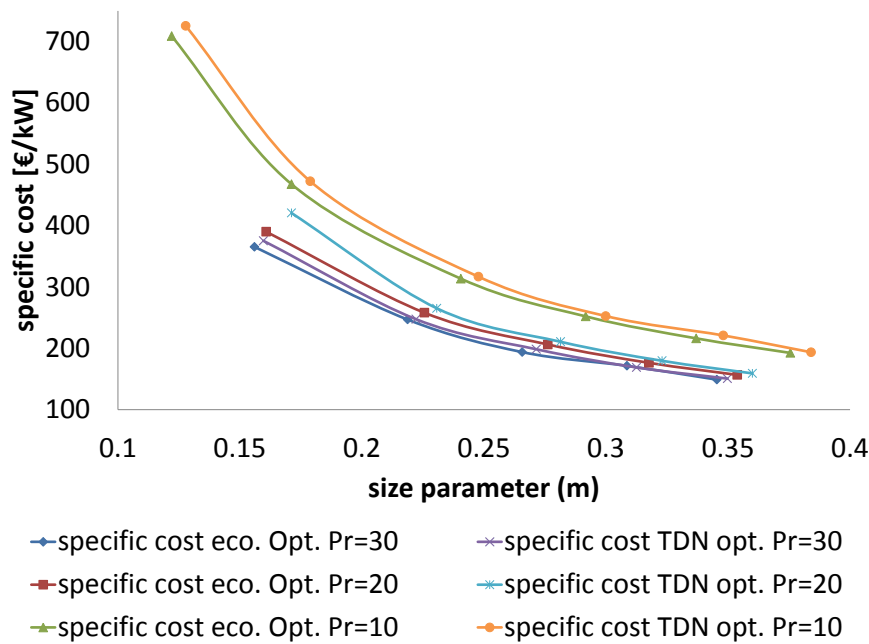
Figure **5.33.**: Specific cost for both thermodynamic and techno-economic optimization, for several values of size parameter and pressure ratio.

For a given set of inlet and boundary conditions, from a theoretical point of view, to maximize the efficiency means to increase the output power and so, this would lead to the minimization of specific cost. However, turbine cost is in principle more strongly related to its volume, rather than efficiency; a useful indication of expander volume is provided by the size parameter, that is the effective number contained inside the cost function in equation 3.18.

According to this formula, to minimize the turbine cost coincides with the minimization of the size parameter which in turn, is a function of the outlet volumetric flow rate. A reduction of $\dot{V}_{out}$ means a higher ρ_{out} and a minor expansion so, at last, a lower efficiency. Therefore, the research of the best efficiency and the reduction of the size parameter are not independent paths: for given boundary conditions, an excessive

reduction of size parameter could lead to low efficiency and so to bad performance in terms of output power, without obtaining therefore an effective reduction of specific cost.

As confirmed by figure 5.33, for each set of boundary conditions there is a range of values for η_t and SP within whom the relative reduction of size parameter is beneficial for the specific cost, irrespective of the correspondent reduction in efficiency. As also reported in figure 5.34, the distance between the curves (representative of this range) is relatively narrow, but the obtained efficiency for a techno-economic optimization is always lower than the corresponding one for the thermodynamic optimization. Figure 5.35 shows the distance between the specific cost curves is substantially reflected in the distance between volumetric flow ratio curves.

Even though the obtained results show a certain difference between the output given by the two optimization processes, this interval is enough narrow not to make possible to state whether there is a certain convenience in adopting this approach with respect to the traditional one, considering also the uncertainty of genetic algorithm and cost function.
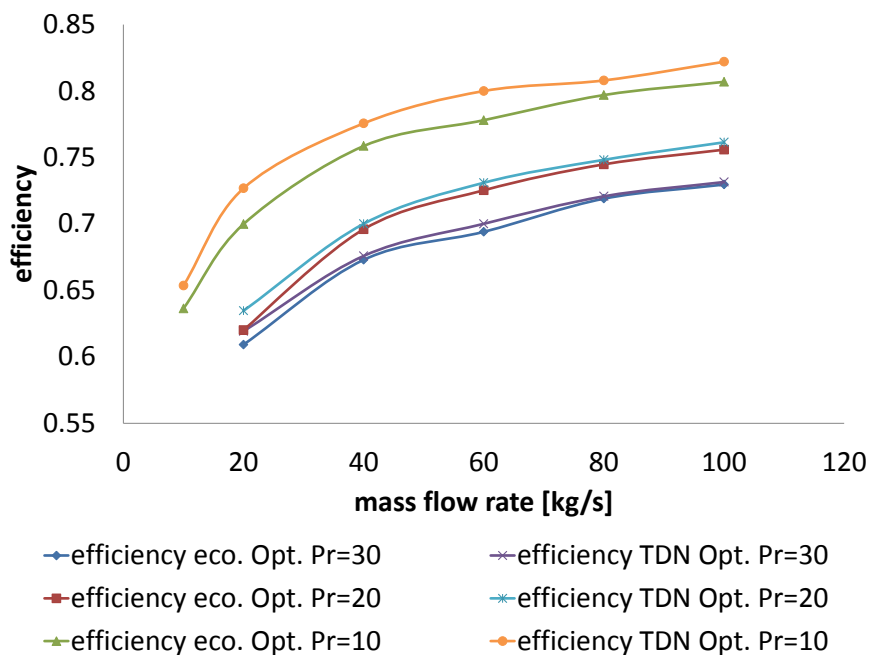
Figure 5.34.: Efficiency for both thermodynamic and techno-economic optimization, for several value of mass flow rate and pressure ratio.
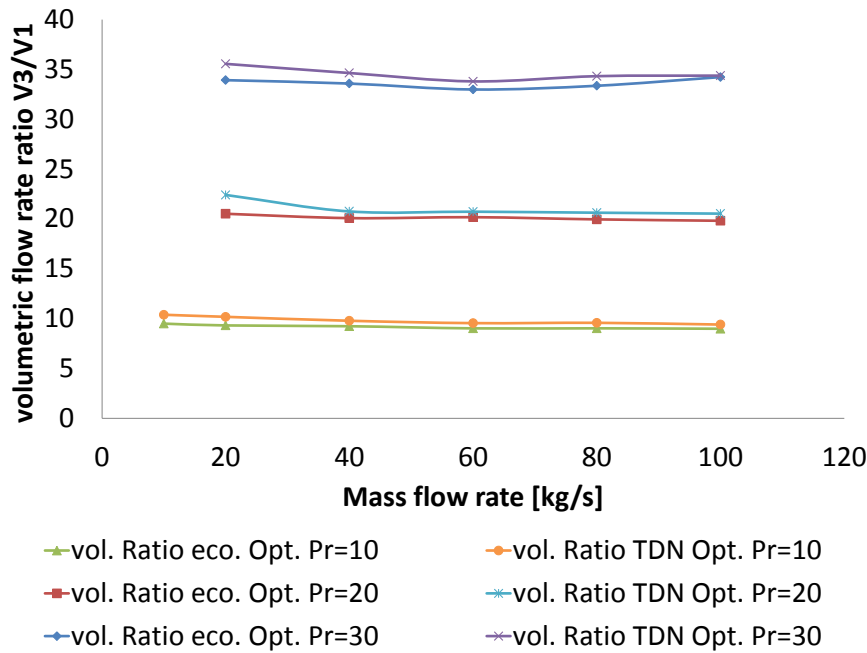
Figure 5.35.: volumetric flow rate ratio $\dot{V}_3/\dot{V}_1$, for both thermodynamic and techno-economic optimization, for several value of mass flow rate and pressure ratio.

5.5 DISCUSSION OF UNCERTAINTIES

As reported in all the figures in section 5.1, the curves of turbine efficiency computed through the maps exhibit a slight fluctuating behaviour: this uncertainty in all the obtained results is due to the approximation and level of accuracy contained in the achieved values of turbine efficiency reported in the maps in figures 5.1 and 5.7.

These data, in turn, are mainly a function of the constraints imposed over the computational routine and accuracy of genetic algorithm which, due to its intrinsic functioning, is affected by a certain component of randomness (see appendix A). As described in chapter 3, some of the applied constraints are due to technological reasons, some to guarantee the validity of the used correlations, some others to ensure the assumption of radially-constant-axial velocity and density profile leads to sufficiently accurate results in the whole solution research span. As also discussed in section 5.1, some constraints play a significant active role on the acceptable solutions and so on the available set of optimizing turbine parameters.

The attainment of many boundary values imposed by these bonds causes the obtained solutions to be slightly superimposed. In fact, for the highest values of pressure ratio, the range of useful values for the eight optimizing parameters is restricted, making the obtained turbine geometric configurations

rather similar as well as, consequently, as the correspondent values of efficiency.

About the uncertainty related to genetic algorithm, it is worth noting that, especially for the map with fixed rotational speed, some episodes of "numerical routine blockage" have been experienced: for some combinations of mass flow rate and pressure ratio, the GA got stuck around a certain value of efficiency without being able to produce different results, so that for some cases more than one optimization had to be performed. For some of them it was observed that, even with a small increase in population size and/or number of generations (see appendix A), no instability arose while for others a more consistent increment in both the parameters was necessary to prevent GA getting stuck during the optimization.
The first map was generated with a starting value of 550 for population size and 150 generations, but for some cases the population size has been risen up to 700. For the second map, in order to account for the addition of one more parameter and the increase of possible solutions, the starting value of population size was set to 650 with 150 generations, but if launched, the second optimizations were performed with 200 generations and a value of 800 for population size. It should be noted the optimal value of these parameters can not be established a priori: in particular, in the context of optimizing turbine design including also rotational speed, it was found that, for some cases, the same population size and number of generations lead to acceptable results in two-three days, while for others the computational time rose up to five-six days. For this latter cases an increase in both the two parameters leads to higher efficiencies and reduces the computational time, while for the first ones a bigger population size and generations number only increases the computational time with no appreciable benefit in output.

Finally, it is also worth reporting that even the possible contribution of the interpolating function in the turbine maps has been examined: as shown from figure 5.1, many optimizations have been performed for values of mass flow rate between 38 and 54 kg/s, being this the active range of mass flow rates in the cycle for the present case of study. However, the increase in data has not brought any appreciable difference in cycle results.

CONCLUSIONS AND POSSIBLE FUTURE WORK

Here the main topics and achieved conclusion of this present work are reported:

- A pre-existing computational code, capable of optimizing the geometry of a single-stage axial-flow turbine to produce the best efficiency for a specific value of inlet temperature, mass flow rate, pressure ratio and rotational speed has been improved and adapted to the purpose of this present work. The code has reported appreciable agreement with previous similar reliable models but some limits have also been identified, mainly due to its incapability to account for radial equilibrium effects; many constraints have been applied in the computational routine to restrain this effect, as well as to ensure the validity of employed correlations and reliability of results from both a technological and thermodynamic point of view;

- The code has been integrated in a complete ORC model and applied in the context of the Draugen offshore platform.
  Two turbine maps have been build, the first one under the assumption of fixed rotational speed, the second one considering this latter parameter among the optimizing ones. Even with different values, both the maps show a similar trend of efficiency, which increases for higher values of mass flow rate and lower values of pressure ratio. For the highest amounts of this latter parameter, many threshold values imposed by constraints, as well as many upper and lower bounds of the optimizing parameters are reached: this causes the obtained geometries to be similar and sometimes superimposed;

- For the present case of study, the minimum value of exhausted gas outlet temperature appears to be the most active constraint. If this constraint is disabled, it is possible to reach higher level of pressure with an increase in output power. For both these cases, the results obtained computing expander performance have been compared with the ones predicted by a constant-turbine-efficiency cycle model; the power curves show a different trend, and no curve based on a constant-efficiency approach can reproduce the behaviour of the one computing expander perfor-

mance: for the case with fixed rotational speed, the efficiency progressively drops down from 0.78 to about 0.67, causing the power curve to flatten and making difficult to evaluate the real optimal configuration from a techno-economic point of view. This demonstrates a turbine map is important for the sake of further investigations.

- The possibility of exploiting also two exhausted gas flows from both the main turbines has been considered. This substantially implies a double value of organic fluid mass flow rate, with a benefit in produced power: due to the increase of turbine efficiency, indeed, the final electric output is more than doubled;

- The optimization of rotational speed increases markedly expander efficiency (values below 0.75 are almost never reached), showing an improvement in output power of about 500 kW in the most general case. However, the insertion of a gearbox implies an additional cost, weight and volume. Only a very rough estimation about the cost is possible and the real profitability of a gearbox insertion should be carefully evaluated, being also weight and volume an important constraint on offshore platforms. The first estimation of possible revenue has been calculated as the difference between the net present value obtained for two plant configurations, respectively with and without gearbox, showing the utilization factor plays a fundamental part in the final result. The gearbox insertion seems profitable, but a more detailed analysis is required to establish the effective convenience.

- A techno-economic optimization of the turbine has been performed for three levels of pressure ratio. In this process, the specific cost, instead of turbine efficiency, has been chosen as the optimizing function. The obtained results are very close to the ones achieved with the "classical" thermodynamic optimization; however, even if there is a range of values for size parameter among which a reduction in fluid expansion (so in efficiency) leads to a benefit in specific cost, this interval is enough narrow not to make possible to state whether there is a certain convenience in adopting this approach with respect to the traditional one.

6.0.1 *Future work*

Here some suggestions for future work are given:

1. The Code structure can be improved, at least considering three levels of blade height to account for fluid variations in radial direction. It would be possible to find out if the higher computational effort is justified in terms of better prediction of efficiency and turbine performances;

2. The off-design performance of the expander can be evaluated: this would be interesting, considering the request of electric energy in the platform is not constant and the turbine is likely to work in part-load regime most of time. Indeed, the analysis of turbine off-design performance can lead to a more accurate estimation of the effective revenue. Both the cases taking into account just one or two gas-turbine exit flows could be examined and compared;

3. A more complex cycle model accounting also for heat exchanger dimensions (and cost) as well as turbine weight and volume can be set up. This would allow to refine the economic analysis here performed, especially to evaluate the real profitability of a gearbox insertion accounting also for eventual weight and volume constraints as well as the aforementioned off-design considerations;

4. It would be interesting to improve the computational code in order to optimize the design of a two-stage turbine. It has been shown there is a maximum available pressure ratio with just one stage: the implementation of a second one could increase the efficiency of the whole expander, possibly making interesting also to set up a supercritical cycle configuration; however, the higher the number of stages, the higher the cost, so it would be worth finding out if there is a real benefit in purchasing a larger and (hopefully) more efficient turbine, both from a thermodynamic and economic point of view, considering also weight and volume are parameters whose importance should not be underestimated in the context of offshore platforms;

5. It is possible to apply the computational code also to fluid mixtures and different case of study. Previous works showed that there is a relevant impact in computing real turbine performances [12], but no attempt of optimizing the whole thermodynamic cycle has been made yet;

6. The behaviour of other organic fluids, especially in terms of maximum available temperature consistent with chemical stability and heat source level can be examined, in the context of this or any other different case of study.

BIBLIOGRAPHY

[1] L. Pantieri and T. Gordini. *L'arte di scrivere con LaTeX*, 2009.

[2] L. Pantieri. *Introduzione allo stile ClassicThesis*, 2008.

[3] JabRef Development Team. *JabRef*, 2014. URL http://jabref.sf.net.

[4] H.R.M. Craig and H.J.A. Cox. Performance estimation of axial flow turbines. *Proc (Part 1)*, pages 407–24, 1972.

[5] Siemens. Sgt-500 gas turbine. URL http://www.energy.siemens.com/us/en/fossil-power-generation/gas-turbines/sgt-500.htm#content=Technical%20Data.

[6] B. Evers and P. Kötzing. Test case e/tu-4 4-stage low speed turbine. *AGARD Report No. AR-275*, 1990.

[7] L. Pierobon, T. Van Nguyen, U. Larsen, F. Haglind, and B. Elmegaard. Multi-objective optimization of organic rankine cycles for waste heat recovery: Application in an offshore platform. *Energy*, 58:538, 2013. ISSN 03605442.

[8] A. Schuster, S. Karellas, E. Kakaras, and H. Spliethoff. Energetic and economic investigation of organic rankine cycle applications. *Applied thermal engineering*, 29(8):1809–1817, 2009.

[9] S. Quoilin, M. Van Den Broek, and S. Declaye. Techno-economic survey of organic rankine cycle (orc) systems. *Renewable and Sustainable Energy Reviews*, 22:168, 2013. ISSN 13640321, 18790690.

[10] C. Osnaghi. *Teoria delle turbomacchine*. Società Editrice Esculapio, 2013.

[11] Offshore Technology. Draugen oil field, norway. URL http://www.offshore-technology.com/projects/draugenoilfieldnorwa/.

[12] P. Gabrielli. Design and optimization of turbo-expanders for organic rankine cycles. Master's thesis, 2014.

[13] The mathworks®. Matlab user's guide, 1998. URL http://www.mathworks.se/.

[14] I. H. Bell, J. Wronski, S. Quoilin, and V. Lemort. Pure and pseudo-pure fluid thermophysical property evaluation and the open-source thermophysical property library coolprop. *Industrial & Engineering Chemistry Research*, 53 (6):2498–2508, 2014. doi: 10.1021/ie4033999. URL http://pubs.acs.org/doi/abs/10.1021/ie4033999.

[15] E.W. Lemmon, M.L. Huber, and M.O. McLinden. Refprop, nist standard reference database 23, version 8.0. *National Institute of Standards and Technology, Gaithersburg, MD*, 2007.

[16] Autodesk®. Autocad 2015. URL http://www.autodesk.com/.

[17] A. Warren Adam. Organic rankine engines. *Encyclopedia of Energy Technology and the Environment*, 4, 1995.

[18] J. Bao and L. Zhao. A review of working fluid and expander selections for organic rankine cycle. *Renewable and Sustainable Energy Reviews*, 24:325, 2013. ISSN 13640321, 18790690.

[19] M. Astolfi, M. C. Romano, and P. Bombarda. Binary ORC (organic Rankine cycles) power plants for the exploitation of medium-low temperature geothermal sources - part A: Thermodynamic optimization. *Energy*, 66:423, 2014. ISSN 03605442.

[20] M. Astolfi, M. C. Romano, P. Bombarda, and E. Macchi. Binary ORC (organic Rankine cycles) power plants for the exploitation of medium-low temperature geothermal sources - part B: Techno-economic optimization. *ENERGY*, 66:435–446, 2014. ISSN 03605442. doi: 10.1016/j.energy.2013.11.057.

[21] D. M. Ginosar, L. M. Petkovic, and D. P. Guillen. Thermal stability of cyclopentane as an organic rankine cycle working fluid. *Energy & Fuels*, 25(9):4138–4144, 2011.

[22] P. Klonowicz, F. Heberle, M. Preissinger, and D. Brueggemann. Significance of loss correlations in performance prediction of small scale, highly loaded turbine stages working in organic rankine cycles. *ENERGY*, 72:322–330, 2014. ISSN 03605442. doi: 10.1016/j.energy.2014.05.040.

[23] E. Macchi. Design criteria for turbines operating with fluids having a low speed of sound. *Von Karman Inst. for Fluid Dyn. Closed Cycle Gas Turbines,*, 2, 1977.

[24] H. I. H. Saravanamuttoo, G. F. C. Rogers, and H. Cohen. *Gas turbine theory*. Pearson Education, 2001.

[25] A. Beccari. *Macchine*. 1993. ISBN 9788879920339.

[26] P. Kundu and I. Cohen. Fluid mechanics, 730 pp, 2000.

[27] E. Macchi and A. Perdichizzi. Efficiency prediction for axial-flow turbines operating with nonconventional fluids. *American Society of Mechanical Engineers (Paper)*, (81), 1981. ISSN 04021215.

[28] G. Lozza. A comparison between the craig-cox and the kacker-okapuu methods of turbine performance prediction. *Meccanica*, 17(4):211–221, 1982. ISSN 00256455, 15729648. doi: 10.1007/BF02128314.

[29] L. Pierobon, F. Haglind, U. Larsen, and T. Van Nguyen. Optimization of organic rankine cycles for off-shore applications. *Proceedings of the ASME Turbo Expo*, 5:–, 2013. doi: 10.1115/GT2013-94108.

[30] Ministry of the Environment (Norway). The government is following up on the climate agreement, 2012. URL http://www.regjeringen.no/en/archive/Stoltenbergs-2nd-Government/Ministry-of-the-Environment/Nyheter-og-pressemeldinger/pressemeldinger/2012/the-government-is-following-up-on-the-cl.html?id=704137.

[31] M.E. Deich, G.A. Filippov, and L. Ya Lazarev. Atlas profilei reshotok osevykh turbomachin, 1965.

[32] D. G. Ainley and G. C. R. Mathieson. An examination of the flow and pressure losses in blade rows of axial-flow turbines. *Aeronautic research council*, 1951.

[33] M.H. Vavra. Axial flow turbines. *Lecture Series*, 15, 1969.

[34] S.C. Kacker and U. Okapuu. A mean line prediction method for axial flow turbine efficiency. *Journal of Engineering for Gas Turbines and Power*, 104(1):111–119, 1982.

[35] M. Obitko. Genetic algorithms. URL http://obitko.com/tutorials/genetic-algorithms/.

[36] A. Galliani and E. Pedrocchi. *Analisi exergetica*. Polipress, 2006.

[37] M. Pasetti, C. M. Invernizzi, and P. Iora. Thermal stability of working fluids for organic rankine cycles: An improved survey method and experimental results for cyclopentane, isopentane and n-butane. *Applied Thermal Engineering*, 73(1):762 – 772, 2014. ISSN 1359-4311. doi: http://dx.doi.org/10.1016/j.applthermaleng.2014.08. 017. URL http://www.sciencedirect.com/science/article/pii/S1359431114006796.

[38] Wikipedia. Net present value, . URL http://en.wikipedia.org/wiki/Net_present_value.

[39] A. Bejan and M. J. Moran. *Thermal design and optimization*. John Wiley & Sons, 1996.

[40] Index mundi, natural gas monthly price, September 2014. URL http://www.indexmundi.com/commodities/?commodity=natural-gas&currency=nok.

[41] Wikipedia. British thermal unit, . URL http://en.wikipedia.org/wiki/British_thermal_unit#For_natural_gas.

[42] K. Rypdal. *Anthropogenic emissions of the greenhouse gases CO_2, CH_4 and N_2O in Norway: A documentation of methods of estimation, activity data and emission factors*. Statistisk sentralbyrêa (Oslo), 1993.

[43] Yahoo Finance. Money currency converter. URL https://it.finance.yahoo.com/valute/convertitore/#from=EUR;to=NOK;amt=1.

[44] Politecnico di Milano. Axtur. URL http://www.energia.polimi.it/.

[45] I. H. Johnston and L. R. Knight. Tests on a single-stage turbine comparing the performance of twisted with untwisted rotor blades. 1953.

[46] M. Mahalakshmi, P. Kalaivani, and E.Kiruba Nesamalar. A review on genetic algorithm and its applications. *International Journal of Computing Algorithm*, 02:415–423, November 2013.

[47] The Mathworks®. Genetic algorithm. URL http://www.mathworks.se/discovery/genetic-algorithm.html.

THE GENETIC ALGORITHM

A detailed description of genetic algorithms and their theoretical background, potential and applications is provided by Obitko [35] or Mahalakshmi et al. [46].
Here follows a more detailed description about the structure and working routine of genetic algorithm (GA). This description is not exhaustive but it would provide a better comprehension of the task in the context of this present work.

The structure of genetic algorithm is inspired by Darwin's theory about evolution. In simple words, the solution obtained by GA is *evolved* during the computational process.

All living organisms are an array of cells, each one containing the same amount of chromosomes which, in turn, are strings of DNA and serves as a model for the whole organism. A chromosome is made of genes, blocks of DNA, and basically each of them encodes a trait of the living organism, for example the colour of skin.

During reproduction, genes from parents recombine in some way (crossover) and a new set of chromosome is so created. Then, some changes in DNA element can occur, mainly due to errors in copying genes from parents (mutation). This means the new set of chromosomes could be different from the pure recombinations of parental genes. The fitness of an organism is measured by its success in life and surviving in the surrounding environment: organisms with higher fitness will survive and, by their reproduction, new offspring with better genes will arise.

The mathematical seek for a optimal solution, coincides with the research of some extreme value (minimum or maximum) for a particular function. The space of all feasible solutions is called search space (also state space). Each point in the search space represent one acceptable solution and each of them can be "marked" by its value or fitness for the problem.

The mathematical structure of GA basically mirrors the aforementioned biological mechanism: for a determined number of chromosomes (population size) a new offspring is created recombining genes of the existing ones. The fitness of each new chromosome is evaluated and the best of each generation is kept in memory. This process goes on until the maximum number of generations is reached or no further change in the found

maximum/minimum value for the optimizing function is obtained[1].

Thus each chromosome is a set of input value for the optimizing function. The goal is to find the chromosome with the best fitness that is, the best set of input values for a certain function that maximises/minimizes it.

However, the "evolution" process is rather more complicated than this, being the new incoming generation a product of crossover, mutation and randomness. The first and second are the most important part of the genetic algorithm while the third is intrinsically contained in the whole process. We define:

1. **Crossover probability**: index of how often crossover is performed. If this value is zero, the offspring is an exact copy of parents. If there is a crossover, offspring is made from parts of parents' chromosome. If crossover probability is 100%, all the new generation is made by crossover. If it is 0%, the new offspring is made from exact copies of chromosomes of the population; it is worth noting this does not mean that the new generation is the same as the previous one. Crossover is made in hope that new chromosomes will have the best parts of old parents, forming a hopefully better generation. However it is good to let some part of old population survive to the next generation.

2. **Mutation probability** states how often parts of a chromosome will be mutated. If there is no mutation, offspring is taken after crossover (or copy) without any change. If a component of mutation fraction exists, at least a small part of the chromosome is changed. If mutation probability is 100%, the whole chromosome genes are changed, if it is 0%, all of them are untouched from the previous step. Mutation process could be completely random or partially/totally governed by a particular probability distribution [47]. This process is made to prevent GA getting stuck into a specific local extreme; even though, theoretically, this problem should not often occur, according to the particular function to be optimized (namely its non-continuity, eventual fluctuating and non-linear trend, presence of local extremes and so on), this could be one of the main causes of uncertainty of this method.

3. **Population size**: the number of chromosomes contained in a single population (or generation). If this number is

---

1 If no change is observed in the optimizing function within the next 50 generations, the algorithm stops calculating.

too low, the genetic algorithm has a few possibilities to perform crossover and only a small part of search space is explored. On the other hand, if the Population size is too high, the process slows down. It has been demonstrated that after a limit size (which depends mainly on encoding and optimizing function), it is not useful to increase population size, because it does not reduces the computational time nor improves the obtained result [35].

4. **Number of generations**: the number of sets of chromosomes to be consecutively created by the GA. The consequences related to this parameter are very similar to the ones discussed about the population size: a small number of generations could prevent GA finding the optimal solution (or at least getting close to it), a huge value can increase excessively the computational time without any significant benefit; in particular, after a certain number of generations, the optimal solution can have been already found so no further improvement is possible.

5. **migration fraction**: Another problem is how to select the chromosomes from a certain generation to be parents and crossover for the next one; according to Darwin's evolution theory only the best ones should survive and create new offspring. However, when creating a new population by crossover and mutation, there is a big chance for the best chromosomes to be lost; it is so good practice to save the best of them, replicated into the next generation. This approach is called *elitism*: the best chromosomes (in terms of fitness) are copied into the new population, according to a specified value of *migration fraction*. the rest of elements is obtained as previously discussed. Elitism can rapidly increase GA performance, because it prevents losing the best found solutions.

While launching the genetic algorithm function, all these parameters must be specified or, at least, keep the default configuration provided by MATLAB [47].

TABLES AND USEFUL FIGURES
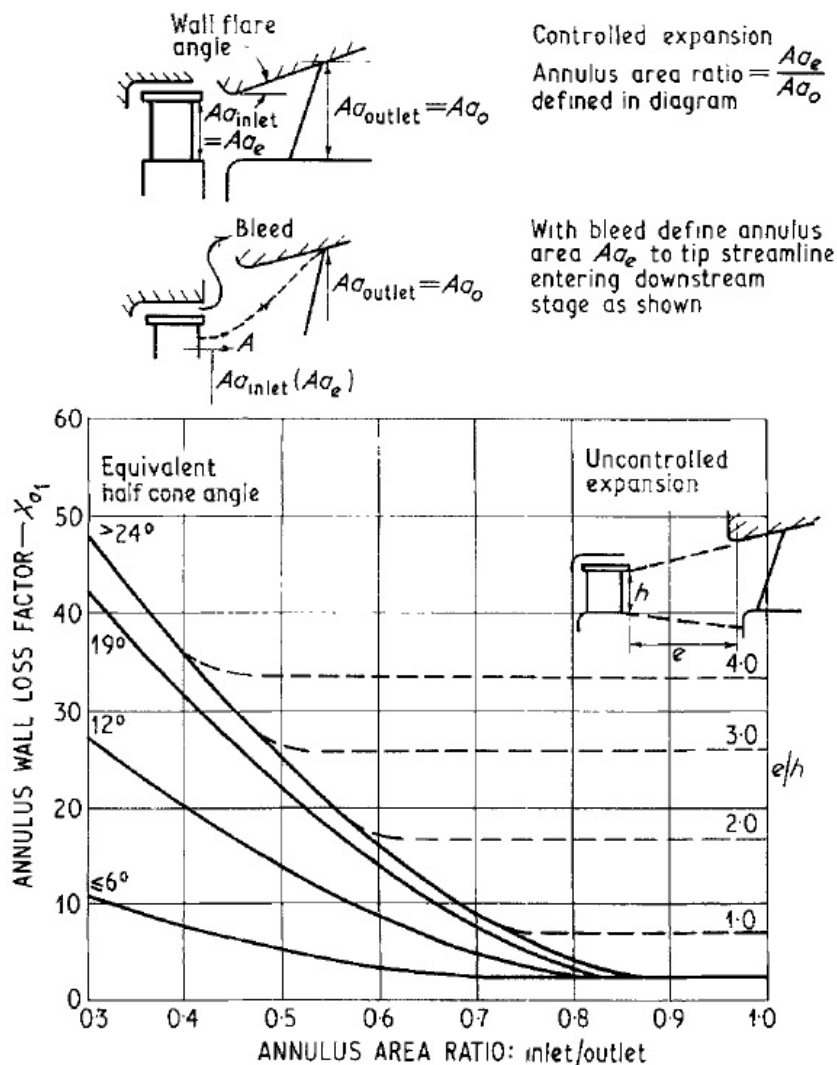
Fig. 19. Annulus wall loss

Figure B.1.: Figure 19 of Craig and Cox losses estimation procedure (Craig and Cox [4]).

Table B.1.: Complete list of required turbine input parameters for the computational routine

Parameter	Unit	Description
Optimizing parameters		
α_1	°	absolute nozzle inlet fluid angle
ψ	-	$\Delta H_{tot}/(u_m^2/2)$
$(o_{min})_n$	m	Nozzle throat section
o_r	m	Rotor throat section
c_n	m	Nozzle axial chord
c_r	m	Rotor axial chord
$\left(\frac{o}{s}\right)_n$	-	Blade outlet section/pitch, nozzle
$\left(\frac{o}{s}\right)_r$	-	Blade outlet section/pitch, rotor
Cycle requirements		
$\dot{m}$	kg/s	Mass flow rate
P_{01}	bar	Total inlet pressure
P_{03}	bar	Total outlet pressure
N	rpm	Rotational speed
T_{01}	K	Total inlet temperature
fluid	-	fluid type
Fixed inputs		
hhh	-	Nozzle outlet/rotor inlet height ratio
Mcd	-	Mach number for conv.-div. Nozzle
$(t_e/o)_n$	-	Trailing edge thickness/outlet section for nozzle
$(t_e/o)_r$	-	Trailing edge thickness/outlet section for rotor
Re	-	Reynolds number
$i_{min,n}$	°	Minimum incidence value for nozzle
$i_{min,r}$	°	Minimum incidence value for rotor
k_{sbr}	-	Relative surface roughness
ε	m	Back surface radius
controlled expansion	-	yes/no
shrouded blades	-	yes/no
overlap	m	overlap
tol_f	-	Tolerance factor for convergence

Table B.2.: Complete list of required input parameters for cycle model

parameter	default value	Unit	Description
$\dot{m}_{gas}$	93.5	kg/s	Exhausted gas mass flow rate
$T_{gas,in}$	376	°C	Inlet gas temperature
$T_{gas,out,min}$	145	°C	Minimum exhausted gas outlet temperature
$c_{p,gas}$	1.1	kJ/(kg K)	Exhausted gas specific heat
η_p	0.8	-	Pump efficiency
η_{gen}	0.98	-	Elecric generator efficiency
η_{turb}	0.8	-	Turbine efficiency (only for constant-efficiency tests)
η_{gear}	0.96	-	Gearbox efficiency (only if gearbox presence ins considered)
fluid	cyclopentane	-	Organic fluid to be used
P_{cond}	1	bar	Condensation pressure
$P_{r,max}$	$0.9 \cdot P_{crit}$	-	Maximum available pressure ratio
$\Delta T_{pp,rec}$	15	°C	Pinch point temperature difference in internal recuperator
ΔT_{pp}	10	°C	Pinch point temperature difference in main heat exchanger
TIT	513.15	K	Turbine inlet temperature
tol_f	0.01	-	Tollerance factor for convergence in turbine map interpolation

Table B.3.: design turbine default values and other input parameters for influence analysis

Input parameter	Value	Unit
α_1	4	°
ψ	3	-
$(o_{min})_n$	0.007	m
o_r	0.009	m
c_n	0.033	m
c_r	0.0311	m
$(o/s)_n$	0.224	-
$(o/s)_r$	0.237	-
m	40	kg/s
P_{01}	20	bar
P_{03}	1	bar
T_{01}	513.15	K
N	3000	rpm
fluid	cyclopentane	-

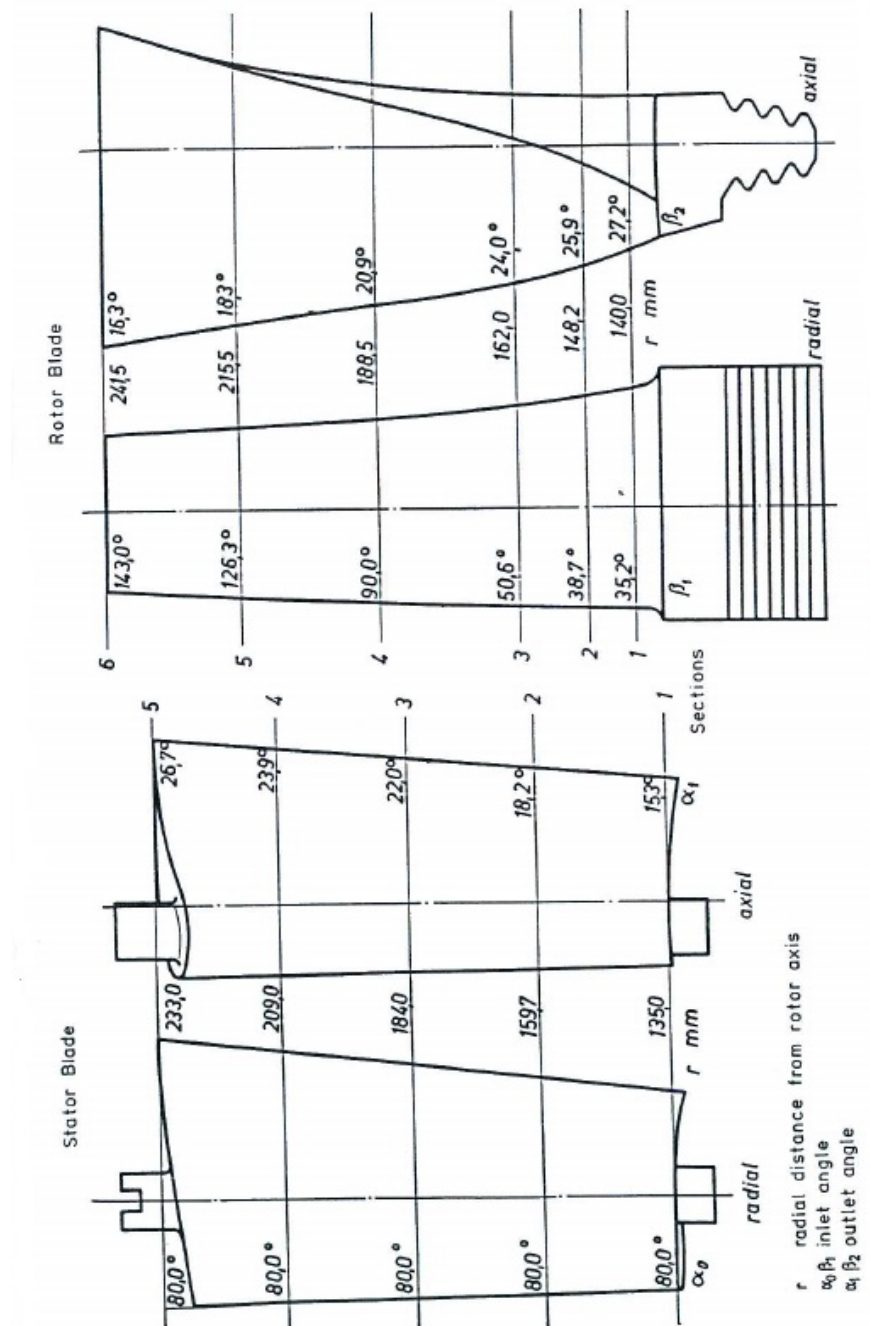# DATA AND PICTURES FROM EVERS AND KÖTZING

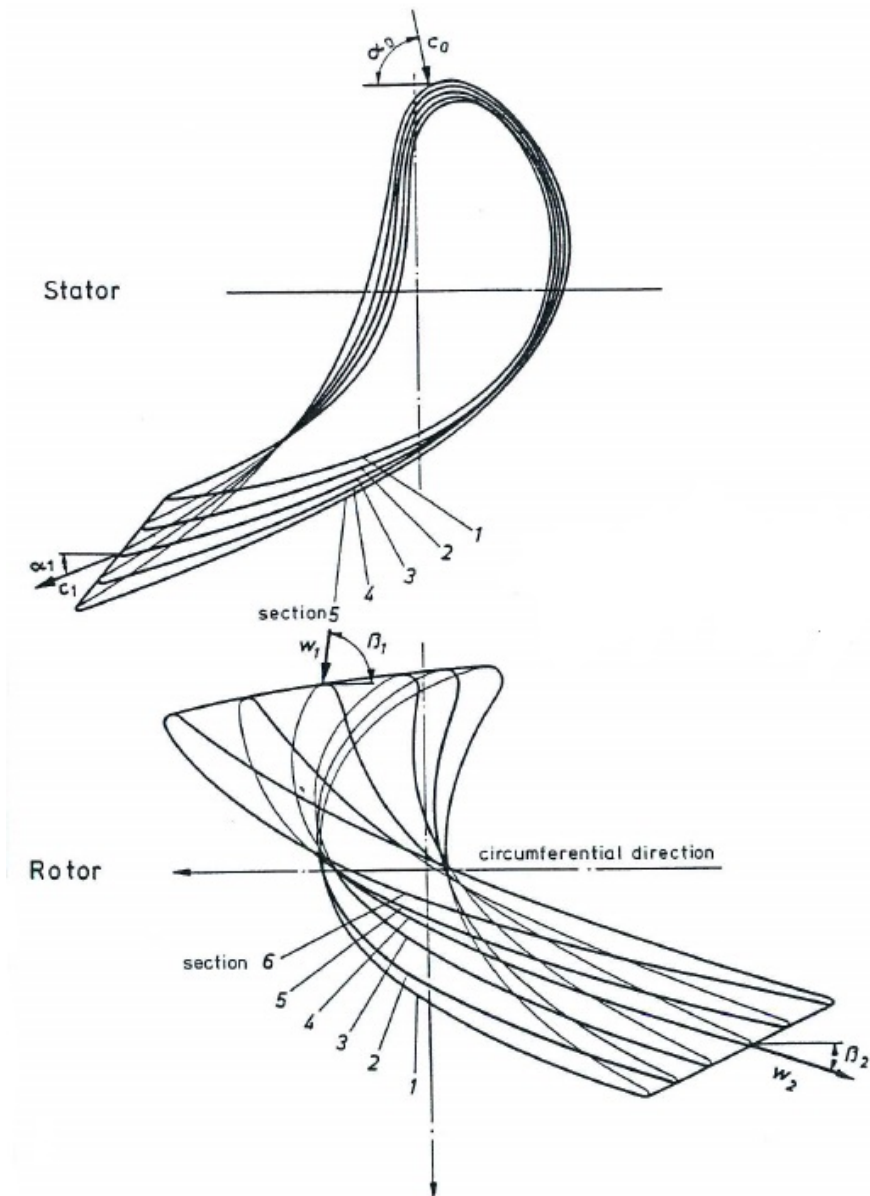**Figure C.1.:** Blade profiles in radial direction, Evers and Kötzing [6].

Figure C.2.: Blade sections in radial direction, Evers and Kötzing [6].

368

Table 3
Traverse data of 4-stage turbine at design condition

Nominal rotational speed n = 7500 rpm
Nominal mass flow   m = 7,8 kg/s

Station 0:

R [m]	PT [Pa]	PS [Pa]	TT [K]	V [m/s]	ALPHA [deg]	GAMMA [deg]
0,1945 tip						
0,1868	259100	254500	405,8	64,2	97,3	11,9
0,1821	258100	253500	406,0	67,5	95,7	9,8
0,1774	258400	253300	405,9	68,0	96,2	5,8
0,1724	257800	253200	405,7	65,2	96,1	4,4
0,1674	258800	253800	405,4	67,4	95,4	-1,8
0,1621	259700	255100	404,8	64,9	95,1	7,1
0,1565	257600	253200	404,2	62,7	94,0	7,0
0,1506	256400	251900	403,3	63,7	95,0	1,2
0,1447	252800	248000	400,8	65,9	94,9	7,0
0,1350 hub						

Station 1:

R [m]	PT [Pa]	PS [Pa]	TT [K]	V [m/s]	ALPHA [deg]	GAMMA [deg]
0,2025 tip						
0,1942	211200	207000	384,9	67,1	92,0	7,7
0,1887	211500	206700	385,0	70,8	92,6	15,7
0,1833	211900	206700	384,8	73,7	91,3	12,1
0,1780	212400	206700	384,6	76,8	90,9	9,6
0,1728	212900	206900	384,8	79,3	90,0	7,6
0,1674	213500	207800	385,4	77,2	85,0	11,1
0,1617	213600	207500	386,2	80,0	79,6	17,1
0,1559	210600	204800	385,4	78,8	79,6	-3,0
0,1488	209200	205400	382,7	62,6	99,9	5,3
0,1350 hub						

Station 2:

R [m]	PT [Pa]	PS [Pa]	TT [K]	V [m/s]	ALPHA [deg]	GAMMA [deg]
0,2125 tip						
0,2031	168900	165400	362,9	94,6	94,6	4,6
0,1966	169300	165400	362,4	95,9	95,9	8,5
0,1900	169400	165600	361,9	97,4	97,4	6,5
0,1833	170100	165700	362,4	98,2	98,2	4,9
0,1769	171100	165900	363,1	95,9	95,9	6,1
0,1706	171300	166000	364,1	93,6	93,6	8,0
0,1640	171200	165900	365,0	85,1	85,1	17,0
0,1570	169900	164800	364,2	82,1	82,1	5,8
0,1493	169000	165500	362,3	88,3	88,3	2,7
0,1350 hub						

Station 3:

R [m]	PT [Pa]	PS [Pa]	TT [K]	V [m/s]	ALPHA [deg]	GAMMA [deg]
0,2242 tip						
0,2140	133500	130500	340,7	66,6	94,9	5,5
0,2067	133700	130400	339,8	69,3	96,5	6,4
0,1990	133700	130500	339,5	68,9	96,0	3,9
0,1913	134300	130700	339,5	72,4	96,4	1,3
0,1836	134800	131000	339,6	74,2	95,5	1,8
0,1758	135200	131300	340,1	75,9	92,9	1,0
0,1678	135000	131200	341,1	74,5	89,2	0,3
0,1592	135600	131100	342,0	81,3	81,8	-5,5
0,1526	135800	131700	340,8	77,1	86,0	-17,9
0,1350 hub						

Station 4:

R [m]	PT [Pa]	PS [Pa]	TT [K]	V [m/s]	ALPHA [deg]	GAMMA [deg]
0,2380 tip						
0,2262	104600	101500	322,7	75,2	83,3	-13,1
0,2175	104300	101400	320,2	71,5	98,1	-1,7
0,2083	104200	101400	319,4	71,8	97,4	-0,9
0,1992	104900	101300	319,4	80,1	96,8	-3,3
0,1906	105200	101200	319,3	84,7	95,4	-3,7
0,1819	105200	101100	319,7	85,5	93,1	-1,9
0,1728	105700	101300	322,4	88,6	85,9	9,8
0,1634	106600	101300	323,6	97,0	78,6	5,6
0,1536	104600	101000	321,8	79,7	90,1	-18,7
0,1350 hub						

Table 4
Traverse data of 4-stage turbine at off-design condition

Rotational speed n= 7500 /min
Mass flow   m= 6.5 kg/s

Station 0:

R [m]	PT [Pa]	PS [Pa]	TT [K]	V [m/s]	ALPHA [deg]	GAMMA [deg]
0.1945 tip						
0.1870	214000	210100	387.6	64.4	95.9	5.0
0.1822	214200	214200	387.6	65.8	95.8	4.2
0.1775	214200	214200	387.6	66.0	95.8	2.2
0.1725	214300	214300	387.5	65.1	95.5	2.1
0.1674	214200	214200	387.5	63.8	95.2	1.3
0.1620	214200	214200	387.3	63.4	94.9	1.9
0.1564	214700	214700	387.3	63.7	94.2	7.0
0.1507	215600	215600	386.8	63.5	93.6	2.0
0.1447	215200	215200	385.7	64.0	94.9	2.4
0.1350 hub						

Station 1:

R [m]	PT [Pa]	PS [Pa]	TT [K]	V [m/s]	ALPHA [deg]	GAMMA [deg]
0.2025 tip						
0.1942	177700	173200	370.1	73.2	81.1	-18.9
0.1888	178100	173800	369.3	72.0	84.9	0.5
0.1836	178500	173800	368.9	75.3	85.6	1.8
0.1783	178700	173900	369.1	76.0	85.8	3.5
0.1729	178700	174000	370.6	75.3	83.0	6.2
0.1672	180000	174500	372.0	81.0	74.2	14.6
0.1616	180500	174200	371.8	87.1	71.4	7.8
0.1560	180400	174500	370.6	83.9	73.2	-22.0
0.1475	176900	174700	367.6	50.6	93.9	-16.9
0.1350 hub						

Station 2:

R [m]	PT [Pa]	PS [Pa]	TT [K]	V [m/s]	ALPHA [deg]	GAMMA [deg]
0.2125 tip						
0.2034	147800	144600	351.9	66.6	80.8	-6.0
0.1971	148300	144900	351.5	67.7	84.4	4.1
0.1909	148500	144900	351.1	69.4	85.9	2.5
0.1845	148800	145100	351.1	70.5	87.4	2.7
0.1781	148800	145300	351.1	69.2	85.6	1.6
0.1711	149000	145500	352.1	69.4	81.8	2.8
0.1640	149500	145600	353.4	73.5	75.7	1.1
0.1569	150300	145800	353.1	76.3	70.8	-8.3
0.1485	148800	146000	351.6	62.4	69.1	-17.1
0.1350 hub						

Station 3:

R [m]	PT [Pa]	PS [Pa]	TT [K]	V [m/s]	ALPHA [deg]	GAMMA [deg]
0.2242 tip						
0.2144	123700	121100	336.2	64.2	74.1	-5.2
0.2073	124000	121300	335.0	64.6	77.8	4.0
0.2002	124000	121300	334.2	64.8	79.2	4.0
0.1928	124100	121400	334.1	64.8	79.7	3.5
0.1851	124200	121600	334.5	63.7	78.8	2.3
0.1769	124400	121800	335.4	64.0	75.2	3.0
0.1685	124800	121900	336.4	66.6	69.9	1.1
0.1595	125400	122100	336.4	71.4	66.9	-3.7
0.1526	125000	122000	335.6	68.3	65.1	-13.2
0.1350 hub						

Station 4:

R [m]	PT [Pa]	PS [Pa]	TT [K]	V [m/s]	ALPHA [deg]	GAMMA [deg]
0.2380 tip						
0.2274	106700	103800	324.4	70.9	54.6	-10.6
0.2192	105700	103800	321.8	59.3	67.8	3.5
0.2109	105700	103700	320.9	60.1	70.1	4.5
0.2023	105500	103600	320.4	58.5	70.9	3.0
0.1934	105600	103600	320.6	59.9	70.2	1.6
0.1840	105700	103600	321.4	61.7	68.3	1.7
0.1744	105900	103600	322.6	63.9	63.6	0.4
0.1639	106300	103600	323.4	69.4	57.8	2.7
0.1533	105900	103400	322.7	66.8	56.0	-14.6
0.1350 hub						

Figure C.3.: Thermodynamic data for all the four stages, Evers and Kötzing [6].